Department of Physics and Astronomy

University of Heidelberg

Master thesis

in Physics

submitted by

Oliver Scholer

born in Trier

2020

On Distinguishing Different $0\nu\beta\beta$ Mechanisms

This Master thesis has been carried out by Oliver Scholer

at the

Max-Planck-Institut für Kernphysik

under the supervision of

Prof. Dr. Dr. h.c. Manfred Lindner

$0\nu\beta\beta$ Mechanismen und wie sie zu finden sind:

In dieser Arbeit untersuchen wir verschiedene Möglichkeiten unterschiedliche Mechanismen, welche zu neutrinolosem doppeltem β-Zerfall führen, experimentell zu unterscheiden und zu identifizieren. Dabei verfolgen wir einen Ansatz der effektiven Feldtheorie bei niedrigen Energien. Wir finden heraus, dass der vielversprechendste Ansatz zur Identifizierung des dominierenden Mechanismus darin besteht, die Verhältnisse der Halbwertszeiten in verschiedenen Isotopen zueinander zu messen und zu vergleichen. Eine ausreichende experimentelle Messgenauigkeit vorausgesetzt, können auf diesem Weg 11 verschiedene Gruppen von effektiven Operatoren voneinander unterschieden werden. Allerdings hängen die genauen Verhältnisse quantitativ von zur Zeit unbekannten niedrig-Energie Konstanten ab, welche besonders bei kurzreichweitigen Mechanismen eine Rolle spielen. Diese Konstanten können in zukünftigen Studien anhand von Gitter-QCD Berechnungen bestimmt werden. Zusätzliche Informationen über den zugrundeliegenden Mechanismus können anhand von Observablen des leptonischen Phasenraums oder über Hochenergie-Beschleunigerexperimente gewonnen werden. Zum Schluss untersuchen wir den Einfluss von drei vollständigen Modellen jenseits des Standardmodells, die wir aus der Literatur entnehmen. Diese vergleichen wir mit dem Standard-Mechanismus des Austauschs leichter Majorana Neutrinos.

On distinguishing different $0\nu\beta\beta$ mechanisms:

In this thesis we study possibilities to distinguish different mechanisms of neutrinoless double-β decay within a low-energy effective field theory framework. We find that the most promising approach towards identifying the dominant contribution experimentally is given by a measurement of half-life ratios in different isotopes. Given the experimental accuracy, we identify 11 different groups of low-energy effective operators that can be distinguished in this way. However, the ratios depend on currently unknown low-energy constants that are especially important when considering short-range mechanisms. These constants can be calculated within lattice QCD and should be obtained in the future. Additional information about the underlying mechanism can be gained from phase space observables as well as high-energy collider data. Finally, we studied the impact of three different models beyond the Standard Model taken from the literature and compared them to the standard mechanism of light neutrino exchange.

Contents

1. Introduction

The Standard Model of particle physics [1] is a story of great success as it has proven to precisely describe nature down to the microscopic scales studied at high energy colliders like the LHC or LEP [2]. However, with the observation of neutrino oscillations [3, 4] we have the first clear experimental evidence of physics beyond the Standard Model. While the Standard Model predicts massless neutrinos, neutrino oscillation necessitates non-vanishing neutrino masses. This fact raises questions about the nature of neutrinos. Being the only electrically neutral fundamental fermions, neutrinos are the only candidates in the Standard Models particle content that could be their own anti-particles, i.e., that could be Majorana fermions. Identifying the true nature of neutrinos is one of the most urging questions in particle physics as it could give us insight into the mechanism of neutrino mass generation as well as it could teach us more about a fundamental question related to the observed baryon asymmetry of the universe, famously quoted as: "Why is there something instead of nothing?" [5]. This question cannot be answered by oscillation experiments. Instead, the most promising experimental project to study the true nature of neutrinos is the search for neutrinoless double-β-decay ($0\nu\beta\beta$). This lepton number violating process is forbidden within the Standard Model. If observed, it would clearly identify neutrinos as Majorana particles [6]. However, things are not quite that easy as also other lepton number violating new physics processes could contribute to or even dominate the $0\nu\beta\beta$-decay amplitude [7, 8]. To really understand the underlying new-physics and to be able to infer the right conclusions one needs to understand the true mechanism of $0\nu\beta\beta$. Therefore this work is dedicated towards studying possibilities to distinguish and identify different mechanisms of $0\nu\beta\beta$-decay.
This thesis is structured as follows: In chapter 2 we will give a rather formal motivation on why one should consider and study the possibility of $0\nu\beta\beta$-decay by explaining the most commonly studied mechanisms of neutrino mass generation. Following up on this, in chapter 3 we will review the most important aspects of the theory of $0\nu\beta\beta$-decay and introduce the effective field theory framework that we applied. In chapter 4 we will then discuss possibilities to distinguish and identify different mechanisms of $0\nu\beta\beta$-decay for both single operators as well as some more complex models taken from the literature. Finally, in the last chapter 5 we will summarize our findings. Throughout this work we use natural units $\hbar = c = 1$.

2. Motivation from Neutrino Physics

Before turning towards our main focus, the $0\nu\beta\beta$-decay, we want to start by giving some motivational context on why this process should be studied. In order to do so, we will start by explaining the problem of vanishing neutrino masses within the Standard Model of Particle Physics and why it is contradicting observations. Building up on this we will show that the most famous approaches towards solving this problem lead to lepton number violation via a Majorana neutrino mass term. Afterwards, we will summarize a few more theoretical motivations for studying lepton number violation within the neutrino sector.

2.1. Neutrinos within the Standard Model

The Standard Model of particle physics is defined by its gauge group $\big(SU(3)_C \times SU(2)_L \times U(1)_Y\big)$, its particle content represented in Tables 2.1 and 2.2, Lorentz invariance and the requirement for renormalizability [9]. The fact that its gauge group distinguishes between left- and right-handed chiral particles (hence the notion $SU(2)_L$) makes the Standard Model a chiral theory. A chiral fermion is defined by the chiral projectors

$$\Psi_{L,R} = P_{L,R}\Psi \quad \text{with} \quad P_{L,R} = \frac{1}{2}\left(1 \mp \gamma_5\right) \ , \tag{2.1}$$

with the chirality operator γ_5, which is given by the Dirac gamma matrices

$$\gamma_5 = i\gamma^0\gamma^1\gamma^2\gamma^3 \tag{2.2}$$

which obey

$$\{\gamma^\mu, \gamma^\nu\} = 2\eta^{\mu\nu} \quad \text{and} \quad \{\gamma^\mu, \gamma_5\} = 0. \tag{2.3}$$

With these properties it is easily shown that $P_{L,R}$ are indeed projectors and obey

$$P_{L,R}P_{R,L} = 0 \quad \text{and} \quad P_{L,R}^2 = P_{L,R}. \tag{2.4}$$

Within the Standard Model, fermions are grouped into right-handed $SU(2)_L$ singlets Ψ_R and left-handed $SU(2)_L$ doublets L_i and Q_i.[1] Ignoring the $SU(3)_C$ part of the gauge symmetry, under the remaining Standard Model gauge group fermions transform as

$$L \longrightarrow U\left(\vec{\theta}(x), \alpha(x)\right) L = \exp\left\{ i\vec{\theta}(x)\frac{\vec{\tau}}{2} + i\hat{Y}\alpha(x) \right\} L, \tag{2.5}$$

$$R \longrightarrow U\left(\alpha(x)\right) R = \exp\left\{ i\hat{Y}\alpha(x) \right\} R, \tag{2.6}$$

[1] In principle there could also be, e.g., $SU(2)$ triplet fermions as we will see later but they are not part of the Standard Models particle content.

		Fermions						
		LH				RH		
		I_3	Y	Q		I_3	Y	Q
Leptons	$L_i = \begin{matrix}\nu_{i,L}\\ l_{i,L}\end{matrix}$	$\begin{matrix}+1/2\\ -1/2\end{matrix}$	-1	$\begin{matrix}0\\ -1\end{matrix}$	$\begin{matrix}/\\ l_{i,R}\end{matrix}$	$\begin{matrix}/\\ 0\end{matrix}$	$\begin{matrix}/\\ -2\end{matrix}$	$\begin{matrix}/\\ -1\end{matrix}$
Quarks	$Q_i = \begin{matrix}u_{i,L}\\ d_{i,L}\end{matrix}$	$\begin{matrix}+1/2\\ -1/2\end{matrix}$	$1/3$	$\begin{matrix}+2/3\\ -1/3\end{matrix}$	$\begin{matrix}u_{i,R}\\ d_{i,R}\end{matrix}$	$\begin{matrix}0\\ 0\end{matrix}$	$\begin{matrix}+4/3\\ -2/3\end{matrix}$	$\begin{matrix}+2/3\\ -1/3\end{matrix}$
		Scalars						
		I_3	Y	Q				
	$\Phi = \begin{matrix}\Phi^+\\ \Phi^0\end{matrix}$	$\begin{matrix}+1/2\\ -1/2\end{matrix}$	$+1$	$\begin{matrix}+1\\ 0\end{matrix}$				

Table 2.1.: Standard Model fermions and scalars and their corresponding weak isospin projection I_3, weak hypercharge Y and electric charge Q [9]

where L defines a $SU(2)_L$ doublet, R a right-handed singlet and $\hat{Y}$ is the hypercharge of the corresponding fermion fields. Neutrinos are part of the left-handed lepton doublets

$$L_i = \begin{pmatrix} \nu_{i,L} \\ l_{i,L} \end{pmatrix} \tag{2.7}$$

with $i \in \{e, \mu, \tau\}$. While the charged leptons l_i and quarks appear as both right-handed singlet and as part of a left-handed doublet, a right-handed neutrino is not part of the Standard Model. This has mainly historic reasons:
After electroweak symmetry breaking (EWSB) which breaks $SU(2)_L \times U(1)_Y \to U(1)_Q$ the electric charge is given by the Gell-Nishijima relation [9]

$$Q = I_3 + \frac{Y}{2} \,, \tag{2.8}$$

where I_3 is the third component of the $SU(2)_L$ generating isospin

$$\vec{I} = \frac{\vec{\tau}}{2} \tag{2.9}$$

with τ_a being the 2×2 Pauli-matrices

$$\tau_1 = \begin{pmatrix} 0 & 1 \\ 1 & 0 \end{pmatrix} \qquad \tau_2 = \begin{pmatrix} 0 & -i \\ i & 0 \end{pmatrix} \qquad \tau_3 = \begin{pmatrix} 1 & 0 \\ 0 & -1 \end{pmatrix} \tag{2.10}$$

acting as

$$\vec{I} L_i = \frac{\vec{\tau}}{2} L_i \qquad \vec{I} \Psi_R = 0. \tag{2.11}$$

		Fermion Generations			Bosons	
		1	2	3	Vector	Scalar
Quarks	u_i	u 2.16 MeV	c 1.27 GeV	t 172.9 GeV	γ $-$	H 125.10 GeV
	d_i	d 4.67 MeV	s 93 MeV	b 4.18 GeV	W 80.379 GeV	
Leptons	ν_i	ν_e < 2 eV	ν_μ < 0.19 MeV	ν_τ < 18.2 MeV	Z 91.1876 GeV	
	l_i	e 0.5110 MeV	μ 105.66 MeV	τ 1.7769 GeV		

Table 2.2.: The experimental masses and mass limits after electroweak symmetry breaking are taken from [10] where the neutrino flavor masses are effective masses given by $m_{\nu_\alpha} = \sqrt{\sum_i |U_{\alpha i}|^2 m_i^2}$ and $m_{\nu_e} = m_{\overline{\nu}_e}$ is assumed.

Consequently, a right-handed neutrino is colourless $C = 0$, electrically neutral $Q = 0$ and due to its right-handedness with $I_3 = 0$ also has $Y = 0$. Hence, it would be a total singlet under the Standard Model gauge group. Such a particle would not interact via any gauge interaction and therefore is also called a "sterile" neutrino. At the times when the Standard Model was constructed, the existence of such a particle was not considered to be necessary.

2.1.1. Dirac Neutrinos

By this construction the left-handed Dirac neutrinos are massless particles due to the lack of a right-handed counterpart. This can easily be seen by taking a look at the definition of a particles mass.
Within a quantum field theory the mass of a particle can be defined as the pole of its propagator. Considering a fermion Ψ, within the path integral formulation of QFT the propagator can be written as [11]

$$S(x-y) = i\left\langle \overline{\Psi}(x)\Psi(y)\right\rangle = i\frac{1}{Z}\frac{\delta}{i\delta\overline{\eta}(x)}i\frac{\delta}{\delta\eta(y)}Z\left[\overline{\eta},\eta\right]\Big|_{\overline{\eta}=\eta=0}. \tag{2.12}$$

Here, $Z\left[\overline{\eta},\eta\right]$ denotes the partition function

$$Z\left[\overline{\eta},\eta\right] = \int \mathcal{D}\overline{\Psi}\,\mathcal{D}\Psi \exp\left\{iS\left[\overline{\Psi},\Psi\right] + i\int_x \left(\overline{\eta}(x)\Psi(x) + \overline{\Psi}(x)\eta(x)\right)\right\} \tag{2.13}$$

given by the action $S\left[\overline{\Psi},\Psi\right]$ and source terms $\overline{\eta}$ and η which are introduced to make calculations of correlation functions easier and are set to zero when calculating observables.

For a free theory of fermions the action is given by

$$S = \int_x \overline{\Psi}(i\not{\partial} - m)\Psi \tag{2.14}$$

such that the partition function becomes a Gaussian integral[2] of the type

$$\int D\overline{\Psi}\, D\Psi \exp\{\overline{\Psi} M \Psi + \overline{\eta}\Psi + \overline{\Psi}\eta\} = \det\{M\} \exp\{-\overline{\eta} M^{-1} \eta\} \tag{2.15}$$

which results in

$$Z\left[\overline{\eta}, \eta\right] = \exp\left\{ i \int_x \overline{\eta}(x) \left[-(i\not{\partial} - m)\right]^{-1} \eta(x) \right\}. \tag{2.16}$$

Here, we have dropped a constant prefactor which does not affect correlation functions. This can be seen by looking at Eq. (2.12). Now it is easy to find that the propagator is given by the solution to the Greens function

$$(-i\not{\partial} + m)\, S(x - y) = \delta(x - y) \tag{2.17}$$

which results in

$$S(x - y) = \int \frac{d^4p}{(2\pi)^4} \exp\{-i(x - y)p\} \frac{\not{p} + m}{p^2 - m^2}. \tag{2.18}$$

We see that the propagator has a pole at $p^2 = m^2$ such that we can identify m with the physical mass of the particle as expected. Hence, the Lagrangian mass term of a Dirac fermion Ψ is given by

$$\mathcal{L}_m = -m\overline{\Psi}\Psi. \tag{2.19}$$

We can rewrite this in terms of chiral fields

$$\begin{aligned} \mathcal{L}_m &= -m\overline{\Psi}\Psi \\ &= -m\left(\overline{\Psi_L} + \overline{\Psi_R}\right)\left(\Psi_L + \Psi_R\right) \\ &= -m\left(\overline{\Psi_L}\Psi_L + \overline{\Psi_L}\Psi_R + \overline{\Psi_R}\Psi_L + \overline{\Psi_R}\Psi_R\right). \end{aligned} \tag{2.20}$$

Noting that

$$\begin{aligned} \overline{\Psi_{L,R}}\Psi_{L,R} &= \left(P_{L,R}\Psi\right)^\dagger \gamma^0 P_{L,R}\Psi \\ &= \Psi^\dagger P_{L,R}\gamma^0 P_{L,R}\Psi \\ &= \Psi^\dagger \gamma^0 P_{R,L} P_{L,R}\Psi \\ &= 0 \end{aligned} \tag{2.21}$$

one finds

$$\begin{aligned} \mathcal{L}_m &= -m\overline{\Psi}\Psi \\ &= -m\left(\overline{\Psi_L}\Psi_R + \overline{\Psi_R}\Psi_L\right). \end{aligned} \tag{2.22}$$

Thus, we see that a non-zero fermion mass term requires the existence of both left and right chiral states. In that sense **a mass term represents a chirality flip** $R, L \to L, R$.

[2]Note that fermions are described by anti-commuting Grassman numbers.

2.1.2. Majorana Neutrinos

The aforementioned is the case for typical Dirac fermions $\Psi = \Psi_L + \Psi_R$. However, one can construct a right-handed fermion field from a left-handed one by taking

$$\Psi_R \to (\Psi_L)^c \tag{2.23}$$

with

$$\Psi^c = C\overline{\Psi}^T \tag{2.24}$$

where C is the charge conjugation operator

$$C = i\gamma^0\gamma^2. \tag{2.25}$$

A particle corresponding to such a field is equal to its own anti-particle as can be seen easily if we take[3]

$$\Psi = \Psi_L + (\Psi_L)^c = (\Psi_L)^c + \Psi_L = \Psi^c\,. \tag{2.26}$$

Therefore, only neutral particles can be Majorana. For a Majorana field the partition function of the free theory is given by

$$Z[\eta] = \int \mathcal{D}\Psi \exp\left\{ iS_M + i\int_x \eta^T\Psi \right\} \tag{2.27}$$

with

$$S_M = \int_x \frac{1}{2}\Psi^T C\left(i\not{\partial} - m\right)\Psi = \frac{1}{2}\int_x \Psi^T S_M(x-y)\Psi. \tag{2.28}$$

The factor of $1/2$ results from the fact that for Majorana fermions $\overline{\Psi}$ and Ψ can no longer be considered as independent.[4] Obviously in this case the propagator is given by

$$S_M(x-y) = S(x-y)C^{-1} = -S(x-y)C \tag{2.29}$$

and we have

$$i\left\langle \Psi_L\Psi_L^T \right\rangle = S_M(x-y). \tag{2.30}$$

That is, the Majorana mass term is given by

$$\mathcal{L}_m = -\frac{m}{2}\Psi^T C\Psi \tag{2.31}$$

or in terms of left-handed chiral fields

$$\mathcal{L}_m = -\frac{m}{2}\Psi_L^T C\Psi_L + h.c.. \tag{2.32}$$

[3] Note that we ignored an arbitrary phase η that can be assigned to either Ψ or Ψ^c resulting in $\Psi = \eta\Psi^c$.

[4] Note that for Majorana fields $\Psi = \Psi^c$ we have $i\Psi^T C\not{\partial}\Psi = i\Psi_L^T C\not{\partial}\Psi_L + i(\Psi_L^T)^c C\not{\partial}(\Psi_L)^c = 2i\Psi_L^T C\not{\partial}\Psi_L$ and similarly for $\Psi^T Cm\Psi$ when considering chiral particles.

We see that in principle one can form such a mass term within a theory which only contains left-handed neutrinos. However, assigning a lepton number of $L = 1$ to the neutrinos it would violate lepton number conservation by $\Delta L = 2$. The question remains whether this is possible within the whole framework of the Standard Model. Before we answer this question, let us first discuss if the assumption of neutrinos being Majorana particles can agree with current experimental results. Afterwards, we will check if neutrinos being Majorana particles is allowed within the Standard Model theory.

2.1.3. Are the Standard Model Neutrinos Majorana Particles?

Neutrinos are electrically neutral particles. Hence, after electroweak symmetry breaking they could be Majorana particles.[5] However, experiments show us that the interactions

$$\begin{aligned} \nu_e + n &\longleftrightarrow e^- + p \\ \nu_e^c + p &\longleftrightarrow e^+ + n \end{aligned} \tag{2.33}$$

are possible, while interactions in which we switch $\nu_e \leftrightarrow \nu_e^c$

$$\begin{aligned} \nu_e^c + n &\longleftrightarrow e^- + p \\ \nu_e + p &\longleftrightarrow e^+ + n \end{aligned} \tag{2.34}$$

are not observed. This result is in accordance with lepton number conservation. On first look, it seems to indicate that $\nu \neq \nu^c$ and thus that neutrinos cannot be Majorana particles. However, one has to take into account that neutrinos interact solely weakly. Weak interactions violate parity maximally, i.e., they treat particles of contrasting chirality differently. Thus, the latter two interactions are forbidden due to the different chiralities of $\nu_e = P_L \nu_e$ and $\nu_e^c = P_R \nu_e^c$. This is also called chiral prohibition [12]. Thus, current experimental findings cannot rule out neutrinos being Majorana particles.
On the theory side however, a fundamental neutrino Majorana mass term is forbidden within the Standard Model framework. We can see this by taking a look at how such a term transforms under the Standard Models symmetries. Neutrinos are color singlets and as such do nott transform under the $SU(3)_C$ part of the Standard Model gauge group. Hence, we only need to consider $SU(2)_L \times U(1)_Y$.
Being part of a $SU(2)_L$ doublet, neutrinos have a weak isospin $I_3 = +1/2$. Knowing that neutrinos are electrically neutral we can use Eq. (2.8) to infer that they have a hypercharge of $Y = -1$. Under a general gauge transformation U with

$$\Psi \longrightarrow U\Psi \tag{2.35}$$

a Majorana mass term transforms as

$$\frac{m}{2}\Psi^T C\Psi \longrightarrow \frac{m}{2}\Psi^T U^T C U\Psi = \frac{m}{2}\Psi^T U^T U C\Psi \,, \tag{2.36}$$

[5] Before EWSB they have a non-zero hypercharge and thus cannot be considered neutral.

where except for $O(N)$ symmetries and especially for $U(1)$ symmetries we have

$$U^T U \neq 1. \tag{2.37}$$

While one can regain $SU(2)$ invariance by inserting $i\tau_2$ and rewriting the mass term as

$$\frac{m}{2}\Psi^T C i\tau_2 \Psi \xrightarrow{U\in SU(2)_L} \frac{m}{2}\Psi^T C U^T i\tau_2 U\Psi = \frac{m}{2}\Psi^T C i\tau_2 \Psi, \tag{2.38}$$

which follows from

$$\tau_2\tau_i\tau_2 = -\tau_i, \tag{2.39}$$

something similar cannot be achieved for a $U(1)$ symmetry. It follows that **a fundamental Majorana mass term can only be formed out of fermion fields which are not charged under any $U(1)$ symmetry**. However, as we can see by looking at the expected Dirac mass terms of the other Standard Model fermions

$$m\overline{\Psi_R}\Psi_L + h.c. \xrightarrow{U\in SU(2)_L} m\overline{\Psi_R}U\Psi_L + h.c., \tag{2.40}$$

the above argument alone is not sufficient to prove that neutrinos are massless within the Standard Model. The reason for this is that also fundamental Dirac mass terms for the remaining massive fermions are forbidden within the Standard Model framework as they are not invariant under the relevant gauge transformations due to the parity violating property of the $SU(2)_L$ symmetry.[6] Hence, we need to discuss the mechanism that generates masses for the remaining Standard Model fermions.

2.1.4. Higgs Mechanism - Generating Fermion Masses via spontaneous Symmetry Breaking

The "problem" of explaining non-zero fermion masses (see Table 2.2) without having explicit fundamental fermion mass terms is solved by the mechanism of spontaneous symmetry breaking (Higgs Mechanism) [9] via the introduction of a complex scalar $SU(2)_L$ doublet

$$\Phi = \begin{pmatrix}\Phi^+\\ \Phi^0\end{pmatrix} \tag{2.41}$$

with a hypercharge $Y = +1$. This scalar doublet couples to the Standard Model fermions via Yukawa interaction terms

$$\mathcal{L}_Y = \sum_{\alpha\beta}\left\{Y^L_{\alpha\beta}\overline{L}_\alpha\Phi l_{R,\beta} + Y^{Q,d}_{\alpha\beta}\overline{Q}_\alpha\Phi d_{R,\beta} + Y^{Q,u}_{\alpha\beta}\overline{Q}_\alpha\tilde{\Phi}u_{R,\beta}\right\} + h.c. \tag{2.42}$$

[6] Actually the fundamental Dirac mass terms formed out of Standard Model fermion fields are also not invariant under the $U(1)_Y$ part of the gauge group, but one non-invariance alone is already sufficient to prove the point.

with

$$\tilde{\Phi} = i\tau_2 \Phi^* \tag{2.43}$$

and the quark doublets

$$Q_i = \begin{pmatrix} u_i \\ d_i \end{pmatrix}. \tag{2.44}$$

The sums are taken over all three fermion generations and $Y^X_{\alpha\beta}$ are the Yukawa coupling matrices.[7] The Higgs potential can be written as

$$V(\Phi) = \mu^2 \Phi^\dagger \Phi + \lambda \left(\Phi^\dagger \Phi\right)^2, \tag{2.45}$$

which has a minimum at

$$\Phi^\dagger \Phi = \frac{v^2}{2}, \tag{2.46}$$

with

$$v = \sqrt{\frac{-\mu^2}{\lambda}} \sim 246\,\mathrm{GeV}. \tag{2.47}$$

We can rewrite Φ as

$$\Phi(x) = \exp\left\{ \frac{i}{2v} \vec{\zeta}(x) \vec{\tau} \right\} \begin{pmatrix} 0 \\ \frac{v+H(x)}{\sqrt{2}} \end{pmatrix} \tag{2.48}$$

where $H(x)$ represents the physical Higgs field as excitation from the vacuum state. The $\zeta(x)$ fields are redundant and do not represent any physical particle as they can be rotated away by a gauge transformation given in Eq. (2.5) with

$$\vec{\theta}(x) = \frac{\vec{\zeta}}{v}, \tag{2.49}$$

such that we end up with Dirac fermion mass terms given by the Yukawa interaction Lagrangian

$$\mathcal{L}_Y = \frac{v}{\sqrt{2}} \sum_{\alpha\beta} \left\{ Y^L_{\alpha\beta} \overline{L}_\alpha l_{R,\beta} + Y^{Q,d}_{\alpha\beta} \overline{Q}_\alpha d_{R,\beta} + Y^{Q,u}_{\alpha\beta} \overline{Q}_\alpha u_{R,\beta} \right\} + h.c.. \tag{2.50}$$

After diagonalizing the above terms the fermion masses are determined by the corresponding Yukawa coupling Y_f and the VEV v

$$m_f = \frac{v}{\sqrt{2}} Y_f. \tag{2.51}$$

[7] Note that again there is only one Yukawa term for the leptonic part of the Standard Model due to the lack of right-handed neutrino singlets.

Obviously, we cannot generate a Dirac mass term for neutrinos via this mechanism because we still lack a right-handed neutrino. We will discuss the possibility of adding right-handed neutrinos to the Standard Model in Sec. 2.3.
Can we use the newly introduced Higgs field to generate a Majorana mass term? The answer to this question is no as well. The reason still being the necessity for gauge invariance. To generate a gauge invariant Majorana mass term via a similar mechanism we need a scalar field Δ which must satisfy 2 conditions:

1. It must posses a hypercharge $Y = 2$ to cancel the hypercharge of the two neutrino fields and make the mass term invariant under $U(1)_Y$ transformations.

2. It must have a neutral component which can gain a VEV, i.e., it must be at least part of an SU(2) triplet to fulfill condition 1.

The only scalar particle within the Standard Model is the Higgs particle which itself does not fulfill the above requirements. However, we can combine two Higgs fields to get a $SU(2)_L$ triplet scalar operator [12]

$$\Delta_{\text{Higgs}} := \Phi^T i\tau_2 \vec{\tau} \Phi \tag{2.52}$$

which we can use to write down a gauge invariant neutrino Majorana mass term

$$\begin{aligned} -\mathcal{L}_{m_\nu} &= \frac{Y^\nu_{\alpha\beta}}{\Lambda} \left(L^T_\alpha C i\tau_2 \vec{\tau} L_\beta\right) \left(\Phi^T i\tau_2 \vec{\tau} \Phi\right) \\ &= \frac{Y^\nu_{\alpha\beta}}{\Lambda} \left(L^T_\alpha C i\tau_2 \Phi\right) \left(\tilde{\Phi}^\dagger L_\beta\right), \end{aligned} \tag{2.53}$$

where Λ is some mass scale, which we have to include to keep the dimension of the Lagrangian at 4. The above operator is known as the Weinberg operator [13]. It generates neutrino Majorana masses, is completely invariant under the Standard Models gauge group and additionally only contains Standard Model fields. However, as its field content is 5 dimensional, it is non-renormalizable. As such, it cannot be a fundamental term, but has to arise from a more fundamental UV complete model treating the Standard Model as a non-renormalizable effective field theory (EFT) with a strict UV-cutoff. Within such an EFT approach Λ resembles the new physics mass scale at which the Weinberg operator is generated after integrating out the heavy new physics components. We will focus more on EFTs in Section 3.4.1. After electroweak symmetry breaking, i.e., after the neutral component of the Higgs field acquires its non-zero vacuum expectation value (VEV) v, the neutrino mass term generated by the Weinberg operator is given by

$$-\mathcal{L}_{m_\nu} = Y^\nu_{\alpha\beta} \frac{v^2}{2\Lambda} \nu^T_{L\,\alpha} C \nu_{L\beta}. \tag{2.54}$$

That is, the neutrino mass is given by

$$m_\nu = Y^\nu_{\alpha\beta} \frac{v^2}{\Lambda}. \tag{2.55}$$

We see that it is suppressed by a factor of v^2/Λ which for large Λ could explain the smallness of the observed neutrino masses. Interestingly, when treating the Standard Model as effective field theory, the Weinberg operator is the only dimension-5 operator that can be formed out of Standard Model fields.

2.2. Neutrino Oscillation

2.2.1. Standard Derivation of Neutrino Oscillation

While we see that within the Standard Model neutrinos are massless, the observation of neutrino oscillations [3, 4] is generally accepted to prove the opposite as it necessitates non-zero mass differences between the different neutrino generations. To show this, we will now go trough the standard derivation of the neutrino vacuum oscillation probability $P_{\nu_\alpha \to \nu_\beta}$ following [9] using the plane-wave assumption. It should be noted that assuming plane waves is actually inconsistent. While plane waves have the nice feature of having a well defined momentum, they are completely delocalized in space making it impossible to define a baseline L between the points of neutrino production and detection. Hence, for a consistent derivation one should treat the propagating neutrinos as wave-packets [14]. Nevertheless, using this approach one finds the correct leading order oscillation probability and additionally the basic idea behind the phenomenon of neutrino oscillation remains the same in both treatments. Therefore, the simpler plane wave derivation is sufficient for us.
Generally speaking, the interaction and the Hamiltonian eigenstates of a particle are not necessarily identical, but can be related via a base transformation given by a unitary matrix U. A famous example is the quark sector in which the weak eigenstates and the Hamiltonian eigenstates are related by the so-called CKM matrix (Cabbibo-Kobayashi-Maskawa) [15, 16]. In such a case we can write

$$|\nu_\alpha\rangle = \sum_i U^*_{\alpha i} |\nu_i\rangle \tag{2.56}$$

and vice versa

$$|\nu_i\rangle = \sum_\alpha U_{\alpha i} |\nu_\alpha\rangle \tag{2.57}$$

where $|\nu_\alpha\rangle$ are the flavor eigenstates and $|\nu_i\rangle$ are the eigenstates of the Hamiltonian. Both form a orthonormal basis, i.e.,

$$\langle \nu_\alpha | \nu_\beta \rangle = \delta_{\alpha\beta} \qquad \langle \nu_i | \nu_j \rangle = \delta_{ij}. \tag{2.58}$$

The time evolution of a free field is governed by Schrödinger's equation

$$i\frac{d}{dt} |\nu_i(t)\rangle = \mathcal{H} |\nu_i(t)\rangle \tag{2.59}$$

and similarly spatial translation is given by

$$-i\nabla \left|\nu_i(\vec{x})\right\rangle = \hat{p} \left|\nu_i(\vec{x})\right\rangle , \tag{2.60}$$

which results in a plane-wave description

$$\left|\nu_i(x,t)\right\rangle = \exp\{-iE_i t + i\vec{p_i}\cdot\vec{x}\} \left|\nu_i\right\rangle . \tag{2.61}$$

Hence, we can infer the evolution of a flavor state

$$\begin{aligned} \left|\nu_\alpha\right\rangle (t,\vec{x}) &= \sum_i U^*_{\alpha i} \exp\{-iE_i t + i\vec{p_i}\cdot\vec{x}\} \left|\nu_i\right\rangle \\ &= \sum_i \left[U^*_{\alpha i} \exp\{-iE_i t + i\vec{p_i}\cdot\vec{x}\} \left(\sum_\beta U_{\beta i} \left|\nu_\beta\right\rangle \right) \right] , \end{aligned} \tag{2.62}$$

with

$$\left|\nu_\alpha(t=0,\vec{x}=0)\right\rangle = \left|\nu_\alpha\right\rangle . \tag{2.63}$$

We can see that for $t \neq 0$ and $\vec{x} \neq 0$ the initial pure flavor state ν_α has transitioned into a state $\nu_\alpha(t,\vec{x})$ which is given by a superposition of pure flavor eigenstates.
To get the transition probability $P_{\nu_\alpha \to \nu_\beta}$ we have to compute the transition amplitude

$$A_{\nu_\alpha \to \nu_\beta}(t,\vec{x}) = \langle \nu_\beta | \nu_\alpha(t,\vec{x}) \rangle = \sum_i U^*_{\alpha i} U_{\beta i} \exp\{-iE_i t + i\vec{p_i}\cdot\vec{x}\}. \tag{2.64}$$

Assuming that all $\vec{p_i}$ are parallel to each other, we can take

$$\vec{p_i}\cdot\vec{x} = |\vec{p_i}| \cdot L \tag{2.65}$$

and for $|\vec{p_i}| \gg m_i$, we can approximate

$$t = L, \tag{2.66}$$

and

$$E_i = \sqrt{\vec{p_i}^2 + m^2} = |\vec{p_i}| + \frac{m_i^2}{2|\vec{p_i}|} + \mathcal{O}\left[\left(\frac{m_i^2}{|\vec{p_i}|} \right)^2 \right] . \tag{2.67}$$

Using this, the transition amplitude simplifies into

$$\begin{aligned} A_{\nu_\alpha \to \nu_\beta}(t,\vec{x}) = \langle \nu_\beta | \nu_\alpha(t,\vec{x}) \rangle &= \sum_i U^*_{\alpha i} U_{\beta i} \exp\{-i(E_i - p_i)L\} \\ &= \sum_i U^*_{\alpha i} U_{\beta i} \exp\left\{ -i \frac{m_i^2}{2|p_i|} L \right\}. \end{aligned} \tag{2.68}$$

	Normal Hierarchy	Inverted Hierarchy
Δm^2_{21}	$(7.53 \pm 0.18) \times 10^{-5}\,\mathrm{eV}^2$	$(7.53 \pm 0.18) \times 10^{-5}\,\mathrm{eV}^2$
Δm^2_{32}	$(2.453 \pm 0.034) \times 10^{-3}\,\mathrm{eV}^2$	$\left(-2.546^{+0.034}_{-0.040}\right) \times 10^{-3}\,\mathrm{eV}^2$
$\sin\theta_{12}$	0.307 ± 0.013	0.307 ± 0.013
$\sin\theta_{23}$	0.545 ± 0.021	0.547 ± 0.021
$\sin\theta_{13}$	$(2.18 \pm 0.08) \times 10^{-2}$	$(2.18 \pm 0.08) \times 10^{-2}$

Table 2.3.: Neutrino mixing parameters [10] for the normal ($\Delta m^2_{32} > 0$) and inverted ($\Delta m^2_{32} < 0$) mass hierarchy.

Thus, assuming $|p_i| = |p_j| \sim E$ we find

$$P_{\nu_\alpha \to \nu_\beta}(t) = |A_{\nu_\alpha \to \nu_\beta}(t)|^2 = \sum_{ij} U^*_{\alpha i} U_{\beta i} U_{\alpha j} U^*_{\beta j} \exp\left\{ -i \frac{\Delta m^2_{ij}}{2E} L \right\}. \tag{2.69}$$

with

$$\Delta m^2_{ij} = m^2_i - m^2_j. \tag{2.70}$$

Eq. (2.71) is often written as

$$P_{\nu_\alpha \to \nu_\beta}(t) = |A_{\nu_\alpha \to \nu_\beta}(t)|^2 = \sum_{ij} U^*_{\alpha i} U_{\beta i} U_{\alpha j} U^*_{\beta j} \exp\left\{ -2\pi i \frac{L}{L^{\mathrm{osc}}_{ij}} \right\}. \tag{2.71}$$

with the oscillation length

$$L^{\mathrm{osc}}_{ij} = \frac{4\pi E}{\Delta m^2_{ij}}. \tag{2.72}$$

Besides the already mentioned caveats about the plane-wave treatment one should note that we ignored any effects coming from the production and detection processes. Within a complete treatment these should be included [14, 9]. Due to the unitarity condition we have

$$\sum_i U^*_{\alpha i} U_{\beta i} = \delta_{\alpha\beta}. \tag{2.73}$$

Hence, the vacuum oscillation probability $P_{\nu_\alpha \to \nu_\beta}$ for $\alpha \neq \beta$ is non-zero only if at least one Δm^2_{ij} is non-zero. Thus, **the observation of neutrino oscillations provides evidence for the existence of non-zero neutrino masses and therefore new physics beyond the Standard Model**. The mixing matrix U is usually referred to as the Pontecorvo-Maki-Nakagawa-Sakata matrix U_{PMNS}. It can be parameterized as [17, 9]

$$U_{PMNS} = \begin{pmatrix} c_{12}c_{13} & s_{12}c_{13} & s_{13}e^{-i\delta_{cp}} \\ -s_{12}c_{23} - c_{12}s_{23}s_{13}e^{i\delta_{cp}} & c_{12}c_{23} - s_{12}s_{23}s_{13}e^{i\delta_{cp}} & s_{23}c_{13} \\ s_{12}s_{23} - c_{13}c_{23}s_{13}e^{i\delta_{cp}} & -c_{12}s_{23} - s_{12}c_{23}s_{13}e^{i\delta_{cp}} & \end{pmatrix} \cdot U_M \tag{2.74}$$

with

$$U_M = \mathrm{diag}\left(1, e^{i\alpha_1}, e^{i\alpha_2}\right) \tag{2.75}$$

where δ_{CP} is a CP violating phase, $\alpha_{1,2}$ are the two Majorana phases which vanish for Dirac neutrinos and we used the abbreviation $\sin\theta_{ij} = s_{ij}$ and $\cos\theta_{ij} = c_{ij}$. The current experimental values measured in oscillation experiments are shown in Table 2.3. Albeit tiny, the measured mass differences are non-zero. Note that the sign of Δm^2_{32} is currently unknown such that two different mass hierarchies the normal hierarchy (NH) $m_1 < m_2 < m_3$ and inverted hierarchy (IH) $m_3 < m_1 < m_2$ can be realized in nature.
The experimental fact of non-vanishing neutrino masses reintroduces the question about the nature of the neutrinos, i.e., Dirac vs. Majorana.

2.3. Generating Neutrino Masses Beyond the Standard Model - The Seesaw Mechanisms

Now that we know that neutrinos are massive, we want to discuss possible extensions to the Standard Model which generate small neutrino masses by following the lectures of [12]. There are countless models which can generate small neutrino masses either at tree-level or radiatively, see e.g. [18] and references therein. The most commonly studied Standard Model extensions which generate the dimension-5 Weinberg operator at tree-level are the so-called seesaw mechanisms depicted in Figure 2.1.
Ignoring gauge invariance or any other constraints, let us first take a look at the most general neutrino mass term for 3 generations of left-handed neutrinos $\nu_{L,i}$ and three generations of right-handed neutrinos $N_{R,i}$. In this case the mass term consists of both Dirac and Majorana mass terms

$$\begin{aligned} -\mathcal{L}_m =& \overline{\nu_L}_{,i} \left(M^D_{ij}\right)^* N_{R,j} \\ &+ \frac{1}{2} \nu^T_{L,i} C M^L_{ij} \nu_{L,j} \\ &+ \frac{1}{2} N^T_{R,i} C \left(M^R_{ij}\right)^* N_{R,j} + h.c., \end{aligned} \tag{2.76}$$

where $M^{D,R,L}$ in general each are complex 3×3 matrices. Additionally, M^L and M^R are symmetric. We can summarize the whole mass term within one Majorana like term

$$-\mathcal{L}_m = \frac{1}{2} n^T_L C \mathcal{M} n_L + h.c. \tag{2.77}$$

with

$$n_L = \begin{pmatrix} \nu_L \\ (N_R)^c \end{pmatrix}, \tag{2.78}$$

where $\nu_L = (\nu_{L\,1}, \nu_{L\,2}, \nu_{L\,3})^T$, $N_R = (N_{R\,1}, N_{R\,2}, N_{R\,3})^T$ and

$$\mathcal{M} = \begin{pmatrix} M^L & M^D \\ M^{D\,T} & M^R \end{pmatrix} \tag{2.79}$$

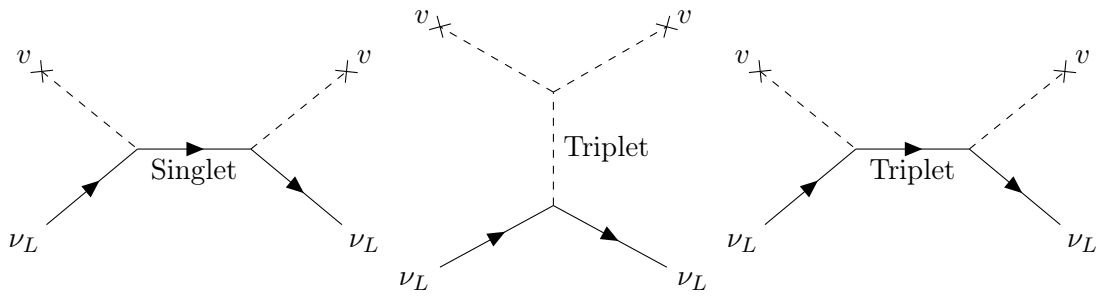

Figure 2.1.: Feynman diagrams of the three standard seesaw models which generate the dimension-5 Weinberg operator.

by noticing that

$$\begin{aligned}
&\frac{1}{2}n_L^T C\mathcal{M}n_L + h.c. \\
=&\frac{1}{2}\nu_L^T C M^L + \frac{1}{2}\overline{N_R}M^R(N_R)^c \\
&+\frac{1}{2}\left(\nu_L^T C M^D\,(N_R)^c + \overline{N_R}\left(M^D\right)^T\nu_L\right) + h.c. \\
=&\frac{1}{2}\nu_L^T C M^L + \frac{1}{2}\overline{N_R}M^R(N_R)^c + \overline{N_R}\left(M^D\right)^T\nu_L + h.c. \\
=&\frac{1}{2}\nu_L^T C M^L + \frac{1}{2}N_R^T C\left(M^R\right)^* N_R + \overline{\nu_L}\left(M^D\right)^* N_R + h.c. \\
=&-\mathcal{L}_m
\end{aligned} \tag{2.80}$$

where we used

$$\begin{aligned}
\nu_L^T C M^D\,(N_R)^c &= \left[\nu_L^T C M^D C\overline{N_R}^T\right]^T \\
&= -\overline{N_R}C^T C^T\left(M^D\right)^T\nu_L \\
&= \overline{N_R}\left(M^D\right)^T\nu_L
\end{aligned} \tag{2.81}$$

with $C^T = C^{-1} = -C$, and

$$\overline{N_R}M^R\,(N_R)^c = \left[(N_R)^c\,M^R N_R\right]^\dagger \tag{2.82}$$

$$\overline{N_R}\left(M^D\right)^T\nu_L = \left[\overline{\nu_L}\left(M^D\right)^* N_R\right]^\dagger. \tag{2.83}$$

One can block diagonalize the mass matrix $\mathcal{M}$ using a base transformation

$$-\mathcal{L}_m \longrightarrow \frac{1}{2}\chi_L^T C\mathcal{M}_{\text{diag}}\chi_L \tag{2.84}$$

with

$$n_L = U\chi_L \tag{2.85}$$

$$\mathcal{M} \longrightarrow \mathcal{M}_{\text{diag}} = U^T \mathcal{M} U = \begin{pmatrix} \tilde{M}_L & 0 \\ 0 & \tilde{M}_R \end{pmatrix}, \tag{2.86}$$

where $\tilde{M}_L$ and $\tilde{M}_R$ are complex 3×3 matrices. That is, up to corrections of order $\left(M^D \cdot (M^R)^{-1}\right)^2$ and $M^L \cdot (M^R)^{-1}$ we have

$$\tilde{M}_L \simeq M^L - M^D \left(M^R\right)^{-1} \left(M^D\right)^T, \qquad \tilde{M}_R \simeq M^R \tag{2.87}$$

The mixing matrix can be approximated as

$$U \simeq \begin{pmatrix} 1 & \rho \\ -\rho^\dagger & 1 \end{pmatrix} \tag{2.88}$$

with

$$\rho \simeq M^D \left(M^R\right)^{-1}. \tag{2.89}$$

Thus, we see that for $M^R \gg M^D$ the base transformation U is almost unity such that ν_L and N_R hardly mix. Thus, in this case $\tilde{M}_L$ describes 3 light neutrino fields which mostly consist out of the Standard Model neutrino fields ν_L, while $\tilde{M}_R$ describes 3 heavy neutrino states which mostly consist out of the right-handed neutrino fields N_R not present in the Standard Model.
The aim of the different seesaw mechanisms is to each generate at least one of the three possible mass matrices M^D, M^L and M^R. Before we go on looking at the specific models, we want to stress that although we started out with the most general mass term which consists of both Dirac and Majorana, we end up with having solely Majorana mass terms after block diagonalization. This general result implies that **the appearance of a Majorana mass term implies that the massive fields are Majorana too**. Or in other words: The only possibility to have Dirac particles is to forbid any Majorana mass term that could appear.

2.3.1. Seesaw Type I

The seesaw type I mechanism represents probably the most obvious Standard Model extension one can think of to generate neutrino masses. We simply add three right-handed neutrino singlets N_R (1,0) to the Standard Models particle content.[8] This enables us to write down a Dirac neutrino mass term

$$-\mathcal{L}_{M^D} = Y^\nu_{\alpha\beta} \overline{L}_\alpha \tilde{\Phi} N_R, \tag{2.90}$$

[8] In principle we can also add any other number. However, one needs at least two in order to generate the observed mass splitting.

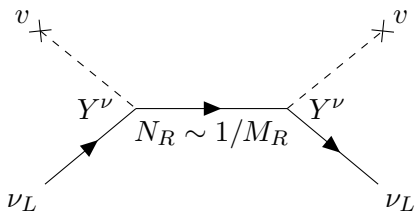

Type I $\sim Y^\nu \frac{v^2}{M_R} Y^\nu$

Figure 2.2.: Seesaw type I mechanism. From the Feynman diagram of the dim 5 Weinberg operator one can intuitively infer the resulting light neutrino masses.

where after EWSB

$$\tilde{\Phi} \longrightarrow \frac{1}{\sqrt{2}} \begin{pmatrix} v \\ 0 \end{pmatrix} + \mathcal{O}(H), \tag{2.91}$$

we have

$$\left(M^D\right)^* = Y^\nu \frac{v}{\sqrt{2}}. \tag{2.92}$$

Additionally, due to N_R being a total Standard Model singlet we can write down a fundamental right-handed Majorana mass term

$$-\mathcal{L}_{M^R} = N_{R,i}^T C M_{ij}^R N_{R,j}. \tag{2.93}$$

Here, M^R is a new fundamental mass scale. Thus, we can see that the small change of introducing right-handed neutrinos to the Standard Model is no simple addition but it changes the general structure of the model which previously only depended on one single mass scale v. Considering our previously introduced general neutrino mass matrix given in Eq. (2.79) we have $M^L = 0$ since in this model we do not have a possibility to generate a Majorana mass term for the left-handed neutrinos in a gauge invariant way. Therefore, we have

$$\mathcal{M} = \begin{pmatrix} 0 & M^D \\ \left(M^D\right)^T & M^R \end{pmatrix} \tag{2.94}$$

and

$$\mathcal{M}_{\text{diag}} = \begin{pmatrix} \tilde{M}_L & 0 \\ 0 & \tilde{M}_R \end{pmatrix} \tag{2.95}$$

with

$$\tilde{M}_L \simeq -M^D \left(M^R\right)^{-1} \left(M^D\right)^T \tag{2.96}$$

$$\tilde{M}_R \simeq M^R. \tag{2.97}$$

It should be noted that the minus sign in $\tilde{M}^L$ has no physical consequences as it can be rotated away. As we noted earlier M^R is a fundamental mass scale which can have any arbitrary values. Thus, for large M^R, $\tilde{M}_L$ is suppressed by a factor of v^2/M_R and we end up with the observed light neutrinos.
A very important point we see is that the simple introduction of a right-handed neutrino singlet N_R, which is necessary to generate a Dirac mass term, also implies the existence of a right-handed Majorana mass term. That is, **when trying the simplest approach to generate light Dirac neutrino masses, we actually end up with massive Majorana neutrinos**. This is a strong motivation towards searching for lepton number violation in the neutrino sector.

2.4. Further Motivations

We have seen in the previous sections, that the most simple Standard Model extensions which generate light neutrino masses result in neutrinos being Majorana particles. In fact, the simple introduction of a right-handed neutrino singlet, which is necessary to generate Dirac masses, will inevitably generate a Majorana mass term for the right-handed neutrino fields. Afterwards, this will generate massive Majorana neutrinos via mixing. One can try to avoid this by extending the model and, e.g., promoting the Standard Models global $U(1)_L$ lepton number symmetry to a local gauge symmetry. Usually instead of $U(1)_L$ one would promote $U(1)_{B-L}$ to a gauge symmetry because lepton number is actually broken already in the Standard Model via non-perturbative so-called *sphaleron* processes [19] while $B-L$ is a Standard Model symmetry even at the non-perturbative level. However, in both cases the introduction of another local $U(1)_L$ or $U(1)_{B-L}$ symmetry will result in the existence of an additional massless gauge boson associated to it and corresponding long-range interactions between leptons. Such interactions are so far not observed in nature. Therefore, to avoid experimental constraints one has to either make the gauge coupling to almost vanish or one could spontaneously break the symmetry through a Higgs like mechanism. The first approach would just swap the problem of explaining small neutrino masses with the problem of explaining a small gauge coupling and hence introduce another fine-tuning like problem. The second approach of breaking the symmetry without reintroducing the right-handed Majorana mass term is only possible within more complex models [20, 21, 22]. Following this line, it is reasonable to assume that neutrinos might actually be Majorana particles. This is one of the main reasons to consider $0\nu\beta\beta$-decay.
Another reason to study $0\nu\beta\beta$ is that while a tree-level neutrino Majorana mass term is the most obvious way to generate $0\nu\beta\beta$-decay, there are actually many different effective lepton number violating operators that can trigger $0\nu\beta\beta$ as we will see in sections 3.3 and 3.4.2. Additional motivation comes from the observed baryon asymmetry of the universe (BAU) [23] which cannot be explained within the Standard Model itself. Instead, one of the most studied mechanism for explaining the observed BAU builds upon lepton number violation beyond the Standard Model in the first place. Such types of mechanisms are called Leptogenesis scenarios [5, 24] and they are another strong motivation to

search for lepton number violation in the neutrino sector. Finally, while the global $B-L$ symmetry forbids $0\nu\beta\beta$-decay within the Standard Model, it is widely expected that a full model of quantum gravity will not contain any global symmetries [25].[9]
Considering all points above, it is reasonable to assume that lepton number is not necessarily conserved. Accordingly, there is a strong motivation towards investigating whether lepton number is indeed a broken symmetry and if neutrinos are actually Majorana particles. In the next chapter we will introduce the basics of $0\nu\beta\beta$-decay and elaborate on how it tests different mechanisms of lepton number violation.

[9] Hence, we should consider that it may be broken at lower scales already.

3. $0\nu\beta\beta$ Theory

3.1. Introduction to double-β Decay

3.1.1. Origin of double-β-Decay

In this chapter we want to discuss and review the important features of $0\nu\beta\beta$-decay. Let us start by discussing the basics.
Within the standard β-decay a neutron (n) inside a nucleus (A, Z) with mass number A and nuclear charge Z transforms into a proton (p) releasing a single electron (e^-) and electron-anti-neutrino ($\overline{\nu}_e$)

$$(A, Z) \longrightarrow (A, Z+1) + e^- + \overline{\nu}_e. \tag{3.1}$$

Ignoring electron binding energies, such a decay can happen if the final state atom has a smaller mass than the initial state atom. The atomic mass is given by the mass of its constituents, i.e., the nucleons (neutrons and protons) the electron shell and the binding energy

$$M(A, Z) = Z(m_p + m_e) + (A - Z)m_n - B(A, Z). \tag{3.2}$$

If we ignore the electron shell for a moment, i.e., we only consider the nucleus, the above formula can be expressed in a parabolic form known as the semi-empirical nuclidic mass equation [26]

$$M(A, Z) = M_A + \frac{1}{2}B_A\left(Z - Z_A\right)^2 + P_A - S(N, Z) \tag{3.3}$$

with a shell correction term S and the pairing coefficient

$$P_A \propto \delta = \begin{cases} +1 & \text{odd-odd} \\ 0 & \text{even-odd} \\ -1 & \text{even-even} \end{cases} \tag{3.4}$$

which is the important part of the formula for our discussion. In Eq. (3.4) "even" and "odd" refer to the number of protons Z and neutrons $N = A - Z$. We see that while for odd mass numbers A the pairing coefficient vanishes and we end up with a single parabola, for even A one can find nuclei with both "even-even" and "odd-odd" structures, such that we have two separate mass parabolas. These are (ignoring the shell correction term) offset by $\Delta_P = 2P_A$. This structure is shown in Figure 3.1. In such a case it can happen that for even-even nuclei next to the minimum of the mass parabola the normal first order β-decay is prohibited due to the neighbouring odd-odd nucleus having

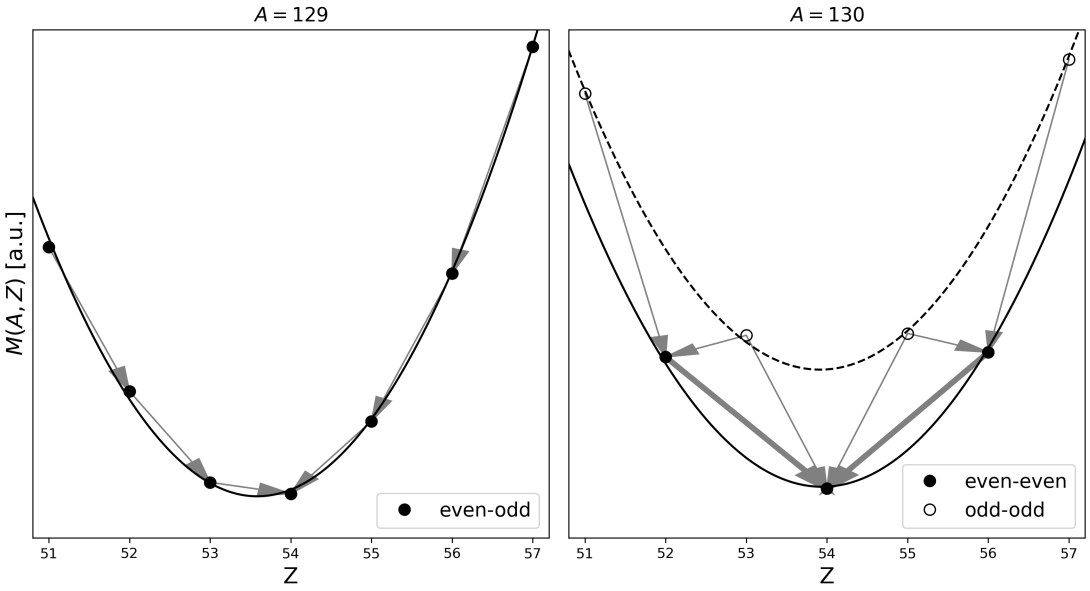

Figure 3.1.: Mass parabolas for even-even and odd-odd nuclei with $A = 130$ and even-odd nuclei with $A = 129$. The arrows represent the leading order decays. While for even-odd nuclei there is only one mass parabola, for even-even and odd-odd nuclei there is a mass split resulting in two parabolas. One can see that due to this mass gap for even-even nuclei close to the minimum of the mass parabola the single β-decay can be blocked due to the neighboring odd-odd nucleus having a higher mass. In such a case the leading order decay is a double-β-decay ($\beta\beta$) or double electron capture (ECEC).

a larger mass. If the standard single-β-decay is blocked in this way, the leading order decay will be a double-β-decay. There are 4 different double-β-decay modes that can be observed. All of them have a 2 neutrinos as well as a possible neutrinoless mode. While the Feynman diagrams for all of these modes are the same (if we ignore the rotation of lines by 180°) they do differ in the necessary mass difference between the mother and daughter atom $\Delta m = m_M - m_D$. This sets the threshold for the process and can suppress certain modes. We summarize all 4 modes below[1]:

1. $\beta^-\beta^-$**:**

$$(A, Z) \rightarrow (A, Z + 2) + 2e^-(+2\overline{\nu}_e) \tag{3.5}$$

$$\Delta m \overset{!}{>} 0 \tag{3.6}$$

[1]Note that we ignore the binding energy of captured electrons in ECβ^+ and ECEC, which are sub keV as well as the masses of the outgoing neutrinos which are expected to be sub eV.

2. $\beta^+\beta^+$**:**

$$(A, Z) \rightarrow (A, Z-2) + 2e^+(+2\nu_e) \tag{3.7}$$

$$\Delta m \overset{!}{>} 4m_e \tag{3.8}$$

3. **EC**β^+**:**

$$(A, Z) + e^- \rightarrow (A, Z-2) + e^+(+2\nu_e) \tag{3.9}$$

$$\Delta m \overset{!}{>} 2m_e \tag{3.10}$$

4. **ECEC:**

$$(A, Z) + 2e^- \rightarrow (A, Z-2)(+2\nu_e) \tag{3.11}$$

$$\Delta m \overset{!}{>} 0 \qquad 2\nu \text{ mode} \tag{3.12}$$

$$\Delta m \overset{!}{=} 0 \qquad 0\nu \text{ mode}^2 \tag{3.13}$$

Here, *EC* denotes electron capture. Note that in principle also the corresponding processes involving positron capture are possible. However, since positrons do not occur naturally inside atoms we will ignore this possibility. Also, every isotope that can decay via $2\nu\beta^+\beta^+$ or $2\nu\text{EC}\beta^+$ will also decay via 2νECEC and the former modes will be suppressed due to the smaller Q-value[3] which represents the released energy given by the summed kinetic energies of the outgoing leptons (electrons/positrons and neutrinos).
Considering the above requirements we find 69 natural elements that decay via at least one double-β mode (35 via $\beta^-\beta^-$ and 34 via ECEC). They are listed in Table 3.1. To find these we used the NIST list of isotopes [28]. While most elements on the list have more than one isotope listed there are two notable elements which both have 4 different naturally occurring isotopes that decay via some double-β mode namely Xe (124, 126, 134 and 136) and Cd (106, 108, 114, 116).

3.1.2. $0\nu\beta\beta$ as a Probe for Lepton Number Violation

The reason we want to study double-β-decay is that this process can be utilized to investigate the nature (Dirac vs. Majorana) of neutrinos as it probes lepton number violation in the neutrino sector. We can immediately see the reason behind this by looking at the Feynman diagram of the standard double-β-decay shown in Figure 3.2. The standard double-β-decay ($2\nu\beta\beta$) basically is just two separate β-decays happening at the same time with two outgoing anti-neutrinos. If, however, neutrinos have a Majorana mass term, neutrinos and anti-neutrinos are equal. Hence, we can connect the two neutrino lines in the left part of Figure 3.2 such that there are no outgoing neutrinos and we end up with the neutrinoless double-β-decay ($0\nu\beta\beta$) represented in the right part of

[3] This suppression does not necessarily hold for the neutrinoless modes.

$2\nu\beta^-\beta^-$		$2\nu\beta^+\beta^+$		$2\nu\mathrm{EC}\beta^+$		$2\nu\mathrm{ECEC}$	
${}^{A}Z$	Q [MeV]	${}^{A}Z$	Q [MeV]	${}^{A}Z$	Q [MeV]	${}^{A}Z$	Q [MeV]
^{46}Ca	0.988576	^{78}Kr	0.802333	^{50}Cr	0.146971	^{36}Ar	0.432581
^{48}Ca	4.266970	^{96}Ru	0.670499	^{58}Ni	0.904313	^{40}Ca	0.193508
^{70}Zn	0.997118	^{106}Cd	0.731391	^{64}Zn	0.072685	^{50}Cr	1.168969
^{76}Ge	2.039061	^{124}Xe	0.820255	^{74}Se	0.187243	^{54}Fe	0.679832
^{80}Se	0.133874	^{130}Ba	0.574761	^{78}Kr	1.824331	^{58}Ni	1.926311
^{82}Se	2.996402	^{136}Ce	0.334556	^{84}Sr	0.767749	^{64}Zn	1.094683
^{86}Kr	1.257542			^{92}Mo	0.629783	^{74}Se	1.209240
^{94}Zr	1.141919			^{96}Ru	1.692497	^{78}Kr	2.846329
^{96}Zr	3.348982			^{102}Pd	0.149915	^{84}Sr	1.789746
^{98}Mo	0.109935			^{106}Cd	1.753389	^{92}Mo	1.651781
^{100}Mo	3.034342			^{112}Sn	0.897811	^{96}Ru	2.714495
^{104}Ru	1.301297			^{120}Te	0.708411	^{102}Pd	1.171913
^{110}Pd	2.017234			^{124}Xe	1.842253	^{106}Cd	2.775387
^{114}Cd	0.542493			^{130}Ba	1.596759	^{108}Cd	0.271810
^{116}Cd	2.813438			^{136}Ce	1.356554	^{112}Sn	1.919809
^{122}Sn	0.372877			^{144}Sm	0.760416	^{120}Te	1.730409
^{124}Sn	2.291010			^{156}Dy	0.983975	^{124}Xe	2.864251
^{128}Te	0.866550			^{162}Er	0.824969	^{126}Xe	0.919757
^{130}Te	2.527515			^{168}Yb	0.387260	^{130}Ba	2.618757
^{134}Xe	0.825751			^{174}Hf	0.076886	^{132}Ba	0.843947
^{136}Xe	2.457984			^{184}Os	0.428879	^{136}Ce	2.378552
^{142}Ce	1.417175			^{190}Pt	0.362202	^{138}Ce	0.693032
^{146}Nd	0.070421					^{144}Sm	1.782414
^{148}Nd	1.928286					^{152}Gd	0.055703
^{150}Nd	3.371357					^{156}Dy	2.005973
^{154}Sm	1.250810					^{158}Dy	0.282802
^{160}Gd	1.730530					^{162}Er	1.846966
^{170}Er	0.655586					^{164}Er	0.025057
^{176}Yb	1.088730					^{168}Yb	1.409257
^{186}W	0.491643					^{174}Hf	1.098884
^{192}Os	0.408274					^{180}W	0.143264
^{198}Pt	1.049142					^{184}Os	1.450877
^{204}Hg	0.419154					^{190}Pt	1.384200
^{232}Th	0.837879					^{196}Hg	0.820190
^{238}U	1.144154						

Table 3.1.: Complete list of natural double-β elements and the corresponding Q-values calculated from the NIST list of elements [28] using the conditions 3.6, 3.8, 3.10 and 3.12. Overall there are 69 different natural elements that can decay via at least one double-β mode.

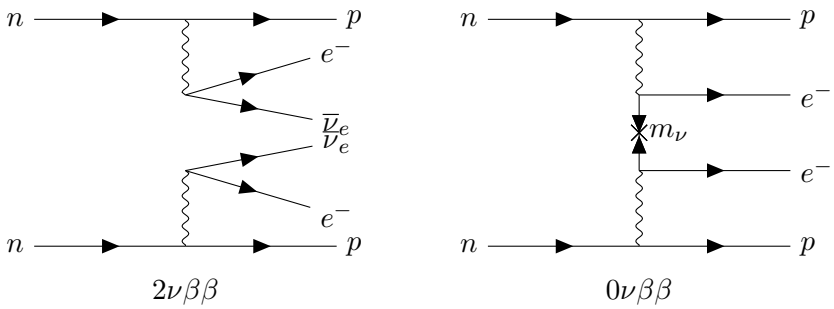

Figure 3.2.: Feynman diagrams of the standard two neutrino (left) and neutrinoless (right) double-β-decays.

Figure 3.2. One should note that this process includes a chirality flip, such that it cannot happen for massless neutrinos which can be described as either Dirac or Majorana. We will discuss this mechanism more detailed in Sec. 3.2 and see that the amplitude of this decay is proportional to the effective electron-neutrino Majorana mass. As we will see in Sec. 3.3 also other mechanisms of lepton number violation can be studied within $0\nu\beta\beta$ experiments.

3.1.3. Experimental Overview

Detecting $0\nu\beta\beta$

The $0\nu\beta\beta$-decay can be distinguished from its main background the $2\nu\beta\beta$-decay via a characteristic signature in the energy spectrum of the emitted electrons. While for $2\nu\beta\beta$

$$(A, Z) \longrightarrow (A, Z+2) + 2e^- + 2\overline{\nu}_e \tag{3.14}$$

the released energy is distributed among 4 outgoing particles[4] out of which only the two electrons can be detected within an experiment, for $0\nu\beta\beta$

$$(A, Z) \longrightarrow (A, Z+2) + 2e^- \tag{3.15}$$

the two outgoing electrons carry all of the released energy and hence have a fixed summed energy T_{sum}. Thus, by measuring the summed energy spectrum of the

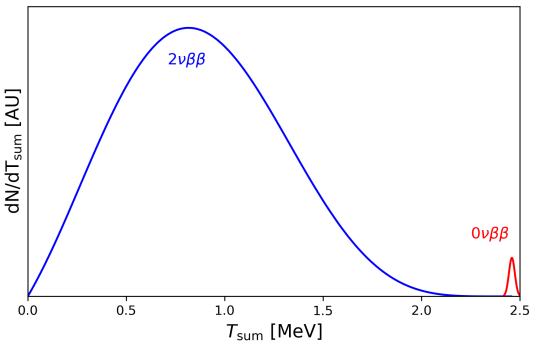

Figure 3.3.: Summed electron energy spectra of the $2\nu\beta\beta$ (blue) and $0\nu\beta\beta$-decays (red) in ^{136}Xe. The $2\nu\beta\beta$ spectrum was calculated in [29]. The width of the $0\nu\beta\beta$ Gauss peak is determined by the experimental accuracy. For the sake of readability the expected height of the $0\nu\beta\beta$ peak is highly exaggerated here.

[4]The kinetic recoil of the nucleus can be ignored due to the high mass compared to m_e.

released electrons one can experimentally distinguish $0\nu\beta\beta$ from $2\nu\beta\beta$. The expected spectra of the $2\nu\beta\beta$ and $0\nu\beta\beta$ modes are shown in Figure 3.3. It is important to note that while one would expect the $0\nu\beta\beta$ mode to have a fixed delta-like spectrum, in reality the experimental uncertainties will smear this into a Gaussian distribution where the width is determined by the accuracy of the experiment. This fact shows the importance of a good energy resolution at the end point of the spectrum to minimize the number of background events coming from the $2\nu\beta\beta$ mode.
Next, we want to give a brief overview covering the experimental efforts towards $0\nu\beta\beta$. These are nicely summarized and explained in [30, 31] which we will refer to. One can distinguish between different types of experiments:

Semiconductors

Semiconductor experiments like GERDA [32] or the MAJORANA DEMONSTRATOR [33] utilize highly enriched high-purity ^{76}Ge (HPGe) diodes. They are able to detect $0\nu\beta\beta$ events by measuring the summed electron spectrum of the decaying ^{76}Ge. HPGe experiments have some notable advantageous properties for being used as a $0\nu\beta\beta$ probe. They can reach a very high energy resolution of $\sim 0.1\%$ [34] at the end point of the $2\nu\beta\beta$ spectrum such that it is possible to reduces the background events which originate from the $0\nu\beta\beta$-decay accompanying $2\nu\beta\beta$-decay. Additionally, they come with a very low intrinsic background. However, they cannot measure the two emitted electrons separately such that neither angular information nor information on the single electron spectra can be recovered from the experimental data.
While GERDA and MAJORANA operate with $\sim 40\,\mathrm{kg}$ and $\sim 30\,\mathrm{kg}$ of highly enriched ^{76}Ge a next-generation ton scale experiment the *Large Enriched Germanium Experiment for Neutrinoless Double beta decay* (LEGEND) [35] will combine the efforts of both previous experiments. LEGEND will reach a sensitivity on the $0\nu\beta\beta$ half-life of $10^{28}\,\mathrm{y}$.

Time Projection Chambers

Time Projection Chamber (TPC) experiments are another favourable technology for the search of $0\nu\beta\beta$. TPC $0\nu\beta\beta$ experiments typically employ (enriched) ^{136}Xe in a gaseous, liquid or dual phase chamber. While the latter are usually used as dark matter searching tools, the first two are used in dedicated $0\nu\beta\beta$ experiments. Within the TPC, decay events generate two different detector signals via ionization and szintillation. These can be used for improved particle discrimination, to locate the event and of course to determine the energy of the emitted electrons. Although one would think that a gaseous TPCs could provide information on the individual electron tracks this is not possible due to the high density of ^{136}Xe within the high-pressure TPCs usually used. Therefore, again only the summed electron energy is measured to identify $0\nu\beta\beta$ events. Examples of experiments that will employ single-phase gaseous-xenon TPCs are the *Particle and Astrophysical Xenon Experiment III* (PandaX-III) [36] which will employ 140 kg of 90%-enriched ^{136}Xe in a high-pressure TPC as well as the *Neutrino Experiment with a Xenon TPC* (NEXT) [37]. These single-phase high-pressure gas TPCs can also reach very high

energy resolutions of $\sim 0.5\%$ [38]. An experimental project that employs liquid-phase TPCs is the *Enriched Xenon Observatory* (EXO) [39] and its planned ton-scale upgrade nEXO [40].
With the first detection of double electron capture in ^{124}Xe [41] which at this point represented the process with the longest half-life ever detected, the XENON collaboration proofed that dual-phase dark matter experiments that are not dedicated directly towards $0\nu\beta\beta$ can indeed provide competitive results for nuclear decay measurements. The future DARWIN experiment [42] will in fact reach sensitivities similar to LEGEND and nEXO even without isotopic enrichement.

Scintillators

There are two types of scintillators used in $0\nu\beta\beta$ experiments. Organic scintillators that are loaded with a $0\nu\beta\beta$-decaying isotope and inorganic scintillator crystals which are build from some chemical compound that contains a $0\nu\beta\beta$ isotope. Examples for the prior are the SNO+ [43] and the KamLAND-Zen [44] experiments searching for $0\nu\beta\beta$ in ^{130}Te and ^{136}Xe, respectively. The main advantage of organic scintillators is the scalability of experiments beyond the ton-scale. However, solar neutrino interactions with electrons in the scintillator atoms induce an additional background. On the other side the *CAlcium fluoride for the study of Neutrinos and Dark matters by Low Energy Spectrometer III* (CANDLES III) [45] experiment utlizes CaF_2 crystal scintillators to search for $0\nu\beta\beta$-decay in ^{48}Ca which out of all naturally occuring double-β isotopes has the highes Q-value.

Bolometers

Bolometers [46] are croygenic calorimeter experiments which typically work at temperatures of $\sim 10\,\mathrm{mK}$. They detect individual decay events via the induced temperature increase which are of $\mathcal{O}(0.1\,\mathrm{mK/MeV})$. To be able to detect such minimal changes in temperature, extremely precise thermometers are necessary. Again, the $0\nu\beta\beta$ isotopes usually come within a crystalline compound. Bolometer experiments have the high advantage of a very precise energy resolution. However, scalability is challenging although not impossible as it is hard to work at such low temperatures. Examples of bolometric experiments are the *Cryogenic Underground Observatory for Rare Events* (CUORE) [47] and its future ton-scale upgrade CUPID [48].

Tracking Calorimeters

Tracking calorimeters are an exciting addition to the other experimental efforts as they are currently the only type of experiment that can gain information on the individual electron tracks in double-β-decays. As such they can give insight into additonal phase-space observables such as angular correlations and the single electron spectra and thereby can help to distinguish different $0\nu\beta\beta$ mechanisms. To achieve this, they us foils of $0\nu\beta\beta$ isotopes that are surrounded by the detector which consists of a tracker module and surrounding calorimeter walls. The only experiments currently using this technology are

NEMO-3 [49] and its next generation successor SuperNEMO [49, 50]. Further advantages of this detector design are the possiblity to employ different $0\nu\beta\beta$ isotopes by switching the foils and a good background discrimination. However, scalability is again not very easy to achieve and the energy resolution is only in the range of $\sim 4\%$ [31].

3.2. Theory of the Standard $0\nu\beta\beta$ Mechanism

The most studied mechanism of $0\nu\beta\beta$ is the mechanism of light Majorana neutrino exchange. We now want to derive the expected $0\nu\beta\beta$-decay rate in this case. In principle the decay rate Γ of a particle which decays from an initial state i into a final state f can be interpreted as the decay probability P per time T. Hence, we can define the differential decay rate as [51]

$$\mathrm{d}\Gamma = \frac{1}{T}\mathrm{d}P. \tag{3.16}$$

The decay probability is given by

$$\mathrm{d}P = \frac{|\langle f|S|i\rangle|^2}{\langle f|f\rangle \langle i|i\rangle}\mathrm{d}\Pi, \tag{3.17}$$

where S represents the evolution operator or scattering-matrix which connects the initial and final states and $\mathrm{d}\Pi$ is the differential phase space volume of the final state particles

$$\mathrm{d}\Pi = \prod_f \frac{V}{(2\pi)^3}\mathrm{d}^3 p_f. \tag{3.18}$$

For $f \neq i$ the transition amplitude is given by

$$\langle f|S|i\rangle = i(2\pi)^4 \delta^4 \left(\sum_{f,i} p_f - p_i\right) \mathcal{M} \tag{3.19}$$

where $\mathcal{M}$ is the usual quantum field theoretical "matrix element". It can be calculated by applying the usual Feynman rules [52, 51]. The delta distribution $\delta\left(\sum p_f - p_i\right)$ accounts for the momentum conservation when going from the initial to the final state. Assuming a finite volume V and time T we can take the square of the transition amplitude and find

$$|\langle f|S|i\rangle|^2 = TV\delta^4 \left(\sum_{f,i} p_f - p_i\right) (2\pi)^4 \left|\mathcal{M}\right|^2. \tag{3.20}$$

Here, one has to use

$$\delta^4(p)\,\delta^4(p) = \delta^4(0)\,\delta^4(p), \tag{3.21}$$

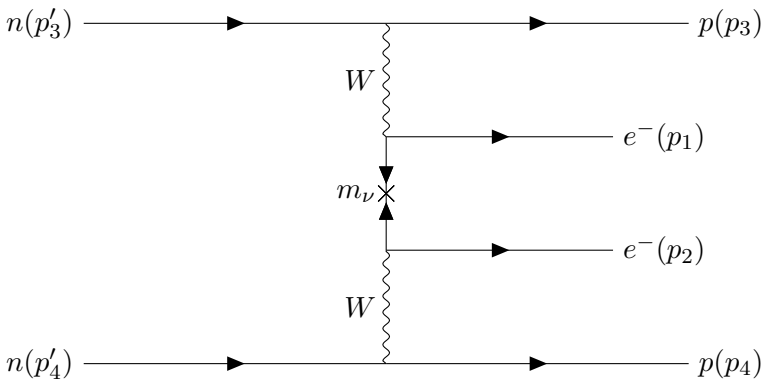

Figure 3.4.: Feynman diagram of neutrinoless double-β-decay in the standard framework of light Majorana neutrino exchange.

and

$$(2\pi)^4 \delta^4(p) = \int \mathrm{d}^4x \exp\{ixp\}, \tag{3.22}$$

which when integrating over finite V and T results in

$$\delta^4(0) = (2\pi)^{-4} \int \mathrm{d}^4x = \frac{TV}{(2\pi)^4}. \tag{3.23}$$

With $|s\rangle = \prod_s |p_s\rangle$ the normalization factors $\langle f|f\rangle$ and $\langle i|i\rangle$ are given by

$$\langle i|i\rangle = (2E_iV), \qquad \langle f|f\rangle = \prod_f (2E_fV) \tag{3.24}$$

and ensure invariance under Lorentz transformations. Plugging all this into Eq. (3.17) we find

$$\mathrm{d}P = \frac{\delta^4\left(\sum_{f,i} p_f - p_i\right) TV (2\pi)^4 |\mathcal{M}|^2}{\left(\prod_f (2E_fV)\right)(2E_iV)} \prod_f \frac{V}{(2\pi)^3} \mathrm{d}^3p_f \tag{3.25}$$

and hence the differential decay rate is given by

$$\mathrm{d}\Gamma = \frac{1}{2E_i} |\mathcal{M}|^2 (2\pi)^4 \delta^4\left(\sum_{f,i} p_f - p_i\right) \prod_f \frac{\mathrm{d}^3p_f}{(2\pi)^3 2E_f}. \tag{3.26}$$

We see T and V drop out of the equation as they should.
Now that we know how to calculate the decay rate in general we can go on deriving the standard $0\nu\beta\beta$-decay rate. The Feynman diagram corresponding to the standard $0\nu\beta\beta$

mechanism induced by light Majorana neutrinos is shown in Figure 3.4. In the case of free particles one would calculate the transition matrix element as

$$\begin{aligned}\mathcal{M} = \left(\frac{g}{2}\right)^4 V_{ud}^2\, \overline{u}_p(p_3)\gamma^\mu P_L u_n(p_3')\frac{ig_{\mu\nu}}{q^2 - m_W^2}\overline{u}_e(p_1) \\ \times \gamma^\nu P_L \sum_i U_{ei}^2 \frac{i\left(\not{p} + m_{\nu_i}\right)}{p^2 - m_{\nu_i}^2} P_L C\gamma^{\alpha T} \\ \times \overline{u}_e^T(p_2)\frac{ig_{\alpha\beta}}{r^2 - m_W^2}\overline{u}_p(p_4)\gamma^\beta P_L u_n(p_4')\end{aligned} \tag{3.27}$$

where g is the weak coupling constant corresponding to $SU(2)_L$ and with

$$P_L = \frac{1-\gamma_5}{2}\,. \tag{3.28}$$

However, since with $0\nu\beta\beta$ we are considering a nuclear decay $N_i \to N_f$, where N_i represents the initial and N_f the final state nucleus, we do not deal with free particles. Rather, the nucleons (p,n) are bound in a nucleus. This means we are actually dealing with a many particle system consisting of bound quark states. We can summarize these nuclear effects in a nuclear matrix element (NME) by rewriting the transition element as

$$\begin{aligned}\mathcal{M} = -\frac{4}{2!}\left(\frac{G_F V_{ud}}{\sqrt{2}}\right)^2 \overline{u}_e(p_1)\gamma^\alpha P_L \sum_i U_{ei}^2 \frac{i\left(\not{p} + m_{\nu_i}\right)}{p^2 - m_{\nu_i}^2} P_L C\gamma^{\beta T}\overline{u}_e^T(p_2) \\ \times \langle N_f|\, J_\alpha(p_1)J_\beta(p_2)\,|N_i\rangle - (p_1 \Leftrightarrow p_2)\end{aligned} \tag{3.29}$$

where we added the $(p_1 \Leftrightarrow p_2)$ term to include the corresponding Feynman diagram which switches the two outgoing electrons. Also, we will absorb the normalization factors for the non-relativistic nuclear states into the nuclear matrix element. The additional factor of 1/2! arises due to the nucleons being bosonic states. Furthermore, we took the limit $\frac{1}{p^2 - m_W^2} \sim \frac{-1}{m_W^2}$. The neutrino propagator can be simplified by noticing that

$$P_L \not{p} P_L = P_L \gamma^\mu p_\mu P_L = \gamma^\mu p_\mu P_R P_L = 0 \tag{3.30}$$

which follows directly from the definition of γ_5 and the anti-commutator rules of the gamma matrices in Eq. (2.3). It is also easy to notice that the second term denoted by $(p_1 \Leftrightarrow p_2)$ will just add another factor of 2. Thus, we can Fourier transform to position space and write

$$\begin{aligned}\mathcal{M} = -4\left(\frac{G_F V_{ud}}{\sqrt{2}}\right)^2 \int \overline{u}_e(x_1)\exp\{ip_1x_1\}\gamma^\alpha \sum_i U_{ei}^2 \\ \times i\int \frac{\mathrm{d}^4p}{(2\pi)^4}\frac{m_{\nu_i}\exp\{-ip\,(x_1 - x_2)\}}{p^2 - m_{\nu_i}^2} P_L C\gamma^{\beta T}\overline{u}_e^T(x_2)\exp\{ip_2x_2\} \\ \times \langle N_f|\,\mathbf{T}\left[J_\alpha(x_1)J_\beta(x_2)\right]|N_i\rangle\,\mathrm{d}^4x_1\mathrm{d}^4x_2.\end{aligned} \tag{3.31}$$

Here, $\mathbf{T}$ denotes the time ordering operator

$$\mathbf{T}\left[J_\alpha(x_1)J_\beta(x_2)\right] = \mathbf{T}\left[J_\alpha(x_2)J_\beta(x_1)\right] = \begin{cases} J_\alpha(x_1)J_\beta(x_2)\,, & x_1^0 > x_2^0 \\ J_\alpha(x_2)J_\beta(x_1)\,, & x_1^0 < x_2^0 \end{cases}. \tag{3.32}$$

From here on we follow the derivation of [53, 54]. However, we use a different definition of the matrix element which one should pay attention to when comparing to [53, 54]. First we can solve the integral over x_i^0 by dividing the integral over x_2^0 into two parts

$$\int_{-\infty}^{+\infty} \mathrm{d}x_2^0 = \int_{-\infty}^{x_1^0} \mathrm{d}x_2^0 + \int_{x_1^0}^{+\infty} \mathrm{d}x_2^0. \tag{3.33}$$

Thus, we have two separate integrals one with $x_1^0 > x_2^0$ and one with $x_1^0 < x_2^0$. In both cases one can solve the integration over p^0 in the neutrino propagator by analytic continuation of p_0 and applying the Residue theorem [55].

Residue theorem: *Let $U \subset \mathbb{C}$ be open. Let f be a function such that $f : U \setminus S \to \mathbb{C}$ is holomorphic where $S \subset U$ is a discrete set of singularities. If $A \subset U$ is a finitely separable set such that $\partial A \cap S = \emptyset$, then*

$$\int_{\partial A} f(z)\mathrm{d}z = 2\pi i \sum_{z_0 \in S \cap A} \mathrm{Res}_{z_0} f. \tag{3.34}$$

In the simple case that $f(z)$ can be written in the form

$$f(z) = \frac{g(z)}{(z - z_0)^n}, \tag{3.35}$$

where $g : U \setminus S \to \mathbb{C}$ is again holomorphic for a pole of order n at z_0 the residue is given by the simple formula

$$\mathrm{Res}_{z_0} f = \frac{1}{(n-1)!} \frac{\mathrm{d}^{n-1} g}{\mathrm{d}z^{n-1}}(z_0). \tag{3.36}$$

Following the above line, we can close the contour integral either in the upper ($x_1^0 > x_2^0$) or lower ($x_1^0 < x_2^0$) complex plane such that the exponential function is non-vanishing only on the real axis. Also we can avoid the poles on the real axis by calculating the actual Feynman propagator. That is, we can shift the poles away from the real axis by a small $i\epsilon$ and afterwards take the limit $\epsilon \to 0$. Doing so results in

$$\begin{aligned} &\lim_{\epsilon \to 0} \frac{1}{(2\pi)^4} \int \frac{\exp\{-ip\,(x_1 - x_2)\}}{p^2 - m_{\nu_i}^2 + i\epsilon} \mathrm{d}^4 p \\ =& -\frac{i}{(2\pi)^3} \int \frac{\exp\left\{\mp ip^0\left(x_1^0 - x_2^0\right) \pm i\vec{p}(\vec{x}_1 - \vec{x}_2)\right\}}{2p_k^0} \mathrm{d}^3 p \end{aligned} \tag{3.37}$$

with

$$p_k^0 = \sqrt{p^2 + m_k^2}. \tag{3.38}$$

Next we need to take a closer look at the nuclear matrix element. The time evolution of the currents J_α is given by the Hamiltonian $\mathcal{H}$ of the system as

$$J_\alpha(x) = \exp\{i\mathcal{H}x^0\} J_\alpha(\vec{x}) \exp\{-i\mathcal{H}x^0\} \tag{3.39}$$

where we have defined

$$J_\alpha(\vec{x}) = J_\alpha(x_0 = 0, \vec{x}). \tag{3.40}$$

Using the normalization condition

$$\sum_n |N_n\rangle \langle N_n| = 1 \tag{3.41}$$

where $|N_n\rangle$ represents the intermediate states we can rewrite the matrix element for $x_1^0 > x_2^0$ as

$$\langle N_f| J_\alpha(x_1) J_\beta(x_2) |N_i\rangle = \sum_n \langle N_f| J_\alpha(x_1) |N_n\rangle \langle N_n| J_\beta(x_2) |N_i\rangle. \tag{3.42}$$

Inserting Eq. (3.39) for $x_1^0 > x_2^0$ we can write

$$\begin{aligned} &\langle N_f| J_\alpha(x_1) |N_n\rangle \langle N_n| J_\beta(x_2) |N_i\rangle \\ =&\sum_n \exp\{i(E_f - E_n)x_1^0\} \exp\{i(E_n - E_i)x_2^0\} \langle N_f| J_\alpha(\vec{x}_1) |N_n\rangle \langle N_n| J_\beta(\vec{x}_2) |N_i\rangle \end{aligned} \tag{3.43}$$

For $x_1^0 < x_2^0$ one can of course do the same just by switching $x_1 \Leftrightarrow x_2$ and $\alpha \Leftrightarrow \beta$. Thus, we are left with the following integrals

$$\begin{aligned} \sum_n \int_{-\infty}^{+\infty} \mathrm{d}x_1^0 \Bigg\{ &\left[\int_{-\infty}^{+x_1^0} \mathrm{d}x_2^0 \exp\{i\left(p_1^0 - p^0 + E_f - E_n\right)x_1^0 + \left(p_2^0 + p_k^0 + E_n - E_i\right)x_2^0\} \right] \\ &\times \langle N_f| J_\alpha(\vec{x}_1) |N_n\rangle \langle N_n| J_\beta(\vec{x}_2) |N_i\rangle \\ &+ \left[\int_{x_1^0}^{+\infty} \mathrm{d}x_2^0 \exp\{i\left(p_1^0 + p^0 + E_n - E_i\right)x_1^0 + \left(p_2^0 - p_k^0 + E_f - E_i\right)x_2^0\} \right] \\ &\times \langle N_f| J_\beta(\vec{x}_2) |N_n\rangle \langle N_n| J_\alpha(\vec{x}_1) |N_i\rangle \Bigg\}. \end{aligned} \tag{3.44}$$

Assuming that interactions are turned off at $x_i = \pm\infty$ we can take

$$\int_{-\infty}^{a} \exp\{ikx\} \to \lim_{\epsilon\to 0} \int_{-\infty}^{a} \exp\{i(k - i\epsilon)x\} = \lim_{\epsilon\to 0} \frac{-i}{k - i\epsilon} \exp\{i(k - i\epsilon)a\} \tag{3.45}$$

for the first integral in Eq. (3.44). Using the above relation and Eq. (3.22) as well as partial integration which results in

$$\int_{-\infty}^{\infty} \mathrm{d}x_1^0 \int_{x_1^0}^{\infty} \mathrm{d}x_2^0 ... = \int_{-\infty}^{\infty} \mathrm{d}x_2^0 \int_{-\infty}^{x_2^0} \mathrm{d}x_1^0 ... \tag{3.46}$$

one can perform the integration in Eq. (3.44) which leads to

$$\begin{aligned}
\sum_n \int_{-\infty}^{+\infty} \mathrm{d}x_1^0 \Bigg\{ & \left[\int_{-\infty}^{+x_1} \mathrm{d}x_2^0 \exp\left\{ i \left(p_1^0 - p^0 + E_f - E_n \right) x_1^0 + \left(p_2^0 + p_k^0 + E_n - E_i \right) x_2^0 \right\} \right] \\
& \times \langle N_f | \, J_\alpha(\vec{x}_1) \, | N_n \rangle \, \langle N_n | \, J_\beta(\vec{x}_2) \, | N_i \rangle \\
& + \left[\int_{x_1}^{+\infty} \mathrm{d}x_2^0 \exp\left\{ i \left(p_1^0 + p^0 + E_n - E_i \right) x_1^0 + \left(p_2^0 - p_k^0 + E_f - E_i \right) x_2^0 \right\} \right] \\
& \times \langle N_f | \, J_\beta(\vec{x}_2) \, | N_n \rangle \, \langle N_n | \, J_\alpha(\vec{x}_1) \, | N_i \rangle \Bigg\}. \\
= -i2\pi \sum_n \Bigg[& \frac{\langle N_f | \, J_\alpha(\vec{x}_1) \, | N_n \rangle \, \langle N_n | \, J_\beta(\vec{x}_2) \, | N_i \rangle}{E_n + p_2^0 + p_k^0 - E_i} \\
& + \frac{\langle N_f | \, J_\beta(\vec{x}_2) \, | N_n \rangle \, \langle N_n | \, J_\alpha(\vec{x}_1) \, | N_i \rangle}{E_n + p_1^0 + p_k^0 - E_i} \Bigg] \delta \left(E_f + p_1^0 + p_2^0 - E_i \right)
\end{aligned} \tag{3.47}$$

Thus, we can finally write the matrix element $\mathcal{M}$ as

$$\begin{aligned}
\mathcal{M} = & 2i \left(\frac{G_F V_{ud}}{\sqrt{2}} \right)^2 \overline{u}\left(p_1\right) \gamma^\alpha P_L \gamma^\beta C \overline{u}^T\left(p_2\right) \int \mathrm{d}^3x_1 \mathrm{d}^3x_2 \exp\{-i \left(\vec{p}_1 \cdot \vec{x}_1 + \vec{p}_2 \cdot \vec{x}_2 \right)\} \\
& \times \sum_k U_{ek}^2 m_k \frac{1}{\left(2\pi\right)^3} \int \frac{\exp\{i\vec{p} \cdot \left(\vec{x}_1 - \vec{x}_2 \right)\}}{p_k^0} \mathrm{d}^3p \\
& \times \sum_n \Bigg[\frac{\langle N_f | \, J_\alpha(\vec{x}_1) \, | N_n \rangle \, \langle N_n | \, J_\beta(\vec{x}_2) \, | N_i \rangle}{E_n + p_2^0 + p_k^0 - E_i} \\
& + \frac{\langle N_f | \, J_\beta(\vec{x}_2) \, | N_n \rangle \, \langle N_n | \, J_\alpha(\vec{x}_1) \, | N_i \rangle}{E_n + p_1^0 + p_k^0 - E_i} \Bigg] \delta \left(E_f + p_1^0 + p_2^0 - E_i \right).
\end{aligned} \tag{3.48}$$

We see that this formula, while representing the exact solution at tree-level, is still quite impractical if one actually wants to calculate the expected decay rate. To arrive at a more handy description one typically takes a few approximations [53]:

1. **Small neutrino masses:** From laboratory experiments we know that the neutrino mass scale is [56]

$$m_\nu \lesssim 1\,\mathrm{eV} \tag{3.49}$$

while cosmological bounds on the sum of the different neutrino masses are even more stringent giving [57]

$$\sum_k m_k \lesssim 0.2\,\mathrm{eV}. \tag{3.50}$$

Considering these experimental results we can compare the expected neutrino mass scale m_k to the expected momentum transfer p via the neutrino propagator which from the uncertainty principle can be estimated as

$$p \sim \frac{1}{r_n} \sim 100\,\mathrm{MeV} \tag{3.51}$$

where $r_n \sim 10^{-15}\,\mathrm{m}$ is the average distance between two nucleons inside the nucleus. We can see that

$$m_k \ll p \tag{3.52}$$

and hence we can take

$$p_k^0 = \sqrt{p^2 + m_k^2} \to p \tag{3.53}$$

2. **Long-wave approximation:** Since the decay takes place inside a nucleus with a finite radius R which can be approximated as

$$R = 1.2A^{1/3} \times 10^{-15}\,\mathrm{m} \tag{3.54}$$

we have

$$|\vec{p}_{1,2} \cdot \vec{x}_{1,2}| < |\vec{p}_{12}|\, R \sim A^{1/3} \frac{p_{1,2}}{100\,\mathrm{MeV}}. \tag{3.55}$$

Typical Q-values are of the order $Q = \mathcal{O}(1\,\mathrm{MeV})$ such that we can take

$$|\vec{p}_{1,2} \cdot \vec{x}_{1,2}| \to 0 \tag{3.56}$$

and consequently

$$\exp\{i\vec{p}_i \cdot \vec{x}_i\} \to 1. \tag{3.57}$$

This also means that one can assume the two outgoing electrons to be in the S-state.

3. **Closure approximation:** We want to get rid of the sum over the intermediate states. However, we cannot just take $\sum_n |N_n\rangle \langle N_n| \to 1$ since each term is weighted by the intermediate states energy E_n. In order to be able to calculate the sum we need to notice that the momentum transfer p via the neutrino propagator is much larger than the typical excitation energies of the intermediate nuclei

$$p \gg E_n - E_i. \tag{3.58}$$

Therefore, we can replace the sum over E_n by the average energy of the intermediate states

$$E_n \to \overline{E} \tag{3.59}$$

and afterwards calculate the sum in the laboratory frame $E_{f,i} \to M_{f,i}$

$$\begin{aligned}\sum_n \Bigg[& \frac{\langle N_f| J_\alpha(\vec{x}_1) |N_n\rangle \langle N_n| J_\beta(\vec{x}_2) |N_i\rangle}{E_n + p_2^0 + p - E_i} \\ & + \frac{\langle N_f| J_\beta(\vec{x}_2) |N_n\rangle \langle N_n| J_\alpha(\vec{x}_1) |N_i\rangle}{E_n + p_1^0 + p - E_i} \Bigg] \\ = & \frac{1}{p + \overline{E} - \frac{M_i + M_f}{2}} \langle N_f| J_\alpha(\vec{x}_1) J_\beta(\vec{x}_2) + J_\beta(\vec{x}_2) J_\alpha(\vec{x}_1) |N_i\rangle\end{aligned} \tag{3.60}$$

where we used

$$\overline{E} + p + p_{1,2}^0 - M_i \approx \overline{E} + p + \frac{p_1^0 + p_2^0}{2} - M_i = \overline{E} + p - \frac{M_i + M_f}{2} \tag{3.61}$$

with

$$p_{1,2}^0 = \frac{p_1^0 + p_2^0}{2} \pm \frac{p_1^0 - p_2^0}{2} \approx \frac{p_1^0 + p_2^0}{2} \tag{3.62}$$

and ignoring nuclear recoil

$$p_1^0 + p_2^0 = M_i - M_f. \tag{3.63}$$

4. **Non-relativistic impulse approximation:** In the non-relativistic approximation the hadronic charged current $J_\alpha(\vec{x})$ can be written as

$$J_\alpha(\vec{x}) = \sum_n \delta(\vec{x} - \vec{r}_n) \tau_n^+ g_{\alpha\beta} J_n^\beta(p^2) \tag{3.64}$$

with

$$J_n^\mu(p^2) = g_V(p^2) g^{\mu 0} + \left[g_A(p^2) + i g_M(p^2) \frac{\vec{\sigma}_n \times p}{2M_N} - g_p(p^2) \frac{\vec{\sigma}_n \cdot \vec{p}}{2M_N} \vec{p} \right] g^{\mu k} \tag{3.65}$$

Here, $\vec{\sigma}_n$ is the spin operator represented by the 3 Pauli matrices and acting on the $n-$th nucleon while τ_n^+ is the isospin raising operator which is also given in terms of Pauli matrices

$$\tau^+ = \frac{1}{2}(\tau_1 + i\tau_2) \tag{3.66}$$

which connects $u-$ and $d-$type quarks. Since σ and τ act on different spaces we denote them by different signs although they both represent Pauli-matrices. Again, we

have ignored the impact of nuclear recoils. The formfactors $g_V\left(p^2\right), g_A\left(p^2\right), g_P\left(p^2\right)$ and $g_M\left(p^2\right)$ represent the charged current vector, axial-vector, pseudoscalar and magnetic formfactors

$$\begin{aligned} g_V(0) &\approx 1 \\ g_A(0) &\approx 1.27 \\ g_P(p^2) &= 2M_N \frac{g_A(p^2)}{p^2 + m_\pi^2} \\ g_M(0) &= \mu_p - \mu_n \end{aligned} \tag{3.67}$$

where $\mu_{p,n}$ is the anomalous magnetic moment of the proton or neutron respectively. Once more, p denotes the momentum transfer.

By applying the above approximations (1-3) and by defining the effective neutrino Majorana mass

$$m_{\beta\beta} = \sum_k U_{ek}^2 m_k \tag{3.68}$$

we can write the matrix element as

$$\begin{aligned} \mathcal{M} =& 4i\pi m_{\beta\beta} \left(\frac{G_F V_{ud}}{\sqrt{2}}\right)^2 \overline{u}\left(p_1\right) \gamma^\alpha P_L \gamma^\beta C \overline{u}^T\left(p_2\right) \\ & \times \int \mathrm{d}^3x_1 \mathrm{d}^3x_2 \frac{1}{(2\pi)^3} \int \mathrm{d}^3p \frac{\exp\{i\vec{p}\cdot(\vec{x}_1 - \vec{x}_2)\}}{p\left(p + \overline{E} - \frac{M_i + M_f}{2}\right)} \\ & \times \langle N_f | J_\alpha(\vec{x}_1) J_\beta(\vec{x}_2) + J_\beta(\vec{x}_2) J_\alpha(\vec{x}_1) | N_i \rangle \, \delta\left(M_f + p_1^0 + p_2^0 - M_i\right). \end{aligned} \tag{3.69}$$

Further, in the non-relativistic impulse approximation we have

$$J_\alpha\left(\vec{x}_1\right) J_\beta\left(\vec{x}_2\right) = \sum_{n,m} \delta\left(\vec{x}_1 r_n\right) \delta\left(\vec{x}_2 r_m\right) \tau_n^+ \tau_m^+ \left(J_n^0 J_m^0 - \vec{J}_n \cdot \vec{J}_m\right) \tag{3.70}$$

and

$$J_\alpha\left(\vec{x}_1\right) J_\beta\left(\vec{x}_2\right) = J_\beta\left(\vec{x}_2\right) J_\alpha\left(\vec{x}_1\right). \tag{3.71}$$

Using Eq. (2.3) we can then write

$$\gamma^\alpha \gamma^\beta = g^{\alpha\beta} + \frac{1}{2}\left(\gamma^\alpha \gamma^\beta - \gamma^\beta \gamma^\alpha\right). \tag{3.72}$$

We can see that the second term when including the hadronic currents will vanish. Thus, combining the above relations in the matrix element we find

$$\begin{aligned} \mathcal{M} =& 4i\pi m_{\beta\beta} \left(\frac{G_F V_{ud}}{\sqrt{2}}\right)^2 \overline{u}\left(p_1\right) P_R C \overline{u}^T\left(p_2\right) \\ & \times \langle N_f | \left[\sum_{n,m} \int \frac{\mathrm{d}^3p}{(2\pi)^3} \frac{\exp\{i\vec{p}\cdot(\vec{r}_n - \vec{r}_m)\}}{p\left(p + \overline{E} - \frac{M_i + M_f}{2}\right)} \tau_n^+ \tau_m^+ \left(J_n^0 J_m^0 - \vec{J}_n \cdot \vec{J}_m\right)\right] | N_i \rangle \\ & \times \delta\left(M_f + p_1^0 + p_2^0 - M_i\right). \end{aligned} \tag{3.73}$$

After switching to spherical coordinates we can solve angular parts of the integral over d^3p via

$$\int_0^\pi \exp\{ik\cos(\theta)\}\sin(\theta)\,\mathrm{d}\theta = 2\frac{\sin(k)}{k}, \tag{3.74}$$

such that we can write

$$\begin{aligned}
&\int \frac{\mathrm{d}^3p}{(2\pi)^3}\frac{\exp\{i\vec{p}\cdot(\vec{r}_n-\vec{r}_m)\}}{p\left(p+\overline{E}-\frac{M_i+M_f}{2}\right)}\\
=&\int_0^{2\pi}\mathrm{d}\phi\int_0^{\pi}\mathrm{d}\theta\int_0^{\infty}\frac{\mathrm{d}p}{(2\pi)^3}p\sin(\theta)\frac{\exp\{i|p||r_{nm}|\cos(\theta)\}}{p\left(p+\overline{E}-\frac{M_i+M_f}{2}\right)}\\
=&\frac{1}{2\pi^2 r_{nm}}\int_0^{\infty}\frac{\sin(pr_{nm})}{p+\overline{E}-\frac{M_i+M_f}{2}}\mathrm{d}p\\
=&\frac{1}{4\pi R}H\left(r_{nm},\overline{E}\right),
\end{aligned} \tag{3.75}$$

where

$$H\left(r_{nm},\overline{E}\right) = \frac{2R}{r_{nm}}\int_0^{\infty}\frac{\sin(pr_{nm})}{p+\overline{E}-\frac{M_i+M_f}{2}}\mathrm{d}p \tag{3.76}$$

is the so-called *neutrino potential* and we defined

$$r_{nm} = r_n - r_m. \tag{3.77}$$

Plugging this back into the matrix element one finds

$$\mathcal{M} = -i\frac{m_{\beta\beta}}{R}\left(\frac{G_F V_{ud}}{\sqrt{2}}\right)^2 \overline{u}(p_1)\,P_R C\overline{u}^T(p_2)\,\mathrm{M}^{0\nu}\delta\left(p_1^0+p_2^0+M_f-M_i\right) \tag{3.78}$$

with the nuclear matrix element defined as

$$\mathrm{M}^{0\nu} = \langle N_f|\sum_{n,m}H\left(r_{nm},\overline{E}\right)\tau_n^+\tau_m^+\left(\vec{J}_n\cdot\vec{J}_m - J_n^0J_m^0\right) \tag{3.79}$$

and with R being the radius of the nucleus. To calculate the differential decay rate we need to take the absolute square of the matrix element $|\mathcal{M}|^2$ which contains the leptonic

currents

$$\begin{aligned}
&\sum_{\text{spins}} \left|\overline{u}\left(p_1\right) P_R u^c\left(p_2\right)\right|^2 \\
=&\sum_{\text{spins}} \left\{\overline{u}\left(p_1\right) P_R u^c\left(p_2\right) \overline{u^c}\left(p_2\right) P_L u\left(p_1\right)\right\} \\
=&\sum_{\text{spins}} \frac{1}{4} \operatorname{Tr}\{\left(1+\gamma_5\right) u^c\left(p_2\right) \overline{u^c}\left(p_2\right) \left(1-\gamma_5\right) u\left(p_1\right) \overline{u}\left(p_1\right)\} \\
=&\frac{1}{4} \operatorname{Tr}\{\left(1+\gamma_5\right) \left(\not{p}_2-m_e\right) \left(1-\gamma_5\right) \left(\not{p}_1+m_e\right)\} \\
=&\frac{p_1^\mu p_2^\nu}{4} \operatorname{Tr}\{\left(1+\gamma_5\right) \left(\gamma^\nu-m_e\right) \left(1-\gamma_5\right) \left(\gamma^\mu+m_e\right)\} \\
=&2 p_1^\mu p_{2\mu}=2\left(E_1 E_2-p_1 p_2 \cos\theta\right)
\end{aligned} \tag{3.80}$$

To solve the leptonic currents we used the fact that one can always take the trace of a scalar without changing the result. Additionally, we applied the following relations

$$\begin{aligned}
&\operatorname{Tr}\{ABC\}=\operatorname{Tr}\{CAB\}=\operatorname{Tr}\{BCA\} \qquad \text{(Cyclic Permutation)} \\
&\operatorname{Tr}\{A+B\}=\operatorname{Tr}\{A\}+\operatorname{Tr}\{B\} \\
&\left.\begin{array}{l}\sum_{\text{spins}} u(p)\overline{u}(p)=\not{p}+m_e \\ \sum_{\text{spins}} u^c(p)\overline{u^c}(p)=\not{p}-m_e\end{array}\right\} \qquad \text{(Completeness relation)} \\
&\left.\begin{array}{l}\operatorname{Tr}\{\gamma^\mu\}=0 \\ \operatorname{Tr}\{\gamma^\mu\gamma_5\}=0\end{array}\right\} \qquad \text{(Trace of odd number of } \gamma^\mu \text{ vanishes)} \\
&\operatorname{Tr}\{\gamma_5\}=\operatorname{Tr}\{\gamma^\mu\gamma^\nu\gamma_5\}=0 \\
&\operatorname{Tr}\{\gamma^\mu\gamma^\nu\}=4g^{\mu\nu} \\
&\left(\gamma_5\right)^2=1 \\
&\{\gamma_5,\gamma^\mu\}=0.
\end{aligned} \tag{3.81}$$

While the above result holds for free electrons, we have to take electromagnetic interactions between the outgoing electrons and the charged nucleus into account by multiplying the electron currents by the Fermi function

$$F(Z,E)=\frac{2\pi\eta}{1-\exp\{-2\pi\eta\}} \tag{3.82}$$

with

$$\eta=Z\alpha\frac{m_e}{p}. \tag{3.83}$$

Combining all of these findings into the differential decay rate one finally finds

$$\begin{aligned}
\mathrm{d}\Gamma^{0\nu}=&\left|m_{\beta\beta}\right|^2\left|\mathrm{M}^{0\nu}\right|^2 \frac{G_F^4 V_{ud}^4}{\left(2\pi\right)^5 R^2}\left(E_1 E_2-p_1 p_2\cos\theta\right) \\
&\times F\left(Z+2,E_1\right) F\left(Z+2,E_2\right) p_1 p_2 \sin\theta\,\mathrm{d}\theta\,\mathrm{d}E_1
\end{aligned} \tag{3.84}$$

and thus with

$$\left(T_{1/2}^{0\nu}\right)^{-1} = \frac{\Gamma^{0\nu}}{\log 2} \tag{3.85}$$

the half-life can be written in the well known form

$$\boxed{\left(T_{1/2}^{0\nu}\right)^{-1} = |m_{\beta\beta}|^2 \left|\mathrm{M}^{0\nu}\right|^2 G^{0\nu}(Q,Z)} \tag{3.86}$$

where $G^{0\nu}$ is the so-called phase space factor (PSF) which is given by the integration over the leptonic phase space

$$\begin{aligned} G^{0\nu}(Q,Z) =& \frac{G_F^4 V_{ud}^4}{2\log 2\,(2\pi)^5 R^2} \int_0^Q \mathrm{d}T_1 \int_0^\pi \mathrm{d}\theta \sin\theta p_1 p_2 \left(E_1 E_2 - p_1 p_2 \cos\theta\right) \\ & \times F(Z+2, E_1)\, F(Z+2, E_2)\,. \end{aligned} \tag{3.87}$$

From Eq. (3.86) we can see that the expected half-life within the mechanism of light neutrino exchange depends on

1. The *effective Majorana mass* $m_{\beta\beta}$ which is a parameter that has to be generated somehow beyond the Standard Model and is a priori **completely unknown**

2. The *nuclear matrix element* $\mathrm{M}^{0\nu}$ which cannot be calculated exactly but rather has to be **calculated approximately** within multi body nuclear simulations.

3. The *phase space factor* $G^{0\nu}$ which within the above approximations can be **calculated exactly**.

While we used the S-wave approximation to calculate the PSFs to show the principles of the calculation, significantly better and more exact methods [29, 58] do exist which differ by up to 30% from the above approximation. We want to point out that from Eq. (3.87) we can see that the half-life will be proportional to Q^5. This is an important feature as it determines the relevance of different isotopes for experimental usage.

3.3. Non-Standard Mechanisms

3.3.1. Long- and Short-Range Mechanisms

In the last section we have discussed the formal description of the standard picture of $0\nu\beta\beta$ generated by the exchange of light Majorana neutrinos. While this is the most commonly studied mechanism to generate $0\nu\beta\beta$, it does not necessarily have to be the dominating mechanism. We know that to generate a non-zero neutrino Majorana

mass term, we need new-physics beyond the Standard Model. However, we do not know if the resulting neutrino Majorana mass term will be the dominating $\Delta L = 2$ operator within this theory as we do not know if an explicit Majorana mass term actually exists. Additionally, even in the case that the light neutrino masses are described by a Majorana mass term, cancellation effects resulting from the additional Majorana CP-phases can in the case of normal mass hierarchy lead to a vanishing effective mass $m_{\beta\beta}$. The effective mass $m_{\beta\beta}$ in dependence on the lightest neutrino mass m_{min} is shown in Figure 3.5.
The usual way to try to describe the possibility of additional different mechanisms is to use effective lepton number violating operators which could arise from some more complete model by integrating out heavy degrees of freedom. We will discuss the formal definition of this process in the following section 3.4.1. These effective operators are then classified into three types of mechanisms represented in Figure 3.6. These are the usual mass mechanism, long-range mechanisms and short-range mechanisms [61, 7].

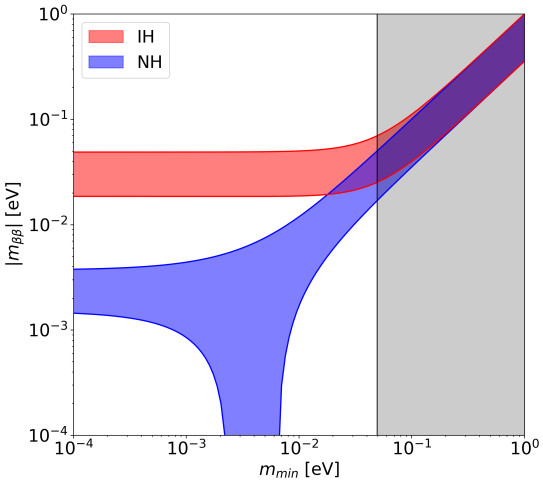

Figure 3.5.: Effective Majorana mass $m_{\beta\beta}$ plotted in dependency on the mass of the lightest neutrino mass eigenstate for both mass hierarchies. As one can see, in the case of normal hierarchy (NH) cancellation can appear. To arrive at this plot, we varied the currently unknown Majorana CP-phases from $0 - \pi$ [59]. The parameter region shaded grey is excluded from measurements on the sum of neutrino masses $\sum_i m_i < 0.17\,\text{eV}$ [60].

Long-range mechanisms:

The diagrams (b) and (c) in Figure 3.6 are what is usually referred to as long-range mechanisms. That is, they are mechanisms which include a light neutrino propagator. In this work we assume that all new-physics will come from additional heavy particles and therefore that no additional light degrees of freedom exist. Within this assumption, contributions from diagrams of the (c) type can be safely ignored since they will be highly suppressed by two small effective couplings $C^{(6,7)}$ and the necessity of another neutrino mass insertion. Even if one considers the existence of additional light mediators connecting the two effective couplings instead of the usual neutrino propagator, diagrams of type (c) would be suppressed by presumably small $\left(C^{(6,7)}\right)^2$ and could only be relevant in case there is no contribution from other diagrams.
We therefore only consider diagrams of type (b) when talking about long-range mecha-

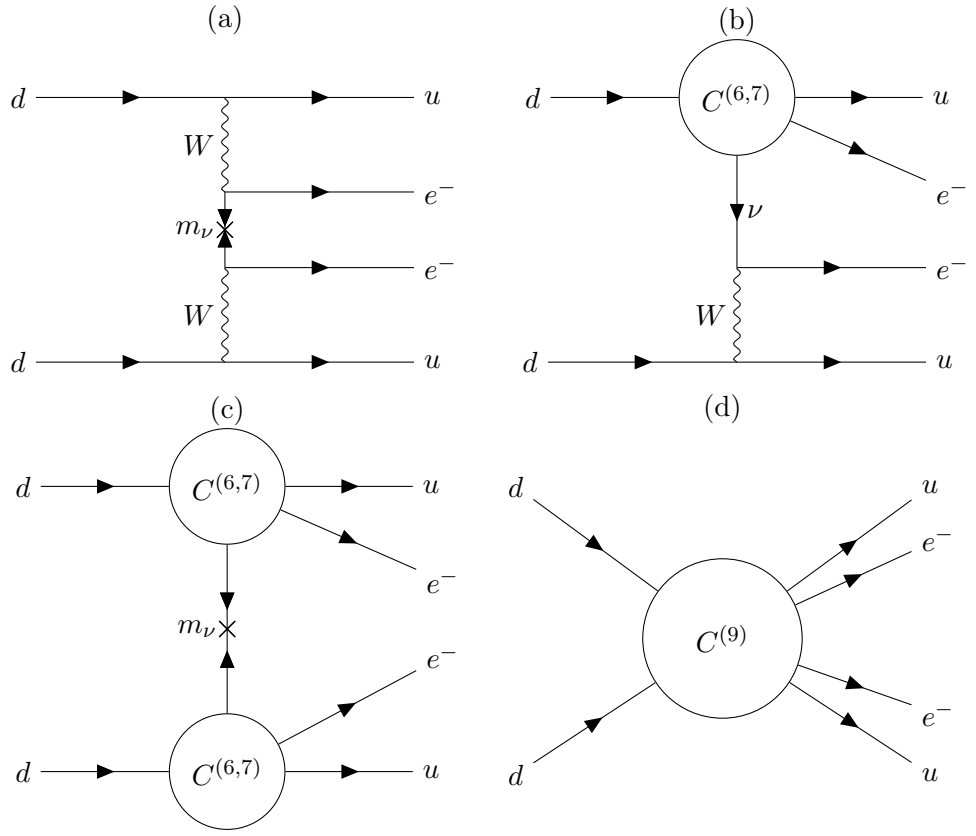

Figure 3.6.: Feynman diagrams of neutrinoless double-β-decay including low-energy effective couplings. (a) is the standard mechanism of light neutrino exchange. The diagrams (b) and (c) with vertices denoted by $C^{(6,7)}$ represent so-called long-range mechanisms while the diagram (d) labeled with $C^{(9)}$ represents so-called short-range mechanisms.

nisms. The couplings $C^{(6,7)}$ represent effective operators of the type

$$C^{(6,7)}\,[\overline{u}d]\;[\overline{e}\nu^c]\,, \tag{3.88}$$

which can have different Lorentz structures. Such operators are of mass dimension-6 or 7 if they include a derivative term.

Short-range mechanisms:

Short-range mechanisms refer to diagrams of the type (d) in Figure 3.6 which do not include any light mediator. A short-range mechanism hence at low energy corresponds to an effective 6 fermion dimension-9 operator of the type

$$C^{(9)}\,[\overline{u}d]\;[\overline{u}d]\;[\overline{e}e^c]\,, \tag{3.89}$$

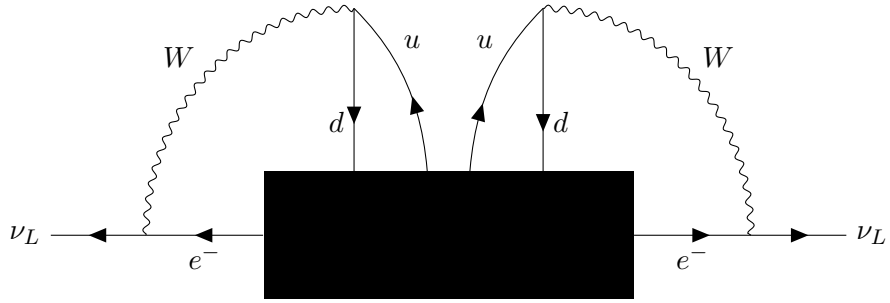

Figure 3.7.: Feynman diagram of the black box theorem by Schechter and Valle [6].

again with different possible Lorentz structures. Thus, short-range mechanisms correspond to an effective $0\nu\beta\beta$ vertex which connects the external fermions without any internal structure. If we include derivative terms also higher dimensional operators can contribute to short-range mechanisms. However, we will ignore this possibility here.

Schechter-Valle Black Box Theorem

The famous black box theorem first discussed by Schechter and Valle [6] gives a connection between non-standard mechanisms and neutrino masses. Its statement is that **a possible observation of neutrinoless double-β-decay would be equivalent to neutrinos being Majorana fermions independently of the actual mechanism responsible for** $0\nu\beta\beta$. The argument is relatively easy to follow. We know that $0\nu\beta\beta$ corresponds to an effective 6-fermion interaction. If we do not care about the exact mechanism we can treat the internal connections of the $0\nu\beta\beta$ diagram as an effective black box vertex with two outgoing electrons, two outgoing up-quarks and two incoming down quarks similar to the short-range mechanisms discussed above. By closing the lines of the external quarks and adding two W-propagators one can generate an effective 4-loop diagram which contributes to the Majorana propagator of the left-handed neutrino fields. The procedure is depicted in Figure 3.7. Therefore, if one does not assume some spurious cancellation this 4-loop diagram will generate some non-zero contribution to the neutrino Majorana mass term. Only shortly after Schechter and Valle had proposed the black box theorem, [62] and [63] showed that there cannot be a symmetry argument continuous or discrete to generate such a cancellation to all orders in perturbation theory. Following the seesaw formula in Eq. (2.87) we know that formally the existence of a Majorana mass term independently of any additional Dirac mass term will result in the mass eigenstates being Majorana particles. Thus, the observation of $0\nu\beta\beta$ would indeed mean that neutrinos are Majorana particles. However, it should be noted that the contribution to the neutrino mass assuming a half-life of $\mathcal{O}\left(10^{25}\,\mathrm{y}\right)$ would result in an extremely small contribution to the neutrino mass δm by the above mechanism of [64]

$$\delta m = \mathcal{O}\left(10^{-28}\,\mathrm{eV}\right). \tag{3.90}$$

Considering the mass differences measured in oscillation experiments (see Table 2.3) the above contribution is many orders of magnitude smaller and hence cannot be the

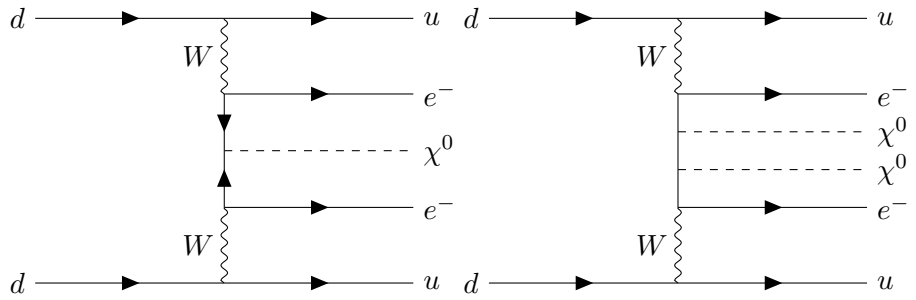

Figure 3.8.: Feynman diagrams of Majoron models with the emission of 1 (left) and 2(right) Majorons. Note that there are a lot of different $0\nu\beta\beta$ Majoron models and the above two diagrams only show two examples.

only neutrino mass generating mechanism. With this knowledge in mind, the black box theorem although important remains of rather academic interest.

3.3.2. Majoron Models

While the above discussion about long- and short-range mechanisms covers all aspects of the usually considered $0\nu\beta\beta$-decay with

$$(A, Z) \longrightarrow (A, Z + 2) + 2e^{-1} \tag{3.91}$$

which have only 3 final state particles, there is another class of possible models which incorporate additional light final state particles χ^0 that cannot be detected directly within the decay experiment

$$(A, Z) \longrightarrow (A, Z + 2) + 2e^{-1} + \chi^0. \tag{3.92}$$

Models of this kind are usually referred to as *Majoron* models. Historically the term Majoron referred to the Goldstone boson of a spontaneously broken global lepton number symmetry [65].
Experimentally, Majoron models would lead to a different signature than the usual $0\nu\beta\beta$ long- and short-range mechanisms. While the latter result in a sharp peak at the end of the measured summed electron energy spectrum, Majoron models will not result in such a signature. This is because the additionally emitted scalar(s) will carry away some portion of the released energy similar to the two neutrinos in the usual $2\nu\beta\beta$-decay. However, Majoron models can still result in a different spectral shape [66] and hence can be distinguished from the $2\nu\beta\beta$-decay background. We will not consider Majoron models any further within this work.

3.4. Effective Field Theory Approach

To be able to study the effect of the aforementioned possible non-standard $0\nu\beta\beta$ mechanisms in a model-independent way, we will now give a brief introduction into the concept

of effective field theories which we will utilize for this purpose.

3.4.1. Introduction to Effective Field Theories

Let us start by introducing the general aspects of effective field theories (EFTs). There exist several comprehensive reviews and introductory lectures on EFTs in the literature, e.g., [67, 68, 69, 70]. Here, we mostly follow [71] and [51].
Oftentimes, when dealing with physics at (macroscopic) low energy scales, it is convenient or even necessary to work within a so-called effective field theory rather than within the full (microscopic) theory. Within such an EFT we include the dynamical degrees of freedom (d.o.f.) which are relevant at the considered energy or length scales and for the physical processes of interest and we ignore any additional d.o.f..[5] To visualize the principles of EFTs let us disregard the field aspect for a moment and consider a more handy picture. Imagine for example the process of two billiard balls scattering off each other. This macroscopic process is very well described by Newtonian mechanics and, as long as we keep the scattering process at an energy that is small enough for the balls not to break, we do not need to worry about the microscopic structure of the balls. The principle stays the same when talking about particle physics and quantum field theory. In this sense, EFTs can be used in two ways:

1. **Top-Down:** If the microscopic physics, i.e., the "full theory" is known, EFTs can be used to simplify calculations of, e.g., scattering amplitudes and study the impact of the microscopic d.o.f. onto the low-energy physics.

2. **Bottom-Up:** If the microscopic theory is unknown but a low-energy theory exists, one can promote the low-energy theory to an EFT by systematically including all possible operators which respect the symmetries of the low-energy theory. If we know that the microscopic theory has to break down into a low-energy theory with the considered symmetries, we automatically include all possible new-physics interactions in this EFT framework. In this way one can study physics beyond the Standard Model in a completely model-independent way.

For now, let us concentrate on the first direction and see how we can generate an EFT from a microscopic UV complete theory. We will concentrate on the second aspect in the following sections. Usually,[6] one can arrive at a simplified particle physics EFT model by "integrating out" heavy degrees of freedom Φ_h of the full model which cannot be generated on-shell at the relevant energy scales and hence can be considered non-dynamical at low energy. In such a case, we can define the effective action S_{eff} in terms of the action of the full theory S as

$$\int \mathcal{D}\Phi_l \exp\{iS_{\text{eff}}\left[\Phi_l\right]\} = \int \mathcal{D}_{\Phi l}\mathcal{D}\Phi_h \exp\{iS\left[\Phi_l, \Phi_h\right]\}. \tag{3.93}$$

[5] It should be noted that there might be more or fewer degrees of freedom compared to the full theory due to possible redefinitions, e.g., there are more bound quark states than there are quarks.

[6] but not always. E.g., to arrive at chiral perturbation theory which is a low-energy approximation to QCD and describes interactions in terms of neutrons, protons, pions etc. one does not integrate out "heavy" up- and down quarks.

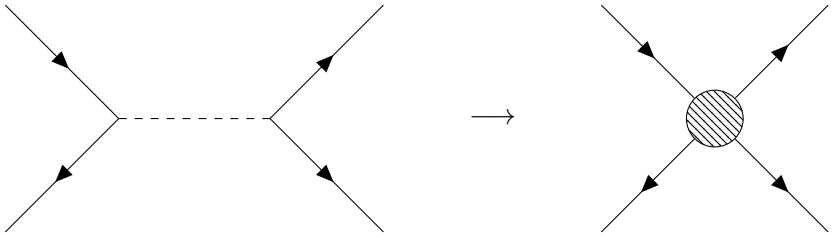

Figure 3.9.: Visualization of integrating out and matching Feynman diagrams of the microscopic full theory (left) and the corresponding macroscopic EFT (right).

In D dimensions the corresponding effective Lagrangian $\mathcal{L}_{\text{eff}}$ can be expressed as a series of local operators $\mathcal{O}_i(x)$

$$\mathcal{L}_{\text{eff}}[\Phi_l] = \sum_{i,d>0} \frac{C_i^{(d)}}{\Lambda^{d-D}} \mathcal{O}_i^{(d)}(x) \tag{3.94}$$

where Λ is the microscopic scale at which new dynamical degrees of freedom become relevant. The coefficients $C_i^{(d)}$ are known as *Wilson coefficients*. We see that at energies $\omega \ll \Lambda$ the Wilson coefficients of operators of dimension $d > 4$ get suppressed by powers of $\mathcal{O}(\omega/\Lambda)$ and thus decouple with increasing operator dimension. For this reason one may truncate the infinite operator expansion of the Lagrangian at a finite dimension N while still capturing the essential low-energy physics.
As an example, let us now consider a Yukawa theory with a real massive scalar ϕ and a massless fermion Ψ. The microscopic Lagrangian is given by

$$\mathcal{L}_Y = i\overline{\Psi}\not{\partial}\Psi - \frac{1}{2}\phi\left(\partial^\mu\partial_\mu + m_\phi^2\right)\phi + \lambda\phi\overline{\Psi}\Psi. \tag{3.95}$$

Instead of solving the functional integral in Eq. (3.93) excplicitly, we can "integrate out" ϕ by demanding that at low energies it satisfies its classical equations of motion given by the Euler-Lagrange equation

$$\frac{\partial\mathcal{L}}{\partial\phi} - \partial_\mu\frac{\partial\mathcal{L}}{\partial(\partial_\mu\phi)} = 0. \tag{3.96}$$

Solving Eq. (3.96) one finds

$$\phi = \lambda\left(\partial^\mu\partial_\mu + m_\phi^2\right)^{-1}\overline{\Psi}\Psi \tag{3.97}$$

and plugging this back into Eq. (3.95) gives us

$$\mathcal{L}_{\text{eff}} = i\overline{\Psi}\not{\partial}\Psi + \frac{\lambda^2}{2}\left(\partial^\mu\partial_\mu + m_\phi^2\right)^{-1}\overline{\Psi}\Psi\overline{\Psi}\Psi. \tag{3.98}$$

This now non-local effective Lagrangian will result in the same correlation functions as the original Lagrangian without containing the heavy field ϕ. To get an expression in

terms of local operators we can Taylor expand $\mathcal{L}_{\text{eff}}$. Doing so and switching to momentum space one finds

$$\mathcal{L}_{\text{eff}} = i\overline{\Psi}\not{\partial}\Psi + \frac{\lambda^2}{2m_\phi^2}\overline{\Psi}\Psi\overline{\Psi}\Psi - \frac{\lambda^2 p^2}{2m_\phi^4}\overline{\Psi}\Psi\overline{\Psi}\Psi + \mathcal{O}\left(\frac{p^4}{m_\phi^6}\right) \tag{3.99}$$

with $p^2 \ll m_\phi^2$. This procedure can also be understood in terms of Feynman diagrams, as represented in Figure 3.9, where we Taylor expand the scalar propagator which results in a new 4-fermion vertex.

3.4.2. Low-Energy Effective Field Theory

Let us now focus on the bottom-up aspect of EFTs turning towards our main topic, i.e., neutrinoless double-β-decay. In the previous section we addressed the possibility of non-standard long- and short-range mechanisms that can contribute to or possibly even dominate the $0\nu\beta\beta$-decay rate. Here, we will introduce an EFT framework which allows us to study the impact of different $0\nu\beta\beta$ mechanisms.
At energies below the masses of the W and Z bosons we can treat particle interactions within a low-energy EFT (LEFT) by integrating out particles with masses above $m_W \sim 80\,\text{GeV}$. Since we are now at energies below the scale of EWSB the remaining gauge symmetry of the model is $SU(3)_C \times U(1)_Q$. We can now study possible new-physics contributions to $0\nu\beta\beta$ by considering all possible effective operators which can contribute to $0\nu\beta\beta$ at tree-level within this LEFT framework. Studying limits from $0\nu\beta\beta$ experiments on the relevant LEFT operators can then give us insight into possible new high energy physics.
Looking at the Feynman diagrams of Figure 3.6 we can see that at LEFT-scale long-range mechanisms correspond to lepton number violating 4-fermion $\Delta L = 2$ interactions which contain a single quark bilinear. Hence, they should be represented by effective operators of dimension-6. If we include derivative terms, also dimension-7 and higher operators will contribute to the long-range part. Following the same line, short-range mechanisms correspond to lepton number violating $\Delta L = 2$ point-like 6-fermion interactions including 2 quark biliniears.
A $0\nu\beta\beta$ LEFT framework was first developed in [7] and [8] for the long- and short-range mechanisms respectively. They found the most general set of dimension-6 and 9 lepton number violating operators contributing to $0\nu\beta\beta$ to be given by

$$\mathcal{L}_6 = \frac{G_F}{\sqrt{2}}\sum_{i,k}\epsilon_k^i j_i J_k \tag{3.100}$$

for the long-range part with $i,k \in \{V \pm A, S \pm P, T_L, T_R,\}$ and

$$\begin{aligned}\mathcal{L}_9 = \frac{G_F^2}{2m_N}\sum_{l,m,n}\Big[&\epsilon_1^{lmn} J_l J_m j_n + \epsilon_2^{lmn} J_l^{\mu\nu} J_{\mu\nu m} j_n + \epsilon_3^{lmn} J_l^{\mu} J_{\mu m} j_n \\ &+ \epsilon_4^{lmn} J_l^{\mu} J_{\mu\nu m} j^{\nu} + \epsilon_5^{lmn} J_l^{\mu} J_m j_{\mu n}\Big]\end{aligned} \tag{3.101}$$

for the short-range part with $l, m, n \in \{L, R\}$. ϵ_k^i and ϵ^{lmn} are the Wilson coefficients of the different long- and short-range operators. The quark currents J are given by[7]

$$\begin{aligned} J_{S\pm P} &= J_{R,L} = \overline{u}\,(1 \pm \gamma_5)\, d \\ J_{V\pm A} &= J^{\mu}_{R,L} = \overline{u}\gamma^{\mu}\,(1 \pm \gamma_5)\, d \\ J_{T_{R,L}} &= J^{\mu\nu}_{R,L} = \overline{u}\sigma^{\mu\nu}\,(1 \pm \gamma_5)\, d \end{aligned} \tag{3.102}$$

and the lepton currents j are given by

$$\begin{aligned} j_{S\pm P} &= \overline{e}\,(1 \pm \gamma_5)\, \nu^c \\ j_{V\pm A} &= \overline{e}\gamma^{\mu}\,(1 \pm \gamma_5)\, \nu^c \\ j_{T_{R,L}} &= \overline{e}\sigma^{\mu\nu}\,(1 \pm \gamma_5)\, \nu^c \\ j_{R,L} &= \overline{e}\,(1 \pm \gamma_5)\, e^c \\ j^{\mu}_{R,L} &= \overline{e}\gamma^{\mu}\,(1 \pm \gamma_5)\, e^c. \end{aligned} \tag{3.103}$$

While this framework captures the most relevant operators, one should note that it contains several redundancies so that it can be further simplified. In order to do so, one needs to notice a few things:

1. In the long-range part of the Lagrangian, only operators with a right-handed lepton current will contribute to $0\nu\beta\beta$ at first order. This is because the propagating neutrino has to couple to the standard left-handed weak interaction. Other interactions will be suppressed either by a neutrino mass insertion which can flip the chirality of the propagating neutrino or by an additional effective operator with corresponding small Wilson coefficient. That is, we can take

$$\epsilon_{\alpha}^{V-A} = \epsilon_{\alpha}^{S-P} = \epsilon_{\alpha}^{T_L} = 0. \tag{3.104}$$

2. Combinations of tensor currents with different chiralities vanish. Thus, we can set

$$\epsilon_{T_L}^{T_R} = \epsilon_{T_R}^{T_L} = 0 \tag{3.105}$$

for the long-range part and similarly

$$\epsilon_2^{LRn} = \epsilon_2^{RLn} = 0 \tag{3.106}$$

for the short-range part. One can verify this by considering the Fierz transformation

[7] We keep the two different types of indices for the short-range currents to stick with the literature

of a combination of two tensor currents

$$\begin{aligned}
&\Big[\overline{\Psi}_1\sigma^{\mu\nu}\Psi_2\Big]\Big[\overline{\Psi}_3\sigma_{\mu\nu}\Psi_4\Big] \\
=&-3\Big[\overline{\Psi}_1\Psi_4\Big]\Big[\overline{\Psi}_3\Psi_2\Big]-3\Big[\overline{\Psi}_1\gamma_5\Psi_4\Big]\Big[\overline{\Psi}_3\gamma_5\Psi_2\Big] \\
&+\frac{1}{2}\Big[\overline{\Psi}_1\sigma^{\mu\nu}\Psi_4\Big]\Big[\overline{\Psi}_3\sigma_{\mu\nu}\Psi_2\Big] \\
=&-3\Big(\Big[\overline{\Psi}_1\Psi_4\Big]\Big[\overline{\Psi}_3\Psi_2\Big]+\Big[\overline{\Psi}_1\gamma_5\Psi_4\Big]\Big[\overline{\Psi}_3\gamma_5\Psi_2\Big]\Big) \\
&+\frac{1}{2}\Big(-3\Big[\overline{\Psi}_1\Psi_2\Big]\Big[\overline{\Psi}_3\Psi_4\Big]-3\Big[\overline{\Psi}_1\gamma_5\Psi_2\Big]\Big[\overline{\Psi}_3\gamma_5\Psi_4\Big]\Big) \\
&+\frac{1}{4}\Big[\overline{\Psi}_1\sigma^{\mu\nu}\Psi_2\Big]\Big[\overline{\Psi}_3\sigma_{\mu\nu}\Psi_4\Big]
\end{aligned} \tag{3.107}$$

which results in

$$\begin{aligned}
&\Big[\overline{\Psi}_1\sigma^{\mu\nu}\Psi_2\Big]\Big[\overline{\Psi}_3\sigma_{\mu\nu}\Psi_4\Big] \\
=&-4\Big[\overline{\Psi}_1\Psi_4\Big]\Big[\overline{\Psi}_3\Psi_2\Big]-4\Big[\overline{\Psi}_1\gamma_5\Psi_4\Big]\Big[\overline{\Psi}_3\gamma_5\Psi_2\Big] \\
&-2\Big[\overline{\Psi}_1\Psi_2\Big]\Big[\overline{\Psi}_3\Psi_4\Big]-2\Big[\overline{\Psi}_1\gamma_5\Psi_2\Big]\Big[\overline{\Psi}_3\gamma_5\Psi_4\Big].
\end{aligned} \tag{3.108}$$

Inserting $\Psi_2 = P_{L,R}\Psi_2$ and $\Psi_4 = P_{R,L}\Psi_4$ gives the desired result.

3. We can omit the last index in the Wilson coefficients $\epsilon_{4,5}$ and take

$$\epsilon_{4,5}^{lmn} \longrightarrow \epsilon_{4,5}^{lm} \tag{3.109}$$

by noticing that[8]

$$\begin{aligned}
\overline{\Psi}\gamma^\mu\Psi^c &= \overline{\Psi}\gamma^\mu C\overline{\Psi}^T \\
&= \left(\overline{\Psi}\gamma^\mu C\overline{\Psi}^T\right)^T \\
&= -\overline{\Psi}C^T\gamma^{\mu T}\overline{\Psi}^T \\
&= -\overline{\Psi}\gamma^\mu C\overline{\Psi}^T \\
\Rightarrow&\overline{\Psi}\gamma^\mu\Psi^c = 0
\end{aligned} \tag{3.110}$$

Additionally, we then have to redefine

$$j_{R,L}^\mu \to j^\mu = \overline{e}\gamma^\mu\gamma_5 e^c. \tag{3.111}$$

4. In the short-range part ϵ_1^{lmn} and ϵ_3^{lmn} are symmetric in the first two indices. That is, we have

$$\epsilon_{1,3}^{lmn} = \epsilon_{1,3}^{mln} \tag{3.112}$$

[8] remember that fermions are represented by anti-commuting Grassmann numbers

and can therefore choose to set

$$\epsilon_{1,3}^{LRn} = 0 \tag{3.113}$$

and only keep $\epsilon_{1,3}^{RLn}$.

Considering the above discussion about redundancies, we are left with 30 independent LEFT operators. One is given by the standard mass mechanism of light neutrino exchange, 5 operators represent different long-range mechanisms and the remaining 24 operators represent different short-range operators. After getting rid of the redundant operators we will refer to this framework as the ϵ-*basis*.
More recently [72] has introduced a different basis of $SU(3)_C \times U(1)_Q$ invariant dimension-9 operators. Together with two additional dimension-7 operators and a relabeled description of the dimension-6 operators above which were introduced by [73] the relevant Lagrangians in this basis can be written as

$$\begin{aligned}\mathcal{L}^{(6)}_{\Delta L=2} = \frac{2G_F}{\sqrt{2}}\Big[& C^{(6)}_{\mathrm{VL}} \left(\overline{u_L}\gamma^\mu d_L\right)\left(\overline{e_R}\gamma_\mu \nu_L^c\right) \\ & + C^{(6)}_{\mathrm{VR}} \left(\overline{u_R}\gamma^\mu d_R\right)\left(\overline{e_R}\gamma_\mu \nu_L^c\right) \\ & + C^{(6)}_{\mathrm{SL}} \left(\overline{u_R} d_L\right)\left(\overline{e_L}\nu_L^c\right) \\ & + C^{(6)}_{\mathrm{SR}} \left(\overline{u_L} d_R\right)\left(\overline{e_L}\nu_L^c\right) \\ & + C^{(6)}_{\mathrm{T}} \left(\overline{u_L}\sigma^{\mu\nu} d_R\right)\left(\overline{e_L}\sigma_{\mu\nu}\nu_L^c\right)\Big] + h.c.\end{aligned} \tag{3.114}$$

and

$$\begin{aligned}\mathcal{L}^{(7)}_{\Delta L=2} = \frac{2G_F}{\sqrt{2}v}\Big[& C^{(7)}_{\mathrm{VL}} \left(\overline{u_L}\gamma^\mu d_L\right)\left(\overline{e_L}\overset{\leftrightarrow}{\partial}_\mu \nu_L^c\right) \\ & + C^{(7)}_{\mathrm{VR}} \left(\overline{u_R}\gamma^\mu d_R\right)\left(\overline{e_L}\overset{\leftrightarrow}{\partial}_\mu \nu_L^c\right)\Big] + h.c.\end{aligned} \tag{3.115}$$

for the long-range part, where

$$\alpha \overset{\leftrightarrow}{\partial} \beta = (\partial\alpha)\beta - \alpha(\partial\beta). \tag{3.116}$$

The dimension-9 short-range operators can be written as

$$\begin{aligned}\mathcal{L}^{(9)}_{\Delta L=2} = \frac{1}{v^5}\sum_i \Big[& \Big(C^{(9)}_{i,R} \left(\overline{e_R} e_R^c\right) \\ & + C^{(9)}_{i,L} \left(\overline{e_L} e_L^c\right)\Big)\, \mathcal{O}_i \\ & + C^{(9)}_{i} \left(\overline{e}\gamma_\mu\gamma_5 e^c\right)\, \mathcal{O}_i^\mu\Big]\end{aligned} \tag{3.117}$$

with the scalar $\mathcal{O}_i$ and vector $\mathcal{O}_i^\mu$ four-quark operators [72, 74]

$$\mathcal{O}_1 = \left(\overline{u_L}^\alpha \gamma_\mu d_L^\alpha\right)\left(\overline{u_L}^\beta \gamma^\mu d_L^\beta\right), \qquad \mathcal{O}'_1 = \left(\overline{u_R}^\alpha \gamma_\mu d_R^\alpha\right)\left(\overline{u_R}^\beta \gamma^\mu d_R^\beta\right), \tag{3.118}$$

$$\mathcal{O}_2 = \left(\overline{u_R}^\alpha d_L^\alpha\right)\left(\overline{u_R}^\beta d_L^\beta\right), \qquad \mathcal{O}'_2 = \left(\overline{u_L}^\alpha d_R^\alpha\right)\left(\overline{u_L}^\beta d_R^\beta\right), \tag{3.119}$$

$$\mathcal{O}_3 = \left(\overline{u_R}^\alpha d_L^\beta\right)\left(\overline{u_R}^\beta d_L^\alpha\right), \qquad \mathcal{O}'_3 = \left(\overline{u_L}^\alpha d_R^\beta\right)\left(\overline{u_L}^\beta d_R^\alpha\right), \tag{3.120}$$

$$\mathcal{O}_4 = \left(\overline{u_L}^\alpha \gamma_\mu d_L^\alpha\right)\left(\overline{u_R}^\beta \gamma^\mu d_R^\beta\right), \tag{3.121}$$

$$\mathcal{O}_5 = \left(\overline{u_L}^\alpha \gamma_\mu d_L^\beta\right)\left(\overline{u_R}^\beta \gamma^\mu d_R^\alpha\right), \tag{3.122}$$

$$\mathcal{O}_6^\mu = \left(\overline{u_L}\gamma^\mu d_L\right)\left(\overline{u_L} d_R\right), \qquad \mathcal{O}_6^{\mu\prime} = \left(\overline{u_R}\gamma^\mu d_R\right)\left(\overline{u_R} d_L\right), \tag{3.123}$$

$$\mathcal{O}_7^\mu = \left(\overline{u_L}\lambda^A\gamma^\mu d_L\right)\left(\overline{u_L}\lambda^A d_R\right), \qquad \mathcal{O}_7^{\mu\prime} = \left(\overline{u_R}\lambda^A\gamma^\mu d_R\right)\left(\overline{u_R}\lambda^A d_L\right), \tag{3.124}$$

$$\mathcal{O}_8^\mu = \left(\overline{u_L}\gamma^\mu d_L\right)\left(\overline{u_R} d_L\right), \qquad \mathcal{O}_8^{\mu\prime} = \left(\overline{u_R}\gamma^\mu d_R\right)\left(\overline{u_L} d_R\right), \tag{3.125}$$

$$\mathcal{O}_9^\mu = \left(\overline{u_L}\lambda^A\gamma^\mu d_L\right)\left(\overline{u_R}\lambda^A d_L\right), \qquad \mathcal{O}_9^{\mu\prime} = \left(\overline{u_R}\lambda^A\gamma^\mu d_R\right)\left(\overline{u_L}\lambda^A d_R\right), \tag{3.126}$$

where α, β are color-indices and $\lambda^A, A = 1...8$ are the generators of SU(3) in the fundamental representation given by the 8 Gell-Mann matrices. The operators $\mathcal{O}$ and $\mathcal{O}'$ are related via parity transformation. We will refer to this framework as the *C-basis*. Compared to the *ϵ-basis* the *C-basis* contains no tensor currents but instead contains color-octet operators. Including the standard mass mechanism and the corresponding coefficient $m_{\beta\beta}$, it also consists of 32 instead of 30 operators due to the addition of the two dimension-7 operators.

The short-range parts of the ϵ-*basis* and the C-*basis* are related via Fierz transformations.

$$C_{1L}^{(9)} = \frac{2v}{m_N}\epsilon_3^{LLL}, \quad C_{1L}^{(9)\prime} = \frac{2v}{m_N}\epsilon_3^{RRL}, \quad C_{1R}^{(9)} = \frac{2v}{m_N}\epsilon_3^{LLR}, \quad C_{1R}^{(9)\prime} = \frac{2v}{m_N}\epsilon_3^{RRR} \tag{3.127}$$

$$\begin{aligned} C_{2L}^{(9)} &= \frac{2v}{m_N}\left(\epsilon_1^{LLL} - 4\epsilon_2^{LLL}\right), \quad C_{2L}^{(9)\prime} = \frac{2v}{m_N}\left(\epsilon_1^{RRL} - 4\epsilon_2^{RRL}\right) \\ C_{2R}^{(9)} &= \frac{2v}{m_N}\left(\epsilon_1^{LLR} - 4\epsilon_2^{LLR}\right), \quad C_{2R}^{(9)\prime} = \frac{2v}{m_N}\left(\epsilon_1^{RRR} - 4\epsilon_2^{RRR}\right) \end{aligned} \tag{3.128}$$

$$C_{3L}^{(9)} = -\frac{16v}{m_N}\epsilon_2^{LLL}, \quad C_{3L}^{(9)\prime} = -\frac{16v}{m_N}\epsilon_2^{RRL}, \quad C_{3R}^{(9)} = -\frac{16v}{m_N}\epsilon_2^{LLR}, \quad C_{3R}^{(9)\prime} = -\frac{16v}{m_N}\epsilon_2^{RRR} \tag{3.129}$$

$$C_{4L}^{(9)} = \frac{2v}{m_N}\epsilon_3^{RLL}, \quad C_{4R}^{(9)} = \frac{2v}{m_N}\epsilon_3^{RLR} \tag{3.130}$$

$$C_{5L}^{(9)} = -\frac{v}{m_N}\epsilon_1^{RLL}, \quad C_{5R}^{(9)} = -\frac{v}{m_N}\epsilon_1^{RLR} \tag{3.131}$$

$$!C_6^{(9)} = \frac{v}{m_N}\left(\epsilon_5^{LRR} + i\frac{5}{3}\epsilon_4^{LRR}\right), \quad C_6^{(9)\prime} = \frac{v}{m_N}\left(\epsilon_5^{RLR} + i\frac{5}{3}\epsilon_4^{RLR}\right) \tag{3.132}$$

$$!C_7^{(9)} = i\frac{v}{m_N}\epsilon_4^{LRR}, \quad C_7^{(9)\prime} = i\frac{v}{m_N}\epsilon_4^{RLR} \tag{3.133}$$

$$C_8^{(9)} = \frac{v}{m_N}\left(\epsilon_5^{LLR} - i\frac{5}{3}\epsilon_4^{LLR}\right), \quad C_8^{(9)\prime} = \frac{v}{m_N}\left(\epsilon_5^{RRR} - i\frac{5}{3}\epsilon_4^{RRR}\right) \tag{3.134}$$

$$!C_9^{(9)} = -i\frac{v}{m_N}\epsilon_4^{LLR}, \quad C_9^{(9)\prime} = -i\frac{v}{m_N}\epsilon_4^{RRR} \tag{3.135}$$

The complete derivation of the above relations is given in appendix A. We want to note that the translations marked by an '!' differ from the translation derived in [74].
While this treatment is suitable to study new-physics at low energies, one can study new-physics aspects at higher energies above EWSB by treating the Standard Model within its full $SU(3)_C \times SU(2)_L \times U(1)_Y$ gauge symmetry as an EFT (SMEFT). Comparing to SMEFT, out of the 24 short-range operators 3 corresponding to $C_{1L}^{(9)}, C_{4L}^{(9)}$ and $C_{5L}^{(9)}$ are induced at SMEFT dimension-7 while eleven operators corresponding to $C_{2-5L}^{(9)}, C_{2L,3L}^{(9)\prime}, C_{1R}^{(9)\prime}$ and $C_{6-9}^{(9)\prime}$ receive contributions from SMEFT dimension-9 operators [72, 74]. These can be considered to give the most relevant contributions from a phenomenological point of view as higher dimensional operators are suppressed by additional powers of v/Λ_{BSM}. A full SMEFT basis up to dimension-9 was unavailable for a long time and has only been found recently [75, 76]. Additionally, we do not know if SMEFT will be the correct completion to a $0\nu\beta\beta$ inducing new-physics. Therefore, we will consider the LEFT basis as our main focus to study as a low-energy theory is the more natural way to go.

3.4.3. Chiral Perturbation Theory

While QCD is asymptotically free, its coupling constant grows with decreasing energy scale and perturbation theory breaks down at a scale of $\Lambda_\chi \sim 2\,\text{GeV}$. A possible way to

describe QCD interactions below this scale, e.g., nuclear processes, is given by the application of the so-called chiral perturbation theory (χPT) [77]. χPT builds upon the fact that in the limit $m_{u,d,s} \to 0$ at GEV scales QCD has a global chiral $SU(3)_L \times SU(3)_R$ symmetry which, however, is not present in the ground state of the theory. The spontaneous breaking of this approximate symmetry induces 8 light pseudoscalar mesons via Goldstone's theorem. Instead of quarks, the relevant fermionic degrees of freedom are given by bound quark states such as protons and neutrons. One can obtain the χPT Lagrangian by including all nucleon-pion operators which obey the chiral symmetry and expanding in terms of a power counting scheme m_π/Λ_χ. The χPT Wilson coefficients are usually referred to as low-energy constants (LECs) and have to be determined experimentally, from lattice calculations or estimated from naive dimensional analysis (NDA) [73]. Given sufficient knowledge about the LECs, χPT can be used to make predictions about low-energy QCD processes which cannot be described within the usual perturbative methods. Hence, χPT is a natural way to go when trying to describe nuclear processes.

3.5. A $0\nu\beta\beta$ Effective Field Theory "Master-Formula"

In this section we want to summarize the EFT framework introduced in [73, 74], the $0\nu\beta\beta$ "master-formula", that we will apply in this work. The general idea behind it is that, assuming no contributions from light new-physics, one can describe $0\nu\beta\beta$-decay in some arbitrary BSM model by a chain of matching onto effective field theories BSM$\to$ SMEFT $\to$ LEFT $\to\chi$PT.[9] At the chiral EFT scale the expected $0\nu\beta\beta$ half-life can be written in terms of the LECs as well as the 32 LEFT operators and of course the corresponding NMEs and PSFs. The most general transition amplitude can be written as [74]

$$\begin{aligned}\mathcal{A} = \frac{g_A^2 G_F^2 m_e}{\pi R}\Big[&\mathcal{A}_\nu \overline{u}\left(p_1\right) P_R u^c\left(p_2\right) + \mathcal{A}_R \overline{u}\left(p_1\right) P_L u^c\left(p_2\right) \\ &+ \mathcal{A}_E \overline{u}\left(p_1\right) \gamma_0 u^c\left(p_2\right) \frac{E_1 - E_2}{m_e} + \mathcal{A}_{m_e} \overline{u}\left(p_1\right) u^c\left(p_2\right) \\ &+ \mathcal{A}_M \overline{u}\left(p_1\right) \gamma_0\gamma_5 u^c\left(p_2\right)\Big]\end{aligned} \tag{3.136}$$

where the subamplitudes $\mathcal{A}_i$ describe the contributions to the different lepton currents. Their definitions are given in Eq. (3.138)-(3.142). To arrive at the half-life formula one again has to take the absolute square of Eq. (3.136). In order to do so, one has to calculate 11 different lepton current traces. These correspond to the usual 11 PSFs given, e.g., in [78]. However, these 11 PSFs contain several redundancies such that only 6 different PSFs are necessary to describe the full half-life formula. The solutions to the different lepton current traces are given in Appendix B. Following this, after taking the absolute

[9] Of course χPT is extended by leptons. If desired one can also skip the first step and directly match onto LEFT. This might even be necessary for some BSM models.

square of the transition amplitude, the half-life can be written as

$$\begin{aligned}\left(T_{1/2}^{0\nu}\right)^{-1} =& g_A^4\Big[G_{01}\left(|\mathcal{A}_\nu|^2+|\mathcal{A}_R|^2\right)-2\left(G_{01}-G_{04}\right)\mathrm{Re}\left[\mathcal{A}_\nu^*\mathcal{A}_R\right]\\ &+4G_{02}\left|\mathcal{A}_E\right|^2+2G_{04}\left(|\mathcal{A}_{m_e}|^2+\mathrm{Re}\left[\mathcal{A}_{m_e}^*\left(\mathcal{A}_\nu+\mathcal{A}_R\right)\right]\right)\\ &-2G_{03}\,\mathrm{Re}\left[\left(\mathcal{A}_\nu+\mathcal{A}_R\right)\mathcal{A}_E^*+2\mathcal{A}_{m_e}\mathcal{A}_E^*\right]\\ &+G_{09}\left|\mathcal{A}_M\right|^2+G_{06}\,\mathrm{Re}\left[\left(\mathcal{A}_\nu-\mathcal{A}_R\right)\mathcal{A}_M^*\right]\Big]\end{aligned} \tag{3.137}$$

which is the aforementioned "master-formula". The sub amplitudes $\mathcal{A}_i$ each depend on different LEFT operators and can be written as

$$\begin{aligned}\mathcal{A}_\nu =& \frac{m_{\beta\beta}}{m_e}\mathcal{M}_\nu^{(3)}\\ &+\frac{m_N}{m_e}\mathcal{M}_\nu^{(6)}\left(C_{\mathrm{SL}}^{(6)},C_{\mathrm{SR}}^{(6)},C_{\mathrm{T}}^{(6)},C_{\mathrm{VL}}^{(7)},C_{\mathrm{VR}}^{(7)}\right)\\ &+\frac{m_N^2}{m_e v}\mathcal{M}_\nu^{(9)}\left(C_{1\mathrm{L}}^{(9)},C_{1\mathrm{L}}^{(9)\prime},C_{2\mathrm{L}}^{(9)},C_{2\mathrm{L}}^{(9)\prime},C_{3\mathrm{L}}^{(9)},C_{3\mathrm{L}}^{(9)\prime},C_{4\mathrm{L}}^{(9)},C_{5\mathrm{L}}^{(9)}\right),\end{aligned} \tag{3.138}$$

$$\mathcal{A}_R = \frac{m_N^2}{m_e v}\mathcal{M}_R^{(9)}\left(C_{1\mathrm{R}}^{(9)},C_{1\mathrm{R}}^{(9)\prime},C_{2\mathrm{R}}^{(9)},C_{2\mathrm{R}}^{(9)\prime},C_{3\mathrm{R}}^{(9)},C_{3\mathrm{R}}^{(9)\prime},C_{4\mathrm{R}}^{(9)},C_{5\mathrm{R}}^{(9)}\right), \tag{3.139}$$

$$\begin{aligned}\mathcal{A}_E =& \mathcal{M}_{E,L}^{(6)}\left(C_{\mathrm{VL}}^{(6)}\right)\\ &+\mathcal{M}_{E,R}^{(6)}\left(C_{\mathrm{VR}}^{(6)}\right),\end{aligned} \tag{3.140}$$

$$\begin{aligned}\mathcal{A}_{m_e} =& \mathcal{M}_{m_e,L}^{(6)}\left(C_{\mathrm{VL}}^{(6)}\right)\\ &+\mathcal{M}_{m_e,R}^{(6)}\left(C_{\mathrm{VR}}^{(6)}\right),\end{aligned} \tag{3.141}$$

$$\begin{aligned}\mathcal{A}_M =& \frac{m_N}{m_e}\mathcal{M}_M^{(6)}\left(C_{\mathrm{VL}}^{(6)}\right)\\ &+\frac{m_N^2}{m_e v}\mathcal{M}_M^{(9)}\left(C_6^{(9)},C_6^{(9)\prime},C_7^{(9)},C_7^{(9)\prime},C_8^{(9)},C_8^{(9)\prime},C_9^{(9)},C_9^{(9)\prime}\right).\end{aligned} \tag{3.142}$$

Here we explicitly emphasized the dependency of each matrix element $\mathcal{M}_i$ on the different operators. The matrix elements $\mathcal{M}_i$ depend on the different LECs and operators. $\mathcal{A}_\nu$ depends on the matrix elements

$$\begin{aligned}\mathcal{M}_\nu^{(3)} &= -V_{ud}^2\left(-\frac{1}{g_A^2}M_F+\mathcal{M}_{GT}+\mathcal{M}_T+2\frac{m_\pi^2\mathbf{g}_\nu^{\mathbf{NN}}}{g_A^2}M_{F,sd}\right),\\ \mathcal{M}_\nu^{(6)} &= V_{ud}\left(\frac{B}{m_N}\left(C_{SL}^{(6)}-C_{SR}^{(6)}\right)+\frac{m_\pi^2}{m_N v}\left(C_{VL}^{(7)}-C_{VR}^{(7)}\right)\right)\mathcal{M}_{PS}+V_{ud}C_{\mathrm{T}}^{(6)}\mathcal{M}_{T6},\\ \mathcal{M}_\nu^{(9)} &= -\frac{1}{2m_N^2}C_{\pi\pi L}^{(9)}\left(M_{GT,sd}^{AP}+M_{T,sd}^{AP}\right)-\frac{2m_\pi^2}{g_A^2 m_N^2}C_{NNL}^{(9)}M_{F,sd},\end{aligned} \tag{3.143}$$

$\mathcal{A}_R$ is given by

$$\mathcal{M}_R^{(9)} = \mathcal{M}_\nu^{(9)}|_{L\to R}, \tag{3.144}$$

for $\mathcal{A}_E$ the different contributions are

$$\begin{aligned}
\mathcal{M}_{E,L}^{(6)} &= -\frac{V_{ud}C_{VL}^{(6)}}{3}\left(\frac{g_V^2}{g_A^2}M_F + \frac{1}{3}\left(2M_{GT}^{AA} + M_T^{AA}\right) + \frac{6\mathbf{g_{V\,L}^E}}{g_A^2}M_{F,sd}\right),\\
\mathcal{M}_{E,R}^{(6)} &= -\frac{V_{ud}C_{VR}^{(6)}}{3}\left(\frac{g_V^2}{g_A^2}M_F - \frac{1}{3}\left(2M_{GT}^{AA} + M_T^{AA}\right) + \frac{6\mathbf{g_{V\,L}^E}}{g_A^2}M_{F,sd}\right),
\end{aligned} \tag{3.145}$$

$\mathcal{A}_{m_e}$ is determined by

$$\begin{aligned}
\mathcal{M}_{m_e,L}^{(6)} &= \frac{V_{ud}C_{VL}^{(6)}}{6}\Bigg(\frac{g_V^2}{g_A^2}M_F - \frac{1}{3}\left(M_{GT}^{AA} - 4M_T^{AA}\right) - 3\left(M_{GT}^{AP} + M_{GT}^{PP} + M_T^{AP} + M_T^{PP}\right)\\
&\qquad - \frac{12\mathbf{g_{V\,L}^{m_e}}}{g_A^2}M_{F,sd}\Bigg),\\
\mathcal{M}_{m_e,R}^{(6)} &= \frac{V_{ud}C_{VR}^{(6)}}{6}\Bigg(\frac{g_V^2}{g_A^2}M_F + \frac{1}{3}\left(M_{GT}^{AA} - 4M_T^{AA}\right) + 3\left(M_{GT}^{AP} + M_{GT}^{PP} + M_T^{AP} + M_T^{PP}\right)\\
&\qquad - \frac{12\mathbf{g_{V\,L}^{m_e}}}{g_A^2}M_{F,sd}\Bigg),
\end{aligned} \tag{3.146}$$

and finally $\mathcal{A}_M$ is given by

$$\begin{aligned}
\mathcal{M}_M^{(6)} &= V_{ud}C_{VL}^{(6)}\Bigg[2\frac{g_A}{g_M}\left(M_{GT}^{MM} + M_T^{MM}\right)\\
&\qquad + \frac{m_\pi^2}{m_N^2}\left(-\frac{2}{g_A^2}\mathbf{g_{VL}^{NN}}M_{F,sd} + \frac{1}{2}\mathbf{g_{VL}^{\pi N}}\left(M_{GT,sd}^{AP} + M_{T,sd}^{AP}\right)\right)\Bigg],\\
\mathcal{M}_M^{(9)} &= \frac{m_\pi^2}{m_N^2}\Bigg[-\frac{2}{g_A^2}\left(\mathbf{g_6^{NN}}C_V^{(9)} + \mathbf{g_7^{NN}}\tilde{C}_V^{(9)}\right)M_{F,sd}\\
&\qquad + \frac{1}{2}\left(\mathbf{g_V^{\pi N)}}C_V^{(9)} + \tilde{\mathbf{g}}_\mathbf{V}^{\pi\mathbf{N}}\tilde{C}_V^{(9)}\right)\left(M_{GT,sd}^{AP} + M_{T,sd}^{AP}\right)\Bigg].
\end{aligned} \tag{3.147}$$

In the above formulas we defined the combined NMEs

$$\begin{aligned}
\mathcal{M}_{GT} &= M_{GT}^{AA} + M_{GT}^{AP} + M_{GT}^{PP} + M_{GT}^{MM},\\
\mathcal{M}_T &= M_T^{AP} + M_T^{PP} + M_T^{MM},\\
\mathcal{M}_{PS} &= \frac{1}{2}M_{GT}^{AP} + M_{GT}^{PP} + \frac{1}{2}M_T^{AP} + M_T^{PP},\\
\mathcal{M}_{T6} &= 2\frac{\mathbf{g_T'} - \mathbf{g_T^{NN}}}{g_A^2}\frac{m_\pi^2}{m_N^2}M_{F,sd} - \frac{8g_T}{g_M}\left(M_{GT}^{MM} + M_T^{MM}\right)\\
&\qquad + \mathbf{g_T^{\pi N}}\frac{m_\pi^2}{4m_N^2}\left(M_{GT,sd}^{AP} + M_{T,sd}^{AP}\right) + \mathbf{g_T^{\pi\pi}}\frac{m_\pi^2}{4m_N^2}\left(M_{GT,sd}^{PP} + M_{T,sd}^{PP}\right).
\end{aligned} \tag{3.148}$$

The short-range dimension-9 LEFT operators contribute to the $C^{(9)}_{V,\pi,\pi NL,NNL}$ couplings that appear in the chiral Lagrangian. They are given by

$$\begin{aligned}
C_V^{(9)} &= C_6^{(9)} + C_6^{(9)\prime} + C_8^{(9)} + C_8^{(9)\prime} \\
\tilde{C}_V^{(9)} &= C_7^{(9)} + C_7^{(9)\prime} + C_9^{(9)} + C_9^{(9)\prime} \\
C_{\pi\pi L}^{(9)} &= g_2^{\pi\pi}\left(C_{2L}^{(9)} + C_{2L}^{(9)\prime}\right) + g_3^{\pi\pi}\left(C_{3L}^{(9)} + C_{3L}^{(9)\prime}\right) \\
&\quad - g_4^{\pi\pi} C_{4L}^{(9)} - g_5^{\pi\pi} C_{5L}^{(9)} - \frac{5}{3} g_1^{\pi\pi} m_\pi^2 \left(C_{1L}^{(9)} + C_{1L}^{(9)\prime}\right) \\
C_{\pi NL}^{(9)} &= \left(\mathbf{g_1^{\pi N}} - \frac{5}{6} g_1^{\pi\pi}\right)\left(C_{1L}^{(9)} + C_{1L}^{(9)\prime}\right) \\
C_{NNL}^{(9)} &= \mathbf{g_1^{NN}}\left(C_{1L}^{(9)} + C_{1L}^{(9)\prime}\right) + \mathbf{g_2^{NN}}\left(C_{2L}^{(9)} + C_{2L}^{(9)\prime}\right) \\
&\quad + \mathbf{g_3^{NN}}\left(C_{3L}^{(9)} + C_{3L}^{(9)\prime}\right) + \mathbf{g_4^{NN}} C_{4L}^{(9)} + \mathbf{g_5^{NN}} C_{5L}^{(9)} \\
C_{\{\pi\pi,\pi N,NN\}R} &= C_{\{\pi\pi,\pi N,NN\}L}|_{L\to R}\,.
\end{aligned} \tag{3.149}$$

The two LECs $g_V^{\pi N}$ and $\tilde{g}_V^{\pi N}$ are defined as

$$\begin{aligned}
\mathbf{g_V^{\pi N}} &= \mathbf{g_6^{\pi N}} + \mathbf{g_8^{\pi N}} \\
\mathbf{\tilde{g}_V^{\pi N}} &= \mathbf{g_7^{\pi N}} + \mathbf{g_9^{\pi N}}
\end{aligned} \tag{3.150}$$

In the above formulas we marked the currently unknown LECs **bold**. This "master-formula" framework depends on the PSFs which can be calculated almost exactly [29], the NMEs which we will cover in the following Sec. 3.6, the different LECs which can be obtained from, e.g., experiments or lattice calculations and finally the different LEFT operators that represent the new-physics components. The necessary LECs were given in the original publication [74] and are summarized for convencience in Table 3.3. This framework has the very nice property that only NMEs appear which can be extracted from simulations of the light neutrino-exchange mechanism as well as from simulations of heavy neutrino-exchange. Since we want to study the impact of different mechanisms in various isotopes, we use the largest set of NMEs that we could find coming from a single approach. These NMEs are calculated within the *quasi-particle random phase approximation* (QRPA) [79]. The numerical values are given in Table 3.2. In this study we do our calculations both with assuming NDA values for the unknown LECs and with assuming the unknown LECs to vanish. However, we want to stress that when taking the unknown LECs to vanish, we do keep $g_{1,6,7}^{NN} = g_V^{\pi N} = \tilde{g}_V^{\pi N} = 1$ since otherwise any contributions from the short-range vector operators would vanish.

3.6. Approaches to Nuclear Matrix Elements

One of the main issues when studying $0\nu\beta\beta$-decay is given by the calculation of the nuclear matrix elements. These are the main source of uncertainty when calculating $0\nu\beta\beta$ half-lives as different calculation methods tend to disagree by factors of two or

NME	^{76}Ge	^{82}Se	^{96}Zr	^{100}Mo	^{110}Pd	^{116}Cd	^{124}Sn	^{128}Te	^{130}Te	^{136}Xe
M_F	-1.74	-1.29	-1.44	-1.63	-2.32	-1.5	-2.33	-1.78	-1.52	-0.89
M_{GT}^{AA}	5.48	3.87	3.17	3.96	6.60	4.24	5.41	5.23	4.28	3.17
M_{GT}^{AP}	-2.02	-1.46	-1.45	-1.68	-2.44	-1.45	-2.27	-2.05	-1.74	-1.19
M_{GT}^{PP}	0.66	0.48	0.50	0.57	0.80	0.47	0.77	0.69	0.59	0.40
M_{GT}^{MM}	0.51	0.37	0.40	0.44	0.62	0.35	0.62	0.53	0.47	0.30
M_{T}^{AA}	-	-	-	-	-	-	-	-	-	-
M_{T}^{AP}	-0.35	-0.27	-0.30	-0.34	-0.37	-0.22	-0.57	-0.54	-0.50	-0.28
M_{T}^{PP}	0.10	0.079	0.10	0.11	0.13	0.08	0.18	0.18	0.16	0.09
M_{T}^{MM}	-0.04	-0.03	-0.04	-0.04	-0.05	-0.03	-0.06	-0.07	-0.06	-0.03
M_{Fsd}	-3.43	-2.51	-2.81	-3.12	-4.13	-2.51	-4.15	-3.41	-2.94	-1.52
M_{GTsd}^{AA}	11.03	7.90	8.52	9.85	13.20	7.73	12.84	11.61	9.98	5.66
M_{GTsd}^{AP}	-5.30	-3.79	-4.22	-4.85	-6.30	-3.65	-6.25	-5.67	-4.90	-2.77
M_{GTsd}^{PP}	1.97	1.41	1.60	1.83	2.33	1.34	2.34	2.13	1.85	1.05
M_{Tsd}^{AP}	-0.84	-0.64	-0.91	-1.10	-1.19	-0.77	-1.58	-1.63	-1.49	-0.91
M_{Tsd}^{PP}	0.31	0.24	0.35	0.43	0.46	0.30	0.61	0.63	0.58	0.35

Table 3.2.: $0\nu\beta\beta$ QRPA NMEs in different isotopes [79]. Note that, due to different definitions, the short-distance NMEs used in [74] are connected to the heavy neutrino exchange NMEs in [79] via rescaling by $\frac{1}{m_e m_p}$.

Known		Unknown	
g_A	1.271	$\lvert g_T' \rvert$	$\mathcal{O}(1)$
g_S	0.97 [80]	$\lvert g_T \pi\pi \rvert$	$\mathcal{O}(1)$
g_M	4.7	$\lvert g^{\pi N}_{1,6,7,8,9} \rvert$	$\mathcal{O}(1)$
g_T	0.99 [80]	$\lvert g^{\pi N}_{VL} \rvert$	$\mathcal{O}(1)$
B	2.2 GeV	$\lvert g^{\pi N}_{T} \rvert$	$\mathcal{O}(1)$
$g_1^{\pi\pi}$	0.36 [81]	$\lvert g^{NN}_{1,6,5} \rvert$	$\mathcal{O}(1)$
$g_2^{\pi\pi}$	2.0 [81]	$\lvert g^{NN}_{2,3,4,5} \rvert$	$\mathcal{O}((4\pi)^2)$
$g_3^{\pi\pi}$	-0.62 [81]	$\lvert g^{NN}_{VL} \rvert$	$\mathcal{O}(1)$
$g_4^{\pi\pi}$	-1.9 [81]	$\lvert g^{NN}_{T} \rvert$	$\mathcal{O}(1)$
$g_5^{\pi\pi}$	-8.0 [81]	$\lvert g^{NN}_{\nu} \rvert$	$\mathcal{O}(1/F_\pi^2)$
		$\lvert g^{E,m_e}_{VL,VR} \rvert$	$\mathcal{O}(1)$

Table 3.3.: Summary of the low-energy constants necessary to calculate the $0\nu\beta\beta$ half-life for all 32 different operators. The table is taken from [74] and restructured. The pion decay constant is $F_\pi = 92.2\,\text{MeV}$.

three. Hence, in the last part of this chapter we want to briefly summarize the most important aspects about nuclear matrix element calculations following [31, 82].
Precisely calculating NMEs is a challenging task as the wave-functions of the initial and final state nuclei cannot be solved exactly. Instead, one needs to calculate the initial

and final state wave-functions approximately by solving the non-relativistic Schroedinger equation in one of a few different nuclear model approaches[10]:

The Nuclear Shell Model

The *nuclear shell model* (NSM) [83] considers only those nucleons near the Fermi surface to be relevant for the $0\nu\beta\beta$ transition amplitude. Thus, the Schrödinger equation is only solved for a small subset of the full many body Hilbert space. Additionally, an effective interaction Hamiltonian is used which is fitted to reproduce nuclear properties and observables such as, e.g., scattering data. The NSM includes all correlations around the Fermi surface. Limiting the configuration space, as it is done here, could lead to an underestimation of the NMEs.

The Quasi-Particle Random Phase Approximation

Together with the nuclear shell model, the *quasi-particle random phase approximation* (QRPA) [79] is probably the major method for NME calculations. While the NSM only includes a few particles mostly within a single shell, QRPA can capture the effects of multiple shells, however, containing fewer correlations. Calculation parameters are usually fixed towards replicating the experimental $2\nu\beta\beta$ half-lives. Typically, QRPA simulations result in larger NMEs compared to the NSM approach.

The Interacting Boson Model

In the *interacting boson model* (IBM) [84, 85] pairs of nucleons are summarized as bosons. The calculation is connected to the shell model. However, more shells are taken into account. Although IBM is build to approximate the shell model, it often gives NMEs close to the ones calculated within QRPA.

Ab initio methods

Recently, ab initio methods have opened a promising new window towards more accurate NME calculations [86]. They try to systematically remove approximations by including the full set of nucleons as well as determining interactions from nucleon-nucleon scattering data and other few-nuclei systems sometimes via relating to χPT. One of the promising features is that such an approach can allow quantifying the uncertainties on the calculations. This would be a huge advancement in the field of NMEs. However, ab initio calculations are typically computationally heavy and therefore hard to apply onto large nuclei which are relevant for $0\nu\beta\beta$ such as, e.g., ^{136}Xe. First calculations for ^{48}Ca have been already obtained [86].

The NMEs we use are calculated within QRPA and given in Table 3.2.

[10] When throwing the closure approximation over board, the calculations become even more complicated and computationally heavy as the intermediate states have to be taken into account.

4. Finding The Underlying Mechanism

In the previous chapter we saw that there are many different effective operators and hence many different models beyond the Standard Model that can induce $0\nu\beta\beta$-decay. Therefore, while a possible observation of $0\nu\beta\beta$ would indeed indicate that neutrinos are Majorana particles, we do not know if the mass mechanism would be the dominating contribution. The question remains how one can possibly distinguish or even identify the leading order contribution and by this infer more information about the full BSM theory. In this chapter we want to discuss and investigate possibilities to distinguish different effective operators as well as some more complex models.

4.1. Distinguishing different Operators

Neutrinoless double-β-decay, if observed, would be characterized by several experimental observables. Precise knowledge of these observables can give us some insight into the underlying mechanism. In general there are three different observables which can be studied in $0\nu\beta\beta$-decay experiments:

1. The decay rate
2. The single electron energy spectrum
3. The angular correlation between the two emitted electrons.

Additional information can be gained by including different double-β modes and by cross-checking with high-energy collider experiments like the LHC. We will start by shortly discussing the last possibility. Afterwards, we will focus on the possibilities to gain insight from $0\nu\beta\beta$-decay experiments which is the focus of this work.

4.1.1. Cross-Checking with High-Energy Collider Experiments

In some sense, nuclear decay experiments can be understood as high luminosity low-energy hadron-collider experiments as the nuclear $0\nu\beta\beta$-decay process resembles a scattering process

$$n + n \longrightarrow p + p + 2e^{-}. \tag{4.1}$$

As with decay experiments, outgoing neutrinos cannot be detected directly within collider experiments and only show up as missing transverse energy. There are three different signatures that can be used to study both long- and short-range operators:

1. Same-Sign Dilepton Signals

$$p + p \longrightarrow 2e^{\pm} + 2\text{jets} \tag{4.2}$$

2. Missing Transverse Energy (MTE)

$$p + p \longrightarrow 1e^{\pm} + 2\text{jets} + \text{MTE} \tag{4.3}$$

3. Dijet with Missing Transverse Energy

$$p + p \longrightarrow 2\text{jets} + \text{MTE}. \tag{4.4}$$

While the appearance of same sign dilepton signals is quite obviously just the same process as $0\nu\beta\beta$ just at higher energies, the remaining two signatures have a high-energy origin. At typical TeV collider energies the LEFT treatment is no longer sufficient and a SMEFT treatment has to be applied. Therefore, low-energy operators coupling to left-handed leptons originate from SMEFT operators containing a left-handed lepton doublet. Hence, at collider energies we have processes with outgoing neutrinos induced by the SMEFT completion of the short-range LEFT operators that contain $e_L^{(c)}$ as well as outgoing electrons resulting from the completion of long-range mechanisms that contain ν_L^c. Following the above reasoning, one can utilize collider data to distinguish $0\nu\beta\beta$ inducing lepton number violating SMEFT operators of three types via their lepton currents[1][2]

1. ... $\left[\overline{L}L^c\right]$ operators induce all three signatures.

2. ... $\left[\overline{L}e_R^c\right]$ operators induce same-sign dilepton signatures as well as single leptons with missing transverse energy.

3. ... $[\overline{e_R}e_R^c]$ operators only result in the same-sign dilepton signature.

One should note that here we assume that no right-handed neutrinos exist at current collider energies and we do not have to include right-handed lepton doublets. While the full set of SMEFT operators which induce the 32 $\Delta L = 2$ LEFT operators is currently unknown, one can find a set of electroweak invariant operators by systematically adding factors of $\Phi^\dagger\Phi$ [72]. When doing this, one finds that out of the 24 short-range operators 11 can be written in a $SU(2)_L \times U(1)_Y$ invariant way without adding any factors of $\Phi^\dagger\Phi$, 12 LEFT operators have to be extended by one factor of $\Phi^\dagger\Phi$ resulting in 19 additional dimension-11 SMEFT operators and finally the single remaining LEFT operator has to be extended by $(\Phi^\dagger\Phi)^2$ to arrive at an electroweak invariant dimension-13 operator. When

[1] Here we do not write down all possible Lorentz structures explicitly. Instead these lepton currents should be understood as a summary of all possible currents with the respective fields but different Lorentz structures.

[2] The ... denote the SMEFT completion of the hadronic structures that appear in the LEFT basis.

G_{01}	G_{02}	G_{03}	G_{04}	G_{06}	G_{09}
$m_{\beta\beta}$	$C_{VL}^{(6)}, C_{VR}^{(6)}$	$C_{VL}^{(6)}, C_{VR}^{(6)}$	$C_{VL}^{(6)}, C_{VR}^{(6)}$	-	$C_{VL}^{(6)}$
$C_{SL}^{(6)}, C_{SR}^{(6)}$	-	-	-	-	$C_6^{(9)}, C_6^{(9)\prime}$
$C_T^{(6)}$	-	-	-	-	$C_7^{(9)}, C_7^{(9)\prime}$
$C_{VL}^{(7)}, C_{VR}^{(7)}$	-	-	-	-	$C_8^{(9)}, C_8^{(9)\prime}$
$C_{1L}^{(9)}, C_{1R}^{(9)}$	-	-	-	-	$C_9^{(9)}, C_9^{(9)\prime}$
$C_{1L}^{(9)\prime}, C_{1R}^{(9)\prime}$	-	-	-	-	$C_9^{(9)}, C_9^{(9)\prime}$
$C_{2L}^{(9)}, C_{2R}^{(9)}$	-	-	-	-	-
$C_{2L}^{(9)\prime}, C_{2R}^{(9)\prime}$	-	-	-	-	-
$C_{3L}^{(9)}, C_{3R}^{(9)}$	-	-	-	-	-
$C_{3L}^{(9)\prime}, C_{3R}^{(9)\prime}$	-	-	-	-	-
$C_{4L}^{(9)}, C_{4R}^{(9)}$	-	-	-	-	-
$C_{5L}^{(9)}, C_{5R}^{(9)}$	-	-	-	-	-

Table 4.1.: Overview of the different PSFs and corresponding operators. The G_{06} PSF is only induced in the presence of multiple operators.

applying this method, matching short-range operators onto the SMEFT, one finds the following correspondences

$$\begin{aligned} \overline{e_R} e_R^c &\longleftrightarrow \overline{e_R} e_R^c \\ \overline{e}\gamma_\mu\gamma_5 e^c &\longleftrightarrow \overline{L}\gamma_\mu e_R^c \\ \overline{e_L} e_L^c &\longleftrightarrow \overline{L} L, \end{aligned} \tag{4.5}$$

between the lepton currents of LEFT operators (left) and SMEFT operators (right). Thus, LHC data could help to distinguish the different scalar short-range LEFT operators coupling to different chiral lepton currents $O_{iL}^{(9)} \leftrightarrow O_{iR}^{(9)}, i \in [1,5]$ from each other as well as it can help to identify the presence of short-range vector operators $C_i^{(9)}, C_i^{(9)\prime}, i \in [5,9]$. As we will see, especially the former possibility of distinguishing between the leptonic currents $\overline{e_L} e_L^c$ and $\overline{e_R} e_R^c$ is important as this is not possible within $0\nu\beta\beta$ experiments. One can follow the same line of argumentation for the long-range operators that are induced at SMEFT dimension-7 [73][3] by replacing $e_L^c \to \nu_L^c$ in Eq. (4.5)[4].

4.1.2. Distinguishing via Phase-Space Observables

Let us now turn towards $0\nu\beta\beta$ experiments, our main focus in this work. As already mentioned there are three different observables that one can investigate with regard to their operator discrimination power. We will start with the observables connected to the leptonic phase space, i.e., the angular correlation of the two outgoing electrons and the

[3] i.e., here one adds a single power of Φ to the dimension-6 long-range LEFT operators
[4] Note that we do not have a ν_R^c

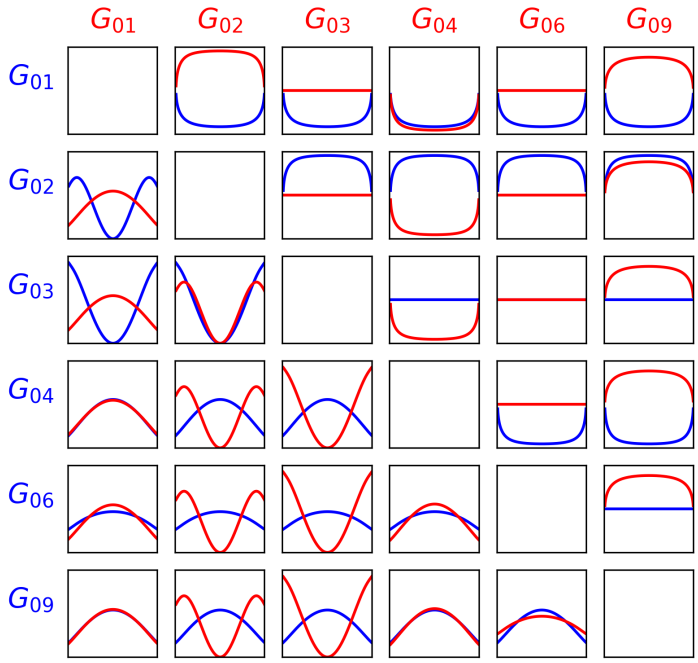

Figure 4.1.: Comparison of the normalized single electron spectra and angular correlation coefficients in ^{136}Xe that result from the 6 PSFs which appear in the $0\nu\beta\beta$ half-life "master-formula". The comparison between the different single electron spectra is represented in the lower left part of the plot while the comparison of the angular correlation coefficients is shown in the upper right part. The color of each curve corresponds to the operator it represents. The x-axis covers the range $\tilde{\epsilon} \in [0 - 1]$.

single electron spectra. These are defined by the different PSFs which again result from traces of the squared lepton currents. Within the simplest approximation these can be calculated analytically. More exact solutions require numeric calculations of the exact electron wave functions [29]. The different PSFs G_{0k} can be written in the form [78]

$$\begin{aligned} G_{0k} = \frac{(G_F V_{ud})^4 m_e^2}{64\pi^5 \ln 2 R^2} \int \delta\Big(\epsilon_1 + \epsilon_2 + E_f - E_i\Big) \\ \times \Big(h_{0k}(\epsilon_1, \epsilon_2, R)\cos\theta + g_{0k}(\epsilon_1, \epsilon_2, R)\Big) \\ \times p_1 p_2 \epsilon_1 \epsilon_2 \, \mathrm{d}\epsilon_1 \, \mathrm{d}\epsilon_2 \, \mathrm{d}(\cos\theta). \end{aligned} \tag{4.6}$$

Here, we split the differential phase space factor into a part h_{0k} which depends on the angle θ between the two outgoing electrons and a part g_{0k} that is independent of it. Of

course, this can always be done. The relations between the electron wave-functions and the functions h_{0k} and g_{0k} are given in [78] to which we will refer here. We apply the simplest approximation scheme 'A'. With Eq. (4.6) one can write the angular correlation coefficient a_1/a_0 which is defined via

$$\frac{\mathrm{d}\Gamma}{\mathrm{d}\cos\theta \mathrm{d}\tilde{\epsilon}_1} = a_0 \left(1 + \frac{a_1}{a_0}\cos\theta\right) \tag{4.7}$$

with

$$\tilde{\epsilon}_i = \frac{\epsilon_i - m_e}{Q_{\beta\beta}} \in [0,1] \tag{4.8}$$

as

$$\frac{a_1}{a_0}(\tilde{\epsilon}) = \frac{\sum_i |M_i|^2 h_{0i}\left(\epsilon, \Delta M_{\text{Nuclei}} - \epsilon, R\right)}{\sum_j |M_j|^2 g_{0j}\left(\epsilon, \Delta M_{\text{Nuclei}} - \epsilon, R\right)} \,. \tag{4.9}$$

Here, ΔM_{Nuclei} is the mass difference between the mother and daughter nuclei. Similarly, the single electron spectra which arise from the different PSFs are given by

$$\begin{aligned}\frac{\mathrm{d}\Gamma}{\mathrm{d}\epsilon_1} =& \frac{(G_F V_{ud})^4 m_e^2}{64\pi^5 \ln 2 R^2} \\ &\times \left(\sum_i |M_i|^2 g_{0i}\left(\epsilon, \Delta M_{\text{Nuclei}} - \epsilon, R\right)\right) \\ &\times p_1 p_2 \epsilon\big(\Delta M_{\text{Nuclei}} - \epsilon\big) \,.\end{aligned} \tag{4.10}$$

Thus, given appropriate knowledge about the electron wave functions, we can easily calculate the expected angular correlation factor and single electron spectra that appear for each of the 32 LEFT operators. The normalized single electron spectra as well as the angular correlation coefficients that arise for each of the 6 PSFs are shown in Figure 4.1. As we can see, the 6 PSFs are in principle all distinguishable from each other, given the experimental accuracy is good enough.[5] However, as we can see from Table 4.1 the different operators do not correspond to a single PSF each. In fact, while

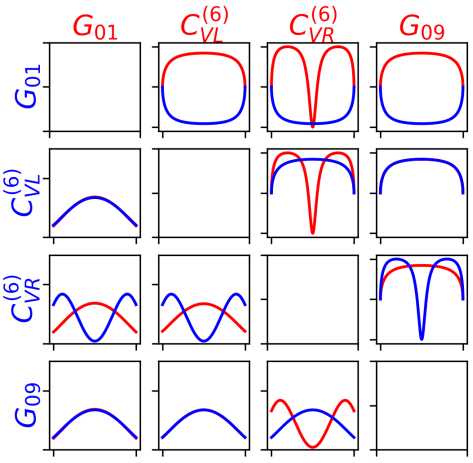

Figure 4.2.: Normalized single electron spectra and angular correlation coefficient for each of the 4 distinguishable groups of operators. The shapes are shown for ^{136}Xe assuming the NDA values for the currently unknown LECs. However, the particular choice does not result in a significant difference in the general shape of the plots. Again, the normalized single electron spectra are shown in the lower left part of the figure while the angular correlation coefficient is shown in the upper right part. The color of each curve corresponds to the operator it represents.

[5] Note that the distinguishability between G_{01} and G_{04} via the anglar correlation is better in elements with a low Q-value like, e.g., ^{128}Te.

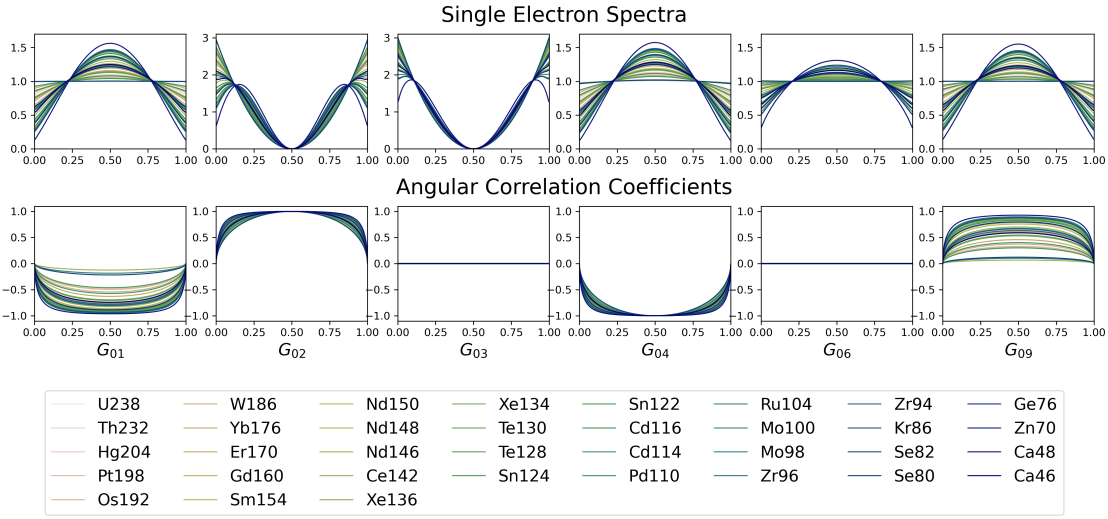

Figure 4.3.: The single electron spectra and the angular correlation for all 35 naturally occurring $0\nu\beta^-\beta^-$ isotopes are shown. One can see that, while the exact quantitative curves do depend on the choice of the isotope, the general shape is mostly independent of this choice. Again, the x-axis shows the normalized electron energy $\tilde{\epsilon}$.

G_{06} is only induced in the presence of multiple operators the dimension-6 vector operators both trigger several of the remaining PSFs. Taking this into account, we can identify 4 different groups of operators that in principle can be distinguished via their leptonic PSF observables namely $C_{VL}^{(6)}, C_{VR}^{(6)}$, the operators corresponding to G_{01} and the ones corresponding to G_{09}. The PSF observables that result from each of these 4 groups are shown in Figure 4.2. Here, we can see that the left-handed vector current operator $C_{VL}^{(6)}$ and the operators corresponding to G_{09}, while in principle distinguishable, are practically indistinguishable as the $C_{VL}^{(6)}$ phase space is dominated by the contribution from G_{09}. The remaining groups are distinguishable from each other in at least one of the considered observables.
Note that while the electron wave-functions do depend on the charge of the daughter nucleus as well as the decay energy, the general shape of the induced observables is not very dependent on the choice of the decaying isotope. In Figure 4.3 we show both the angular correlation as well as the single electron spectra corresponding to the 6 different PSFs in all of the 35 naturally occurring $0\nu\beta^-\beta^-$ isotopes.

4.1.3. Distinguishing via Decay Rate Ratios

The remaining $0\nu\beta\beta$ observable is the decay rate Γ. While the former methods can be used to distinguish operators with different leptonic currents, information about the decay rates in various isotopes can be used to distinguish operators with different hadronic

structures. The reason for this is that different hadronic currents of course represent different NMEs. Current calculations of NMEs in different isotopes do not show a linear behavior as can be seen by looking at Table 3.2. Therefore, we can study the half-life ratios

$$R^{\mathcal{O}_i}({}^AX) = \frac{T^{\mathcal{O}_i}_{1/2}({}^AX)}{T^{\mathcal{O}_i}_{1/2}({}^{76}\mathrm{Ge})} \tag{4.11}$$

where $T^{\mathcal{O}_i}_{1/2}({}^AX)$ is the half-life induced by the operator O_i in the isotope ${}^AX$. This possibility was first discussed in [87]. Here, we take ^{76}Ge as the reference isotope. Of course, one can also work with different reference isotopes. We will later also discuss the optimal isotope combinations for distinguishing different operators. To be able to quantify how well one can distinguish two different operators $\mathcal{O}_{i,j}$ from each other we can take the ratio

$$R_{ij}({}^AX) = \frac{R^{\mathcal{O}_i}({}^AX)}{R^{\mathcal{O}_j}({}^AX)}. \tag{4.12}$$

Specifically the ratio $R_{im_{\beta\beta}}$ will be of interest to compare the effect of different operators to the standard mass mechanism and possibly identify the existence of non-standard mechanisms within a $0\nu\beta\beta$ experiment. Studying the decay rate ratios has several positive benefits: In case only one Wilson coefficient contributes, it drops out completely when taking the ratio. Therefore the ratio corresponding to a certain operator and its Wilson coefficient is a constant that only depends on the corresponding NMEs, LECs and PSFs. If more Wilson coefficients contribute, the overall magnitude can be factored out. The relations between the different coefficients can still change the resulting ratios. However, assuming naturalness, one can still study the expected impact resulting from more complex models. Additionally, when taking ratios of the half-lives, one can expect that the impact of systematic relative errors on the NMEs decreases as they should cancel at least partly. Taking, for example, the values of M_F calculated within QRPA [79] and the shell model [83] in ^{76}Ge and ^{82}Se of

$$\begin{aligned} M^{76Ge}_{F,QRPA} &= -1.74, \qquad M^{82Se}_{F,QRPA} = -1.29 \\ M^{76Ge}_{F,SM} &= -0.59, \qquad M^{82Se}_{F,SM} = -0.55 \end{aligned} \tag{4.13}$$

they differ by a factor of $\sim 2.3 - 2.9$ while the ratios of the NMEs only differ by a factor of ~ 1.3. This is a significant reduction and a sign towards the ratios being less affected by the choice of the calculation method for the NMEs.
Considering the master-formula framework one can identify 11 different groups of operators that can in principle be distinguished from each other. Assuming the unknown LECs to be equal to their NDA values, these 11 groups are summarized in Table 4.2. However, the distinguishability of the short-range operators does strongly depend on the LECs. Taking the unknown LECs to vanish while keeping $g^{NN}_{1,6,7} = g^{\pi N}_V = \tilde{g}^{\pi N}_V = 1$ to not omit the contribution from the short-range vector operators makes it impossible to distinguish the short-range scalar operators $C^{(9)}_{S2-S5}$. On the other hand, improved knowledge about

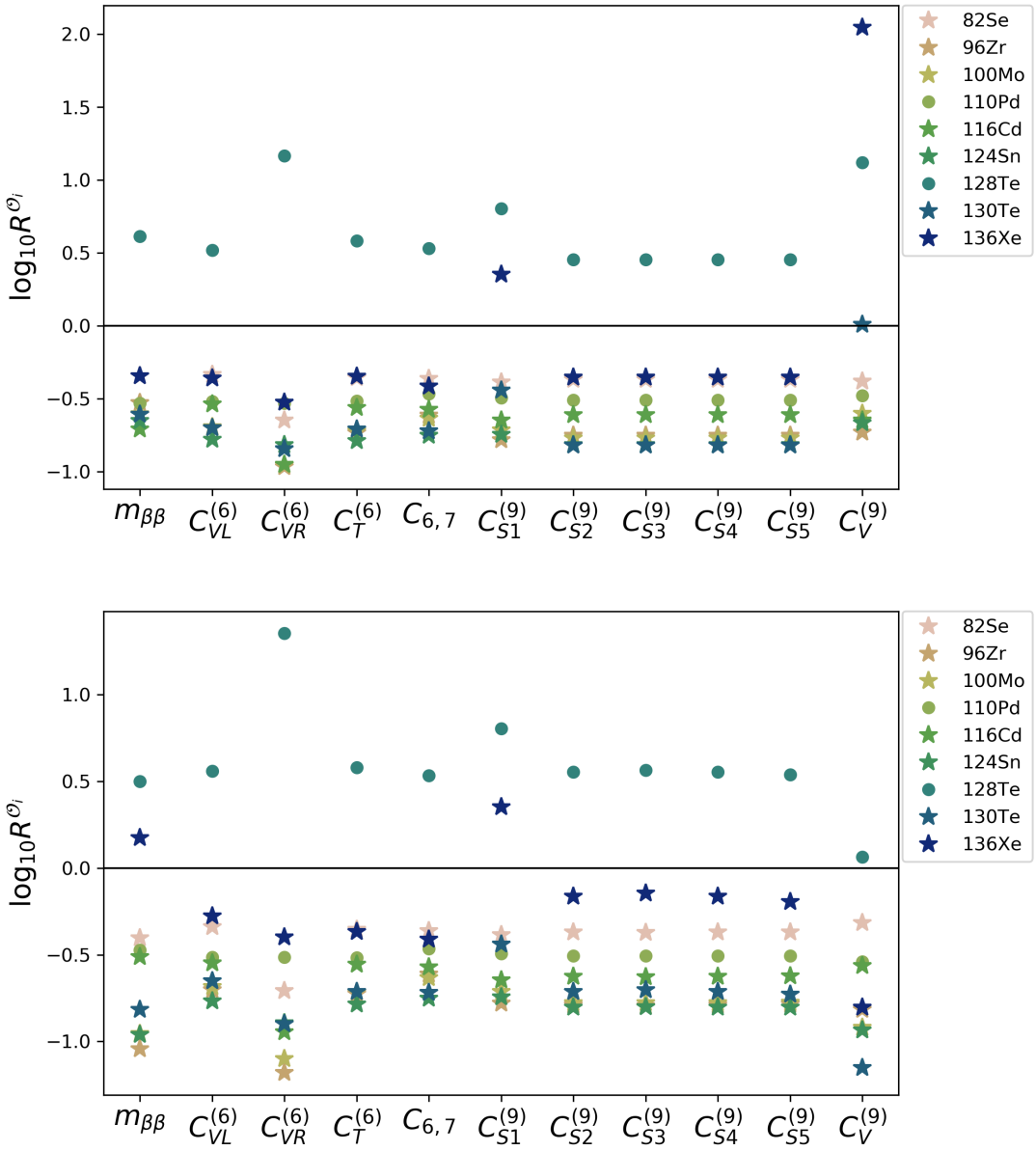

Figure 4.4.: The decay rate ratios R^{O_i} for the different operator groups are shown. In the upper plot we assume the unknown LECs to vanish, whereas in the lower plot we set them to their NDA values. This choice significantly influences the result for the dimension-9 vector operators. However, it hardly changes the ratios for the remaining operators. Isotopes marked with a star have a PSF $G_{01} > 10^{-14} y^{-1}$. The reference isotope is ^{76}Ge.

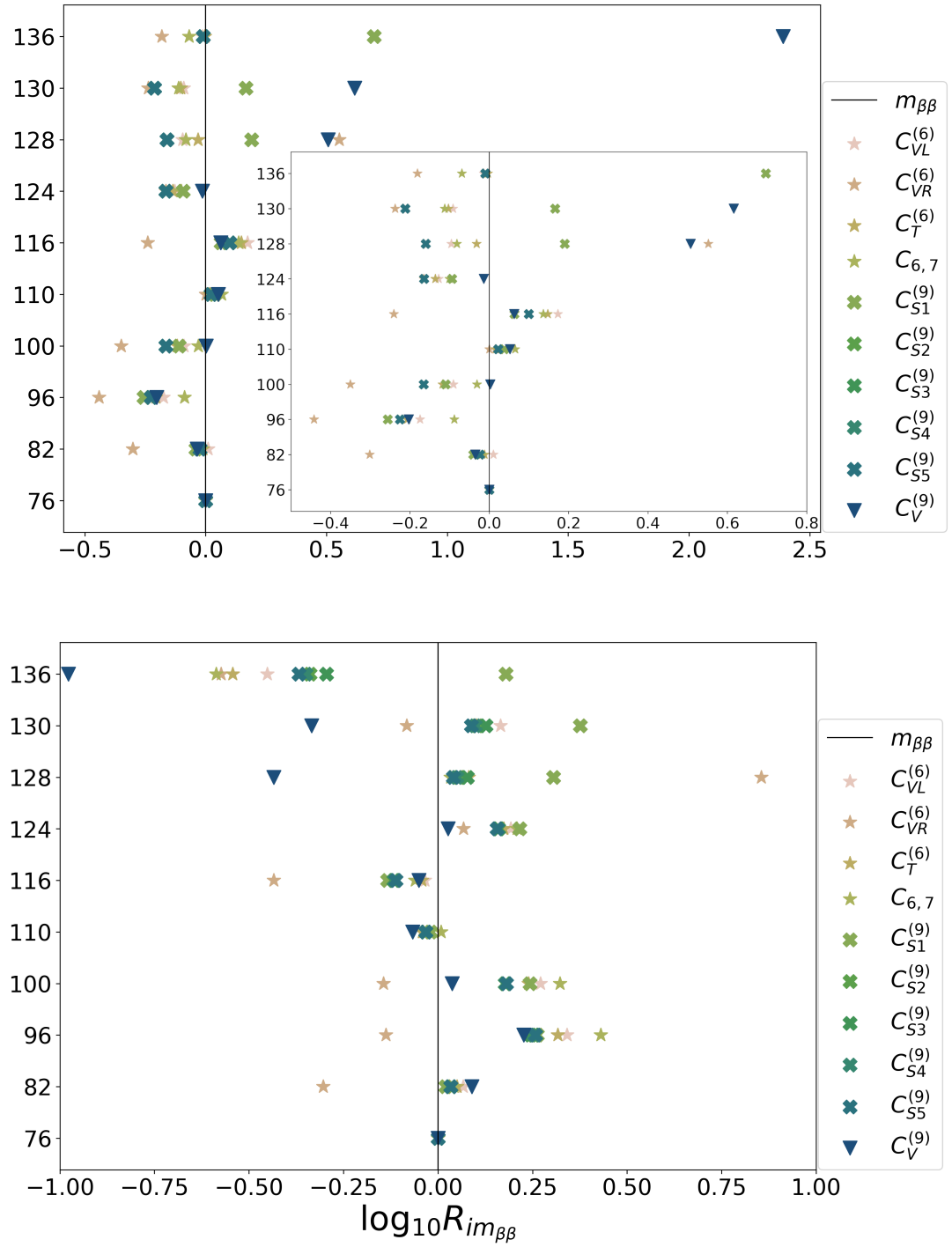

Figure 4.5.: The ratio $R_{im_{\beta\beta}}$ relevant for identifying the standard mass mechanism is shown. In the upper plot we again assume the unknown LECs to vanish while keeping $g_{1,6,7}^{NN} = g_V^{\pi N} = \tilde{g}_V^{\pi N} = 1$. In the lower plot we set them to their NDA values. The long-range mechanisms are marked by a star, the short-range scalar operators by a cross and the short-range vector operators by a triangle. The reference isotope is still ^{76}Ge.

$m_{\beta\beta}$	$C_{VL}^{(6)}$	$C_{VR}^{(6)}$	$C_{T}^{(6)}$	$C_{6,7}$	$C_{S1}^{(9)}$	$C_{S2}^{(9)}$	$C_{S3}^{(9)}$	$C_{S4}^{(9)}$	$C_{S5}^{(9)}$	$C_{V}^{(9)}$
$m_{\beta\beta}$	$C_{VL}^{(6)}$	$C_{VR}^{(6)}$	$C_{T}^{(6)}$	$C_{SL}^{(6)}$	$C_{1L}^{(9)}$	$C_{2L}^{(9)}$	$C_{3L}^{(9)}$	$C_{4L}^{(9)}$	$C_{5L}^{(9)}$	$C_{6}^{(9)}$
-	-	-	-	$C_{SR}^{(6)}$	$C_{1R}^{(9)}$	$C_{2R}^{(9)}$	$C_{3R}^{(9)}$	$C_{4R}^{(9)}$	$C_{5R}^{(9)}$	$C_{6}^{(9)\prime}$
-	-	-	-	$C_{VL}^{(7)}$	$C_{1L}^{(9)\prime}$	$C_{2L}^{(9)\prime}$	$C_{3L}^{(9)\prime}$	-	-	$C_{7}^{(9)}$
-	-	-	-	$C_{VR}^{(7)}$	$C_{1R}^{(9)\prime}$	$C_{2R}^{(9)\prime}$	$C_{3R}^{(9)\prime}$	-	-	$C_{7}^{(9)\prime}$
-	-	-	-	-	-	-	-	-	-	$C_{8}^{(9)}$
-	-	-	-	-	-	-	-	-	-	$C_{8}^{(9)\prime}$
-	-	-	-	-	-	-	-	-	-	$C_{9}^{(9)}$
-	-	-	-	-	-	-	-	-	-	$C_{9}^{(9)\prime}$

Table 4.2.: Operator groups that can be distinguished via taking decay rate ratios. Here, we assume the unknown LECs to be equal to their order of magnitude estimate. The choice of the groups depends on the knowledge of the LECs. If we set the unknown LECs to zero, the short-range scalar operator groups $C_{S2-S5}^{(9)}$ become indistinguishable. On the other hand, improved knowledge of the LECs ,assuming no fine tuning, would allow to distinguish the operators contributing to $C_V^{(9)}$ from the ones contributing to $\tilde{C}_V^{(9)}$ in Eq. (3.149).

the currently unknown LECs, assuming no fine tuning, could allow us to distinguish the operators contributing to $C_V^{(9)}$ from the ones contributing to $\tilde{C}_V^{(9)}$ in Eq. (3.149) resulting in 12 different distinguishable operator groups.
The expected ratios R^{O_i} for both choices of LECs are shown in Figure 4.4 while the values for $R_{im_{\beta\beta}}$ are shown in Figure 4.5.

4.1.4. Utilizing additional $0\nu\beta\beta$ Modes

Until now, we only discussed the usual $0\nu\beta^-\beta^-$-decay mode and ignored the additional modes mentioned in Sec. 3.1.1. In principle it would be interesting to also study these additional modes as any additional decay process might improve the possibilities to distinguish different mechanisms via decay rate ratios. The reason for our "ignorance" is simple, though. The remaining $0\nu\beta\beta$ modes are expected to have a significantly longer half-life than the usual $0\nu\beta^-\beta^-$ mode and are therefore unlikely to show up within an experiment. Nevertheless, we want to discuss this a bit more detailed:

$0\nu\beta^+\beta^+$

This mode can be treated similarly to the usual $0\nu\beta^-\beta^-$ mode just by choosing a negative nuclear charge $Z \to -Z$ to calculate the positron wavefunctions. As such, the expected half-life will also mainly be determined by the PSF which, as we saw earlier, goes with Q^5. Looking at the second column in Table 3.1 we can see that the Q-values for naturally occurring isotopes are up to one order of magnitude smaller than usual $0\nu\beta^-\beta^-$ Q-values. Additionally, the electromagnetic repulsion of the outgoing positrons deforms

the wavefunctions and decreases the decay rate. Thus, we see that $0\nu\beta^+\beta^+$ will be highly suppressed compared to $0\nu\beta^-\beta^-$. Also, from the similarities of the two decay modes we cannot see a natural way to enhance the $0\nu\beta^+\beta^+$-decay rate with respect to $0\nu\beta^-\beta^-$. The relevant PSFs for the $0\nu\beta^+\beta^+$-decay of naturally occuring isotopes have been calculated in [58] and are about 3-5 orders of magnitude smaller than for the usual $0\nu\beta^-\beta^-$ mode.

0νECβ^+

The PSFs for the 0νECβ^+ mode have also been calculated to good precision in [58] and are found to be 3-4 orders of magnitude smaller than for $0\nu\beta^-\beta^-$. The reason is the same as in the discussion about $0\nu\beta^+\beta^+$.

0νECEC

As this decay mode has no outgoing particles additional to the daughter isotope, there needs to be a mass degeneracy between the mother and daughter isotopes to satisfy conservation of energy and momentum. The degeneracy, though, does not have to be exact, but the two isotopes can have a small mass offset due to the width of the bound electrons energy band. In principle, an exact mass degeneracy can result in a resonant enhancement of the decay rate [27, 88]. These resonances are often found when considering excited final state nuclei. The corresponding decay could be detected either by observing the de-excitation of the daughter nucleus or by observation of an overproduction of the daughter isotope via, e.g., extraction. Typically, such a de-excitation results in a rather unique signal of photons and can be very well distinguished from any background [27]. However, studies have shown that the resulting half-lives are still considerably longer than for $0\nu\beta^-\beta^-$ [88] and hence this mode does not have to be considered in detail in our study.
While we see that for the usual mass, long-range and short-range mechanisms the 0νECEC mode can safely be ignored, things might be different when considering Majoron models which do not necessitate a mass degeneracy.

Bound-State $0\nu\beta\beta$

Bound state $0\nu\beta\beta$-decay refers to a decay in which one or both of the two outgoing electrons end up in a bound energy level of the daughter isotope. It is usually referred to as $0\nu\beta$EP and 0νEPEP for the one and two bound final state electrons respectively. Here, EP denotes electron production or electron placement. 0νEPEP again necessitates a mass degeneracy similar to the 0νECEC as it is just the reverse process. It was studied in [27] and found to give even longer half-live times than the double electron capture. The single bound state double-β-decay $0\nu\beta$EP was investigated in [89] and again found to have PSFs 6-7 orders of magnitude smaller than the competing $0\nu\beta^-\beta^-$ mode. The decay rates can be significantly enhanced when considering fully ionized nuclei. For some isotopes [89] showed that in this case the $0\nu\beta$EP-decay rate can exceed the usual $0\nu\beta^-\beta^-$. While this seems like an interesting case to study within experiments, it is currently not

possible to fully ionize a significant number of isotopes at the ton or kilogram scale. Therefore, while the decay rate might be larger, the number of ions would be much too small to reach relevant precision within an experiment.

Artificial Isotopes

While there are only 69 naturally occurring double-β-decaying isotopes, we found about $\sim$ 2700 possible $0\nu\beta\beta$ candidate isotopes when considering the full NIST list of elements [28]. Some of them having considerably larger Q-values of up to 50 MeV.[6] While such a large Q-value of $\sim 50\,\mathrm{MeV}$ would result in a significant enhancement of the decay rate by ~ 8 orders of magnitude, there are several problems that arise when considering real experiments. Although we did not study all of the possible artificial isotopes in detail, we found the following features to be general limiting factors. First, as the name states, artificial isotopes need to be produced within the $0\nu\beta\beta$ experiment. This strongly limits the number of particles that an experiment can contain. Again ton, kilogram and even gram scales are usually not possible. This fact alone typically already cancels out the advantage gained from a larger Q-value. Additionally, many artificial isotopes, especially the ones with large Q-values, come with additional decay modes that strongly dominate and limit the half-life of the isotopes sometimes down to nanosecond scales such that storing them to study the $0\nu\beta\beta$ mode becomes impossible. The resulting necessity to continuously produce the artificial isotopes again strongly limits the number of isotopes that can be studied at once. For these reasons we do not consider artificial isotopes to be relevant for $0\nu\beta\beta$ studies.

To summarize the findings stated above: Despite the fact that many different $0\nu\beta\beta$-decay modes exist the usually studied naturally occurring $0\nu\beta^-\beta^-$-decaying isotopes are by far the most relevant candidates to study. Other possible modes should only become relevant in exotic mechanisms which explicitly forbid or limit the leading $0\nu\beta^-\beta^-$-decay or somehow significantly enhance other decay modes. As the Feynman diagrams for all of the above decay modes are the same (ignoring flipping electron lines by 180°), such models seem rather unnatural from a particle physics point of view. We therefore do not consider them here.

4.1.5. Results - Distinguishing the 32 LEFT Operators

Summary - Distinguishing via $0\nu\beta\beta$ experiments

We found that out of the 32 different LEFT operators one can form 11 operator groups which are theoretically distinguishable via taking ratios of the half-lives. These are given in Table 4.2. Even the inclusion of PSF observables does not allow to distinguish operators within one of these groups. As such, they represent the general set of distinguishable operator groups within $0\nu\beta\beta$ experiments.

[6] Considering only isotopes without a single-β-decay mode already significantly reduces this number down to 86. None of these has a significantly enhanced $Q-$value.

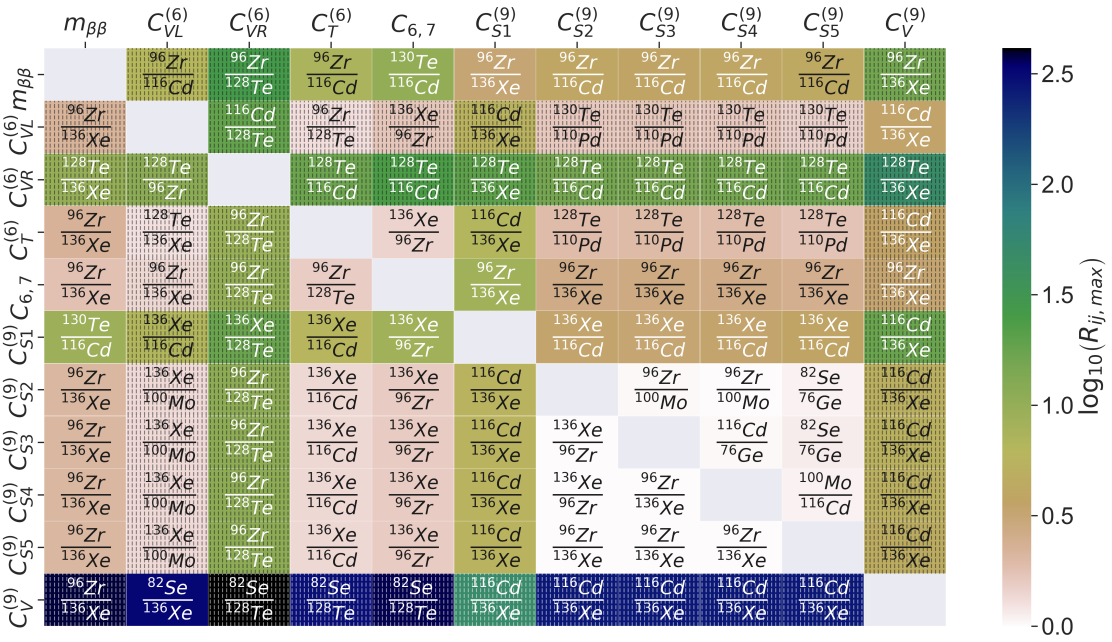

Figure 4.6.: The maximum values of $\log_{10} R_{ij}$ and the corresponding combination of isotopes are shown. Each of the fields showcases the distinguishability of two operator pairs labeled on the x/y-axis. The dashed fields represent operator combinations that can be distinguished via PSF observables. Again, in the lower left half of the plot we assume the unknown LECs to vanish while in the upper right half we take the NDA values. We can see that especially for the dimension-9 vector operators the choice of the LECs makes a significant difference.

As the half-life ratios are of course depending on the studied isotopes, we want to find the optimal choice of isotopes to maximize the ratios R_{ij} and hence maximize the possibility to distinguish the 11 operator groups. Our set of NMEs, as given in Table 3.2, includes 10 different isotopes. In Figure 4.6 we show the maximum ratios $R_{ij,max}$ for each operator combination and the corresponding best choice of isotopes. Again, we studied this for vanishing unknown LECs while keeping $g_{1,6,7}^{NN} = g_V^{\pi N} = \tilde{g}_V^{\pi N} = 1$ as well as for assuming the NDA values for the unknown LECs. Especially for the short-range vector operators this choice does significantly impact the values of the ratios. We find that out of the 10 isotopes studied, 7 (^{82}Se, ^{96}Zr, , ^{100}Mo, ^{116}Cd, ^{128}Te, ^{130}Te and ^{136}Xe) appear in Figure 4.6 when assuming the unknown LECs to vanish while 9 (all but ^{124}Sn) appear if one assumes the NDA values for the unknown LECs. Including PSF observables the number of necessary isotopes for vanishing unknown LECs reduces to 6 as a measurement in ^{100}Mo can be replaced by a measurement of the angular correlation coefficient.
It is important to note that although from looking at Figure 4.6 one would presume that the scalar short-range operators $C_{S2-S5}^{(9)}$, while theoretically distinguishable, are in fact

practically indistinguishable. This is a result of the specific values of the LECs. Different choices can significantly enhance these ratios. Additionally, we want to stress the fact that we study the effects of operators induced at the electroweak scale and not directly at the χPT scale. The RGE running can induce additional operators [74]. However, while this does of course affect the numerical values of the ratio, we find that it does not change the general composition of the different distinguishable operator groups.

Including Measurement Uncertainties

Of course, within a real experiment we will not be able to exactly resolve the half-live ratios. Hence, it is interesting to quantify the experimental precision on the half-lives which is necessary to distinguish different sets of operators. The uncertainty on the decay rate ratios ΔR^{O_i} is directly related to the uncertainty on the half-life measurement $\Delta t_{1/2}$ via

$$\frac{\Delta R^{O_i}}{R^{O_i}} = \sqrt{2}\frac{\Delta t_{1/2}}{t_{1/2}} \tag{4.14}$$

and thus

$$\frac{\Delta R_{ij}}{R_{ij}} = 2\frac{\Delta t_{1/2}}{t_{1/2}} \tag{4.15}$$

where we assumed the same relative uncertainty for all different isotopes. Using the above relation in Eq. (4.15) we can determine the experimental precision that is necessary to identify certain operator groups. Here, we label an operator group O_i as identifiable within experimental accuracy if

$$R_{ij,\max} - \Delta R_{ij,\max} > 1 \quad \forall j \neq i \tag{4.16}$$

which, assuming equal half-live uncertainties in all isotopes, can be written as

$$R_{ij,\max}\left(1 - 2\frac{\Delta t_{1/2}}{t_{1/2}}\right) > 1 \quad \forall j \neq i. \tag{4.17}$$

In Table 4.3 we show the identifiable/rejectable operators when considering different half-life uncertainty levels reaching from $0 - 50\%$. While the results do depend on the values of the different LECs, it is important to note that for the two different choices studied here, if the $0\nu\beta\beta$-decay is observed at a 5σ level, the mass mechanism can be identified or rejected at least with a 1σ significance. We can conclude that, given the $0\nu\beta\beta$-decay is observed in the relevant isotopes for identifying the mass mechanism (^{96}Zr, ^{116}Cd, ^{130}Te, ^{136}Xe), one can distinguish between the mass-mechanism and general non-standard mechanisms. If data on the PSF observables is available, only three different isotopes (^{96}Zr, ^{116}Cd and ^{136}Xe) are necessary in order to achieve this. While ^{136}Xe is studied in many different experiments, ^{96}Zr and ^{116}Cd both can be studied in the future SuperNEMO experiment and they both have a reasonable high Q-value of 3.3 MeV and 2.8 MeV respectively as well as relatively high natural abundances. The same holds for ^{130}Te.

$\frac{\Delta t_{1/2}}{t_{1/2}}$ [%]	Identifiable operator groups										
	$m_{\beta\beta}$	$C_{\mathrm{VL}}^{(6)}$	$C_{\mathrm{VR}}^{(6)}$	$C_{\mathrm{T}}^{(6)}$	$C_{6,7}^{(6)}$	$C_{\mathrm{S1}}^{(9)}$	$C_{\mathrm{S2}}^{(9)}$	$C_{\mathrm{S3}}^{(9)}$	$C_{\mathrm{S4}}^{(9)}$	$C_{\mathrm{S5}}^{(9)}$	$C_{\mathrm{V}}^{(9)}$
	Unknown LECs = NDA										
0	X	X	X	X	X	X	X	X	X	X	X
1	X	X	X	X	X	X		X		X	X
5	X	X	X	X	X	X					X
10	X	X	X	X	X	X					X
15	X	*	X	*	X	X					X
20	X	*	X			X					X
25	X	*	X			X					X
33	X	*	X			X					X
50			*								
	Unknown LECs = 0										
0	X	X	X	X	X	X					X
1	X	X	X	X	X	X					X
5	X	X	X	X	X	X					X
10	X	*	X	*	X	X					X
15	X	*	X		*	X					X
20	X	*	X			X					X
25		*	X			X					X
33		*	X			X					X
50			*								

Table 4.3.: List of operators which are identifiable at least at the 1σ level considering different levels of relative uncertainties on the experimental half-lives. We consider the relative half-life uncertainty independent of the isotope and ignore uncertainties arising from different NME calculations. Operators that are identifiable via ratio taking are marked with an X while operators with a $*$ are only identifiable by including PSF observables. In the upper half we show the results when taking the unknown LECs to their NDA values and in the lower half we show the results assuming the unknown LECs vanish.

The Best Case Scenario

Assuming future knowledge of the LECs does provide that contributions from $C_V^{(9)}$ and $\tilde{C}_V^{(9)}$ are indeed distinguishable and that the ratios for the scalar short-range operators $C_{S2-S5}^{(9)}$ are enhanced up to a level that allows $0\nu\beta\beta$-decay experiments to distinguish among them, one can distinguish 12 different operator groups. If, additionally, high-energy collider data is available one can distinguish 17 different groups of operators as collider data allows to distinguish between the short-range scalar left and right operators $C_{iL,R}^{(9)}$ of which we have 5 pairs. In this case the only indistinguishable operator pairs

remaining are the short-range operators $C_i^{(9)}$ and their primed counterpart $C_i^{(9)\prime}$ as well as the operators denoted by the group $C_{6,7}$.

4.2. Distinguishing specific Models

Now that we introduced methods on how one can experimentally distinguish different LEFT operators, we want to turn towards complete models rather than just single operators. As we will see and as one would expect, lepton number violating BSM models will typically introduce several LEFT operators at a time. While we do not expect that one will be able to identify a specific BSM model by the aforementioned methods as no finite set of BSM models exists and many different models will result in the same low-energy physics, we do expect that, given fixed model parameters, one can at least check if a model fits the observed data and reject it if it does not. In the following parts we want to briefly discuss three different models beyond the Standard Model taken from the literature that would lead to $0\nu\beta\beta$-decay. We will compare each model to the standard mass mechanism. To be on the conservative side we will keep the unknown LECs to zero for the rest of this chapter while still keeping $g_{1,6,7}^{NN} = g_V^{\pi N} = \tilde{g}_V^{\pi N} = 1$.

4.2.1. Minimal Left-Right Model

The Standard Model is a chiral theory. That is, parity is explicitly broken due to the gauged $SU(2)_L$ symmetry and the lacking right-handed neutrino. The latter together with the lack of an $SU(2)_L$ triplet scalar results in vanishing neutrino masses. A simple approach to resolve both of these phenomena is to extend the Standard Model's gauge group to a left-right symmetric model $SU(3)_C \times SU(2)_L \times SU(2)_R \times U(1)_{B-L}$ [90, 91, 92] which afterwards needs to be broken spontaneously to the Standard Model setting $SU(3)_C \times SU(2)_L \times U(1)_Y$. We will give a brief introduction to the minimal left-right symmetric Standard Model (mLRSM). A comprehensive review, which we will often follow, is given in [93]. Extending the Standard Model to a left-right symmetric theory requires the existence of additional scalars and fermions. The minimal setting includes two additional scalar triplets $\Delta_L \in (1, 3, 1, 2)$ and $\Delta_R \in (1, 1, 3, 2)$ as well as a scalar bifield $\Phi \in (1, 2, 2^*, 0)$ instead of the usual higgs doublet and obviously right-handed neutrino fields ν_R $(1, 1, 2, -1)$.[7] It is easy to notice some similarities to the particle content of the seesaw mechanisms that we discussed in Sec. 2.3. Again, the scalar triplets are defined as

$$\Delta_{L,R} = \sum_i \tau_i \Delta_{L,R,i} \tag{4.18}$$

giving

$$\Delta_{L,R} = \begin{pmatrix} \frac{1}{2}\delta_{L,R}^{+} & \delta_{L,R}^{++} \\ \delta_{L,R}^{0} & \frac{1}{2}\delta_{L,R}^{+} \end{pmatrix} \tag{4.19}$$

[7] Note that also other settings have been considered, e.g. [92].

and the bifield Φ is given by

$$\Phi = \begin{pmatrix} \Phi_1^0 & \Phi_1^+ \\ \Phi_2^- & \Phi_2^0 \end{pmatrix}. \tag{4.20}$$

Under $U_{L,R} \in SU(2)_{L,R}$ they transform as

$$\Phi \longrightarrow U_L \Phi U_R^\dagger, \qquad \Delta_L \longrightarrow U_L \Delta_L U_L^\dagger, \qquad \Delta_R \longrightarrow U_R \Delta_R U_R^\dagger. \tag{4.21}$$

The fermions are grouped into left- and right-handed doublets

$$L_L = \begin{pmatrix} \nu_L \\ e_L \end{pmatrix} \in (1,2,1,-1)\,, \qquad Q_L = \begin{pmatrix} u_L \\ d_L \end{pmatrix} \in (3,2,1,1/3)\,, \tag{4.22}$$

$$L_R = \begin{pmatrix} \nu_R \\ e_R \end{pmatrix} \in (1,1,2,-1)\,, \qquad Q_R = \begin{pmatrix} u_R \\ d_R \end{pmatrix} \in (3,1,2,1/3)\,, \tag{4.23}$$

which transform as

$$\Psi_{L,R} \longrightarrow U_{L,R} \Psi_{L,R}. \tag{4.24}$$

It is easy to see that the electric charge of a field is given by

$$Q = I_{3_L} + I_{3_R} + \frac{B-L}{2} \tag{4.25}$$

Obviously, the field content of this theory is symmetric under a transformation $L \leftrightarrow R$. There are two discrete symmetries which can relate left- and right-handed fermions namely parity P and charge transformation C [94]. Thus, one can define two different discrete symmetry transformations

$$P : \Psi_L \Longleftrightarrow \Psi_R, \qquad \Phi \Longleftrightarrow \Phi^\dagger, \qquad \Delta_{L,R} \Longleftrightarrow \Delta_{R,L} \tag{4.26}$$

$$C : \Psi_L \Longleftrightarrow (\Psi_R)^c\,, \qquad \Phi \Longleftrightarrow \Phi^T, \qquad \Delta_{L,R} \Longleftrightarrow \Delta_{R,L}^*. \tag{4.27}$$

Requiring either P or C invariance results in different constraints on the scalar potential as well as the Yukawa coupling matrices [94].[8]

The matching onto the SMEFT and afterwards the relevant LEFT operators has been discussed in the original "master formula" paper [74]. Here, we will summarize their findings and expand on the topic of distinguishing this model from the standard mass mechanism by considering the C symmetric case. Considering Eq. (4.25) we can identify the neutral components of the scalar fields. Assuming that $U(1)_Q$ is an unbroken symmetry only these components can gain a VEV and thus the most general form is given by

$$\langle \Phi \rangle = \frac{1}{\sqrt{2}} \begin{pmatrix} \kappa & 0 \\ 0 & \kappa' \end{pmatrix}, \qquad \langle \Delta_L \rangle = \frac{1}{\sqrt{2}} \begin{pmatrix} 0 & 0 \\ v_L & 0 \end{pmatrix}, \qquad \langle \Delta_R \rangle = \frac{1}{\sqrt{2}} \begin{pmatrix} 0 & 0 \\ v_R & 0 \end{pmatrix}. \tag{4.28}$$

[8] Note that a combination of both does not fit observational constraints [94].

We want to point out that generally all four VEVs can be complex, i.e., $v = v\exp\{i\alpha_v\}$. Two complex phases can be rotated away [95] such that we are left with two complex VEVs and we can write

$$\langle\Phi\rangle = \frac{1}{\sqrt{2}}\begin{pmatrix}\kappa & 0\\ 0 & \kappa' e^{i\alpha}\end{pmatrix}, \qquad \langle\Delta_L\rangle = \frac{1}{\sqrt{2}}\begin{pmatrix}0 & 0\\ v_L e^{i\theta_L} & 0\end{pmatrix}, \qquad \langle\Delta_R\rangle = \frac{1}{\sqrt{2}}\begin{pmatrix}0 & 0\\ v_R & 0\end{pmatrix}, \tag{4.29}$$

with real parameters $\kappa, \kappa', v_L, v_R, \alpha, \theta_L$. The VEVs are related to the parameters of the scalar potential V_{Higgs} by requiring

$$\frac{\partial V_{Higgs}}{\partial v_L} = \frac{\partial V_{Higgs}}{\partial v_R} = \frac{\partial V_{Higgs}}{\partial \kappa} = \frac{\partial V_{Higgs}}{\partial \kappa'} = \frac{\partial V_{Higgs}}{\partial \alpha} = \frac{\partial V_{Higgs}}{\partial \theta_L} = 0 \tag{4.30}$$

As v_R spontaneously breaks $SU(2)_R \times U(1)_{B-L} \longrightarrow U(1)_Y$ it is reasonable to assume it be the largest VEV. The VEVs of the bidoublet Φ play the part of the usual Higgs doublet and break the remaining $SU(2)_L \times U(1)_Y \longrightarrow U(1)_Q$. As such, they are of the order of the electroweak scale. Finally, the remaining VEV v_L should be very small since it generates a Majorana mass term for the left-handed neutrinos and additionally contributes to the masses of the W- and Z-bosons. Thus changes the ρ-parameter at tree-level [96] which is given by [10]

$$\rho = \frac{m_W}{m_Z \cos^2\theta_W} = 1.00038 \pm 0.00020 \tag{4.31}$$

and is equal to unity within the Standard Model at tree-level. Therefore, we assume the following hierarchy

$$v_R \gg \kappa, \kappa' \gg v_L. \tag{4.32}$$

The fermion masses arise from the Yukawa couplings of the different scalars and are given by

$$\begin{aligned}
M^u_{ij} &= \frac{1}{\sqrt{2}}\left[Y^q_{ij}\kappa + \tilde{Y}^q_{ij}\kappa' \exp\{-i\alpha\}\right], & M^d_{ij} &= \frac{1}{\sqrt{2}}\left[Y^q_{ij}\kappa' \exp\{i\alpha\} + \tilde{Y}^q_{ij}\kappa\right]\\
M^\nu_{D,ij} &= \frac{1}{\sqrt{2}}\left[Y^l_{ij}\kappa + \tilde{Y}^l_{ij}\kappa' \exp\{-i\alpha\}\right], & M^l_{ij} &= \frac{1}{\sqrt{2}}\left[Y^l_{ij}\kappa' \exp\{i\alpha\} + \tilde{Y}^l_{ij}\kappa\right]\\
M^\nu_{L,ij} &= \sqrt{2}Y^L_{ij} v_L \exp\{i\theta_L\}, & M^\nu_{R,ij} &= \sqrt{2}Y^R_{ij} v_R
\end{aligned} \tag{4.33}$$

While the quark and charged lepton mass matrices can be diagonalized straight away, the mass matrices for the light and heavy neutrino fields ν_i and N_i can be obtained via the seesaw formula in Eq. (2.87) and must be diagonalized appropriately. The gauge boson masses arise from the kinetic terms of the scalars as

$$\mathcal{L}^{W^\pm}_m = \left(W^{+\mu}_L, W^{+\mu}_R\right) M^2_W \begin{pmatrix}W^-_{L\mu}\\ W^-_{R\mu}\end{pmatrix} + h.c. \tag{4.34}$$

with

$$M_W^2 = \frac{1}{4}\begin{pmatrix} g_L^2\left(2|v_L|^2 + |\kappa|^2 + |\kappa'|^2\right) & -2g_L g_R|\kappa||\kappa'|e^{i\theta} \\ -2g_L g_R|\kappa||\kappa'|e^{-i\theta} & g_R^2\left(2|v_R|^2 + |\kappa|^2 + |\kappa'|^2\right) \end{pmatrix} \tag{4.35}$$

for the charged gauge bosons $W_{L,R}^{\pm}$ given by

$$W_{L,R}^{\pm} = \frac{1}{\sqrt{2}}\left(W_{L,R}^1 \mp i W_{L,R}^2\right). \tag{4.36}$$

Since we want to focus on the impact of mLRSM on $0\nu\beta\beta$ we do not need to care much about the neutral gauge bosons. From Eq. (4.35) we see that the left and right charged W bosons mix due to the coupling to the bidoublet Φ. The massive states $W_{1,2}^{\pm}$ are given by

$$\begin{pmatrix} W_L^+ \\ W_R^+ \end{pmatrix} = \begin{pmatrix} \cos\zeta & -\sin\zeta\exp\{-i\alpha\} \\ \sin\zeta\exp\{i\alpha\} & \cos\zeta \end{pmatrix}\begin{pmatrix} W_1^{\pm} \\ W_2^{\pm} \end{pmatrix} \tag{4.37}$$

with

$$\tan\zeta \sim -2\xi\left(\frac{M_{W_L}}{M_{W_R}}\right)^2, \qquad \xi = \frac{\kappa'}{\kappa} \tag{4.38}$$

Naturally, ξ is expected to be at the order of m_b/m_t [95] such that the mixing angle ζ is strongly suppressed. From this discussion we can already infer the different contributions within the mLRSM to the $0\nu\beta\beta$ amplitude. The relevant Feynman diagrams are shown in Figure 4.7.
After Δ_R gains its VEV it gives masses to the right-handed gauge bosons as well as the right-handed neutrinos, the scalar fields $\Delta_{L,R}$ and parts of Φ. Integrating out the heavy fields with masses proportional to v_R and matching the theory onto SMEFT results in the lepton number violating operators [74]

$$\begin{aligned} \mathcal{L}_{\Delta L} =& C^{(5)}\left(\left(L^T C i\tau_2 \Phi_{SM}\right)\left(\tilde{\Phi}_{SM}^{\dagger} L\right)\right) \\ &+ \left(L^T\gamma^\mu e_R\right) i\tau_2\Phi_{SM}\left(C^{(7)}_{Leu\bar{d}\Phi}\overline{d_R}\gamma_\mu u_R + C_L^{(7)}\Phi_{SM}^T i\tau_2 (D_\mu\Phi_{SM})\right) \\ &+ \overline{e_R}e_R^c\left(C^{(9)}_{eeud}\overline{u_R}\gamma^\mu d_R\overline{u_R}\gamma_\mu d_R + C^{(9)}_{ee\Phi ud}\overline{u_R}\gamma^\mu d_R\left(\left[iD_\mu\Phi_{SM}\right]^\dagger\tilde{\Phi}_{SM}\right)\right. \\ &\left. + C^{(9)}_{ee\Phi D}\left(\left[iD_\mu\Phi_{SM}\right]^\dagger\tilde{\Phi}_{SM}\right)^2\right) \end{aligned} \tag{4.39}$$

where Φ_{SM} is the Standard Model Higgs doublet. The matching scale is at $\sim m_{W_R}$.
Taking a look at Figure 4.7 we see that none of these operators contributes to the Δ_L part of the lower-right diagram which is generated by the exchange of the left-handed doubly charged triplet scalar δ_L^{--}.The corresponding lepton number violating operators which contribute to this diagram are obtained from integrating out the heavy double

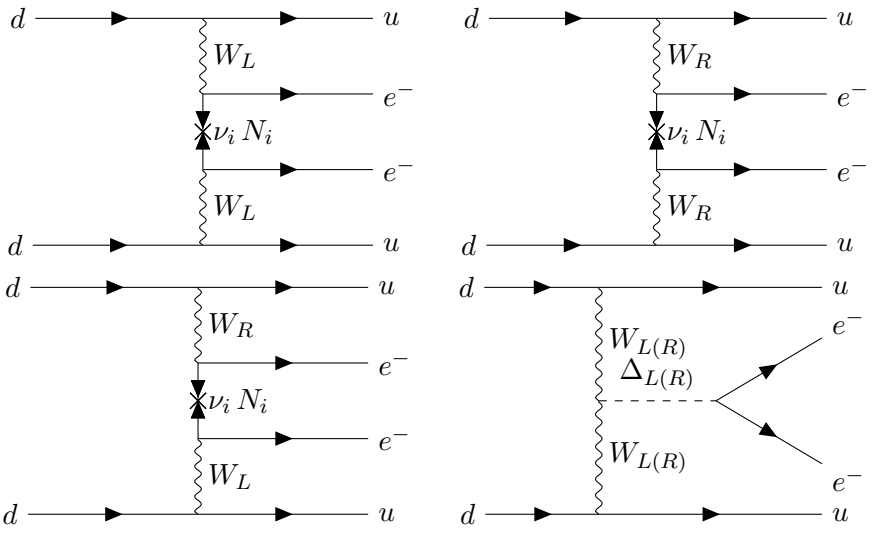

Figure 4.7.: Feynman diagrams arising in the mLRSM that contribute to $0\nu\beta\beta$. Here, ν_i and N_i represent the light and heavy neutrino mass eigenstates. It should be noted that, due to mixing of both left- and right-handed neutrinos and gauge bosons, each diagram (except the triplet exchange diagram) comes with all possible combinations of the outgoing particle's chiralities. However, some diagrams are highly suppressed compared to others.

charged triplet scalars $\delta^{++}_{L,R}$. The relevant parts of the Lagrangian are

$$\begin{aligned}\mathcal{L}_\Delta =& \operatorname{Tr}\Big\{\left(D^\mu \Delta_{L,R}\right)^\dagger \left(D^\mu \Delta_{L,R}\right)\Big\} - \Delta^\dagger_{L,R} M_\Delta \Delta_{L,R} + Y^{L,R} L^T_{L,R} C i\tau_2 \Delta_{L,R} L_{L,R} \\ \supset& \partial^\mu \delta^{--}_{L,R} \partial_\mu \delta^{++}_{L,R} - m^2_{\delta^{++}_{L,R}} \delta^{--}_{L,R} \delta^{++}_{L,R} + \frac{\sqrt{(}2) g_L^2}{2} v_L W_L^+ W_L^+ \delta^{--}_L \\ &+ \frac{\sqrt{(}2) g_L^2}{2} v_L W_L^- W_L^- \delta^{++}_L + Y^L_{ee} e^T_L C e_L \delta^{++}_L .\end{aligned} \tag{4.40}$$

Starting from this Lagrangian and integrating out $\delta^{++,--}_L$ with $M_{\delta^{++}_L} \sim v_R$ one obtains an effective lepton number violating operator of the form

$$Y^L_{ee} \frac{\sqrt{2} g_L^2 v_L}{2 v_R^2} W_L^- W_L^- \bar{e} e^c . \tag{4.41}$$

This operator is proportional to v_L and would break the invariance under the Standard Model gauge group. Hence, it cannot be part of a SMEFT model. However, we can ignore it and still integrate out heavy fields at a scale where the Standard Model gauge group is still intact. The reason for this is that for the process of interest ($0\nu\beta\beta$) it is highly suppressed for typical values of $v_L \sim \mathcal{O}(0.1\,\mathrm{eV})$ and $v_R \sim \mathcal{O}(10\,\mathrm{TeV})$ since the $0\nu\beta\beta$ amplitude corresponding to the operator in Eq. (4.41) will be proportional to $\frac{v_L}{v_R^2 m_W^4}$. This has to be compared to the standard mass mechanism amplitude which depends on

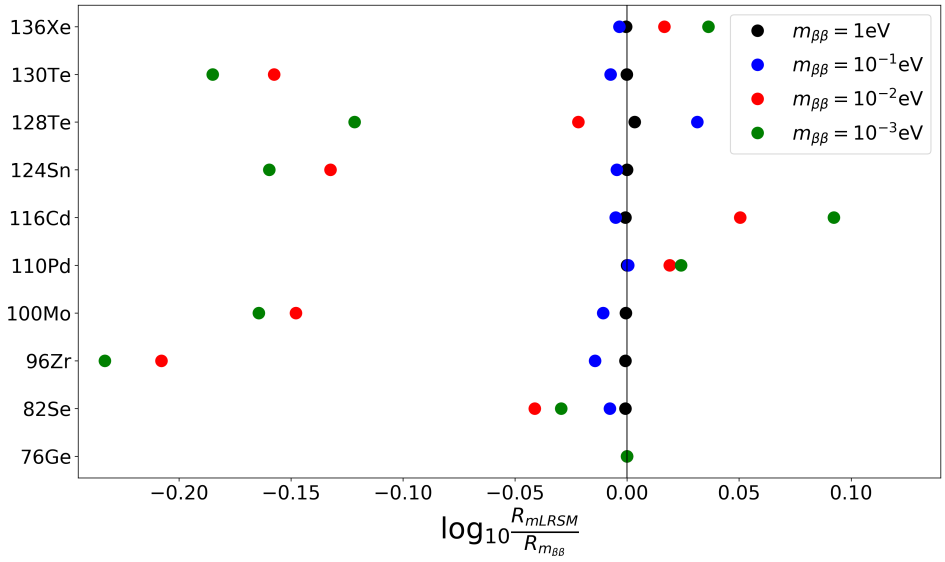

Figure 4.8.: Ratios within the mLRSM for different $m_{\beta\beta}$ ranging from 1 eV to 1 meV.

the same BSM parameters and is proportional to $\frac{v_L}{p^2 m_W^4}$ with $p \sim \mathcal{O}(100\,\text{MeV})$. The Wilson coefficients at SMEFT level are given by [74]

$$\begin{aligned}
C^{(5)} &= \frac{1}{v^2}\left(M_D^{\nu\,T} M_R^{\nu\,-1} M_D^{\nu} - M_L^{\nu}\right) \\
C^{(7)}_{Leu\bar{d}\Phi} &= \frac{\sqrt{2}}{v}\frac{1}{v_R^2}\left(V_R^{ud}\right)^* \left(M_D^T M_R^{\nu\,-1}\right)_{ee} \\
C^{(7)}_{L\Phi De} &= \frac{2i\xi\exp\{i\alpha\}}{(1+\xi^2)\,V_R^{ud*}} C^{(7)}_{Leu\bar{d}\Phi} \\
C^{(9)}_{eeud} &= -\frac{1}{2v_R^4} V_R^{ud2}\left[\left(M_R^{\nu\dagger}\right)^{-1} + \frac{2}{m^2_{\Delta_R}} M_R^{\nu}\right] \\
C^{(9)}_{ee\Phi ud} &= -4\frac{\xi\exp\{-i\alpha\}}{(1+\xi^2)\,V_R^{ud}} C^{(9)}_{eeud} \\
C^{(9)}_{ee\Phi D} &= 4\frac{\xi^2\exp\{-2i\alpha\}}{(1+\xi^2)^2\,V_R^{ud2}} C^{(9)}_{eeud}
\end{aligned} \tag{4.42}$$

where v is the Standard Model Higgs doublets VEV given by

$$v^2 = \kappa^2 + \kappa'^2. \tag{4.43}$$

From the matching scale $\sim m_{W_R}$ the above coefficients have to be evolved down to $m_W \sim 80\,\text{GeV}$ at which one can match onto the relevant LEFT operators by integrating

out the remaining heavy particles with masses above m_W. By doing so one obtains [74]

$$\begin{aligned} m_{\beta\beta} &= -v^2 C_{ee}^{(5)} \\ C_{VL}^{(6)} &= -iV_L^{ud}\frac{v^3}{\sqrt{2}} C_{L\Phi De}^{(7)\,*} \\ C_{VR}^{(6)} &= \frac{v^3}{\sqrt{2}} C_{Leu\bar{d}\Phi}^{(7)\,*} \\ C_{1R}^{(9)}(m_W) &= v^5 V_L^{ud2} C_{ee\Phi D}^{(9)}(m_W) \\ C_{1R}^{(9)\prime}(m_W) &= v^5 C_{eeud}^{(9)}(m_W) \\ C_{4R}^{(9)}(m_W) &= -v^5 V_L^{ud} C_{ee\Phi ud}^{(9)}(m_W). \end{aligned} \tag{4.44}$$

Evolving the above coefficients down to the χPT scale of $\sim 2\,\text{GeV}$ also generates a non-zero $C_{5R}^{(9)}$ coefficient since the RGEs of $C_{4,5}^{(9)}$ mix [74]. Setting $\theta_L = \alpha = 0$ and fixing $\xi = m_b/m_t$, as well as assuming that the light and heavy neutrino mass matrices M_ν and M_{ν_R} are diagonalized by the same matrix and imposing the similar property for the mass matrices of the left- and right-handed Quarks, the Wilson coefficients can be expressed in terms of the different VEVs v, v_L, v_R as well as the physical masses of the heavy neutrinos $m_{\nu_{R1,2,3,}}$, the lightest neutrino mass m_{min} and the mass of the heavy right-handed triplet m_{Δ_R}. For simplicity we will study the limit of 1 fermion generation applying the same mass structure as [74]

$$\begin{aligned} v_L &= 0.1\,\text{eV}, \qquad v_R = 10\,\text{TeV}, \\ m_{\nu_R} &= 10\,\text{TeV}, \quad m_{\Delta_R} = 4\,\text{TeV}. \end{aligned} \tag{4.45}$$

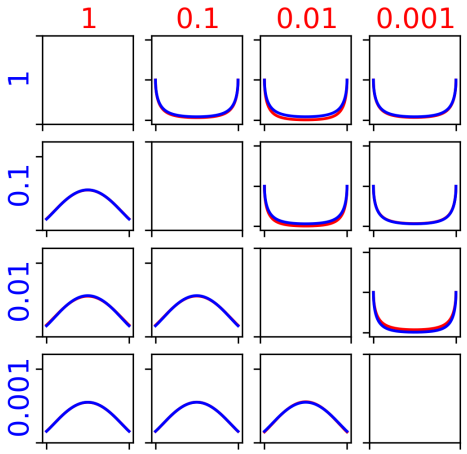

Figure 4.9.: Normalized single electron spectra (lower left) and angular correlation coefficients (upper right) generated in the mLRSM with different effective Majorana masses $m_{\beta\beta} = 1\,\text{eV} - 0.001\,\text{eV}$. The shapes are shown for ^{136}Xe.

Additionally, we adapt M_D^ν to vary the value of $m_{\beta\beta}$ between $1\,\text{eV} - 1\,\text{meV}$ such that we can study the impact of the non-standard operators at different strengths of the mass-mechanism. The ratios are shown in Figure 4.8. One can see that for values $m_{\beta\beta} \leq 10\,\text{meV}$ the ratios start to be distinct from the standard mass mechanism as non-standard operators start to dominate. Here, the main contribution when choosing this parameter setup stems from the scalar short-range LEFT operators. Below $m_{\beta\beta} = 1\,\text{meV}$ the ratios stay at a stable level. The PSF observables are shown in Figure 4.9. As one can see the different settings cannot be

distinguished from each other or from the standard mass mechanism. The reason for this is that either the $m_{\beta\beta}$ or the short-range Wilson coefficients $C_{1,4}^{(9)(,)}$ dominate the decay amplitude which all couple to the same PSF G_{01}.

4.2.2. $\not{R}_p$ - SUSY

Historically, supersymmetric (SUSY) theories have been considered to be attractive extensions to the Standard Model since they offer a wide field of possible explanations to urging questions within the particle physics community as, e.g., the hierarchy problem or the origin of dark matter. A comprehensive review can be found in [97].
Supersymmetric theories contain so-called supermultiplets of fermions and bosons which, under supersymmetry, transform into each other. The most simple constructions are chiral supermultiplets

$$\left(\Psi_{L,R}, \Phi_{L,R}^{\Psi}\right) \tag{4.46}$$

which relate two component chiral spinors ($\Psi_{L,R}$) and a corresponding complex scalar $\Phi_{L,R}$. If we want to make the Standard Model supersymmetric, one also needs to consider gauge supermultiplets

$$\left(A_{\mu}^{a}, \Psi^{a}\right) \tag{4.47}$$

which relate the Standard Model's gauge bosons A_{μ}^{a} to their superpartner fermions Ψ^{a}. One should note that since gauge bosons have 2 degrees of freedom (d.o.f.) and since a transformation obviously cannot change the number of d.o.f., their superpartners Ψ^{a} also have 2 degrees of freedom. Therefore, they are Majorana fermions.[9]
Obviously for SUSY to hold, particles within a supermultiplet must share the same mass, quantum numbers (except spin), interactions and couplings. This fact necessitates that SUSY, if realized in nature, must be broken to hide the superpartners of the Standard Model particles which are yet to be observed. Typically, after breaking SUSY there remains a discrete symmetry called R-parity (R_p) which can be assigned to every field such that we have $R_p = +1$ for Standard Model fields and $R_p = -1$ for the superpartner fields. One can define R-parity as [97]

$$R_p = (-1)^{2s+3(B-L)} \tag{4.48}$$

where s is the spin and B and L are the corresponding baryon and lepton numbers of the field. If R_p is a conserved quantity, it follows that the lightest superpartner cannot decay such that it becomes a candidate for explaining the origin of dark matter.[10] However, R_p conservation also comes with the conservation of both baryon and lepton number [97]. Thus, supersymmetric models which want to explain the baryon asymmetry

[9] Or Weyl fermions in the massless case. However, in the massless case distinguishing Weyl and Majorana fermions is not necessary
[10] It is often referred to as LSP.

of the universe via explicit violation of either lepton or baryon number need to break R_p. This induces new lepton number violating parts to the Lagrangian [98]

$$\begin{aligned}\mathcal{L}^{\Delta L=1}_{\not{R}_p} = &-\lambda'_{111}\Big[(\overline{u}_L, \overline{d}_R) \begin{pmatrix} e^c_R \\ -\nu^c_R \end{pmatrix} \tilde{d}_R \\ &+ (\overline{e}_L, \overline{\nu}_L)\, d_R \begin{pmatrix} \tilde{u}^*_L \\ -\tilde{d}^*_L \end{pmatrix} \\ &+ \left(\overline{u}_L, \overline{d}_L\right) d_R \begin{pmatrix} \tilde{e}^*_L \\ -\tilde{\nu}^*_L \end{pmatrix} \Big] + h.c.\end{aligned} \tag{4.49}$$

which can contribute to $0\nu\beta\beta$-decay. Contributions to $0\nu\beta\beta$ from $\not{R}_p$−SUSY have been studied first by [98, 99]. The resulting Feynman diagrams are shown in Figure 4.10. The relevant gluino ($\tilde{g}$) and neutralino (χ) - fermion interactions are given by [98, 100, 101]

$$\mathcal{L}_{\tilde{g}} = -\sqrt{2} g_3 \sum_a \frac{\lambda^{(a)}_{\alpha\beta}}{2} \left(\overline{q_L}^{\alpha} \tilde{g} \tilde{q}^{\beta}_L - \overline{q_R}^{\alpha} \tilde{g} \tilde{q}^{\beta}_R \right) + h.c. \tag{4.50}$$

and

$$\mathcal{L}_{\chi} = \sqrt{2} g_2 \sum_{i=1}^{4} \left(\epsilon_{Li}\left(\Psi\right) \overline{\Psi_L} \chi_i \tilde{\Psi}_L + \epsilon_{Ri}\left(\Psi\right) \overline{\Psi_R} \chi_i \tilde{\Psi}_R + \right) + h.c.. \tag{4.51}$$

One can arrive at the low-energy effective Lagrangian by integrating out the heavy superfields as well as the Standard Model particles with masses above$\sim m_W$. After integrating out the heavy scalar squarks $\tilde{d}_R$ and $\tilde{u}_L$ as well as the gluino $\tilde{g}$ and neutralinos χ_i by solving the e.o.m. and plugging the solutions back into the Lagrangian one after the other, one finds the different low-energy effective dimension-9 $\Delta L = 2$ operators which contribute to $0\nu\beta\beta$ [99]

$$\begin{aligned}\mathcal{L}_{\not{R}_p} = \frac{G_F^2}{2m_N} \Big[&(\eta_{\tilde{g}} + \eta_{\chi}) \left(\left[\overline{u}(1+\gamma^5)d\right] \left[\overline{u}(1+\gamma^5)d\right] - \frac{1}{4} \left[\overline{u}\sigma^{\mu\nu}(1+\gamma^5)d\right] \left[\overline{u}\sigma_{\mu\nu}(1+\gamma^5)d\right] \right) \\ &+ \left(\eta_{\chi\tilde{e}} + \eta'_{\tilde{g}} - \eta_{\chi\tilde{f}} \right) \left[\overline{u}(1+\gamma^5)d\right] \left[\overline{u}(1+\gamma^5)d\right] \Big] \left[\overline{e}\,(1+\gamma_5)\, e^c\right].\end{aligned} \tag{4.52}$$

These can be translated to the *C-basis* as

$$\begin{aligned} C^{(9)\prime}_{2R} &= \frac{2v}{m_N} \left[2\eta_{\tilde{g}} + 2\eta_{\chi} + \eta_{\chi\tilde{e}} + \eta'_g - \eta_{\chi\tilde{f}} \right] \\ C^{(9)\prime}_{3R} &= \frac{4v}{m_N} \left[\eta_{\tilde{g}} + \eta_{\chi}\right]. \end{aligned} \tag{4.53}$$

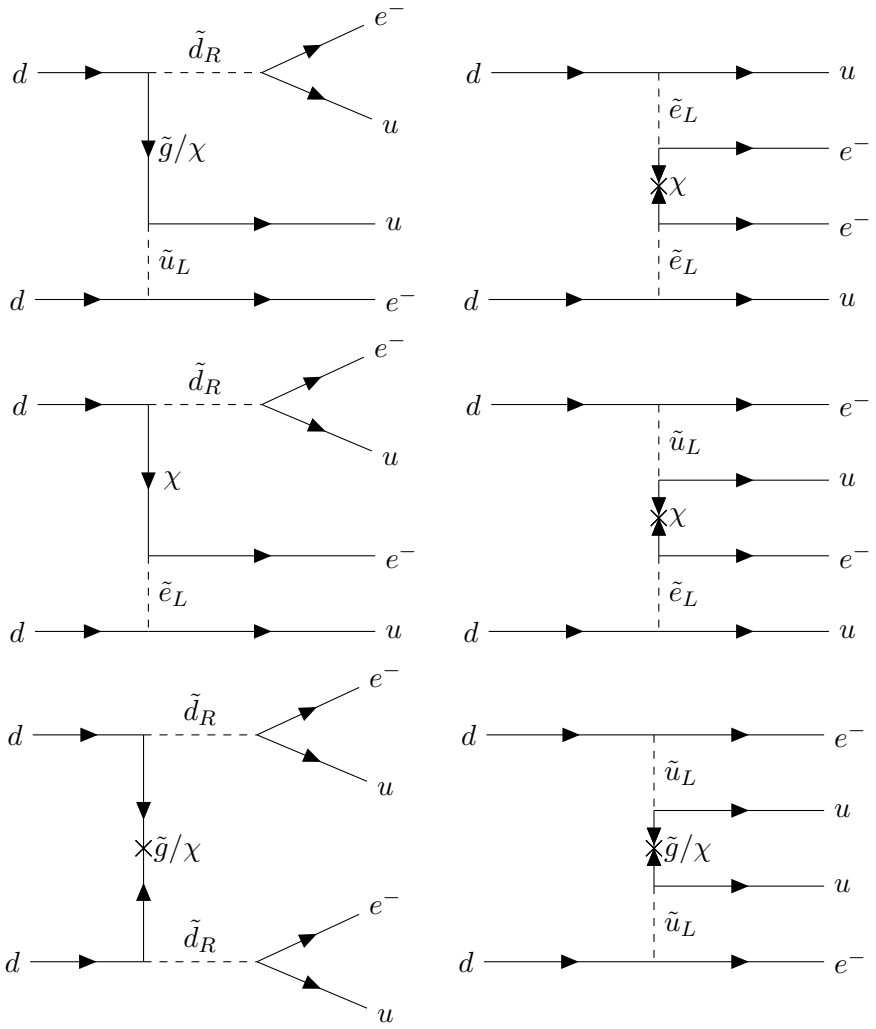

Figure 4.10.: Feynman diagrams contributing to $0\nu\beta\beta$ within the $\not{R}_p$-MSSM [98].

The coupling constants are given in terms of the gluino, neutralino and squark masses as [98]

$$
\begin{aligned}
\eta_{\tilde{g}} &= \alpha_s \Lambda^2 \frac{m_N}{m_{\tilde{g}}} \left[1 + \left(\frac{m_{\tilde{d}_R}}{m_{\tilde{u}_L}} \right)^4 \right] \\
\eta'_{\tilde{g}} &= 2\alpha_s \Lambda^2 \frac{m_N}{m_{\tilde{g}}} \left(\frac{m_{\tilde{d}_R}}{m_{\tilde{u}_L}} \right)^2 \\
\eta_{\chi} &= \frac{3\alpha_2}{4} \Lambda^2 \sum_{i=1}^{4} \frac{m_N}{m_{\chi_i}} \left[\epsilon_{Ri}^2(d) + \epsilon_{Li}^2(u) \left(\frac{m_{\tilde{d}_R}}{m_{\tilde{u}_L}} \right)^4 \right] \\
\eta_{\chi\tilde{e}} &= 9\alpha_2 \Lambda^2 \left(\frac{m_{\tilde{d}_R}}{m_{\tilde{e}_L}} \right)^4 \sum_{i=1}^{4} \epsilon_{Li}^2(e) \frac{m_N}{m_{\chi_i}} \\
\eta_{\chi\tilde{f}} &= \frac{3\alpha_2}{2} \Lambda^2 \left(\frac{m_{\tilde{d}_R}}{m_{\tilde{e}_L}} \right)^2 \sum_{i=1}^{4} \frac{m_N}{m_{\chi_i}} \left[\epsilon_{Ri}(d)\epsilon_{Li}(e) + \epsilon_{Ri}(u)\epsilon_{Li}(d) \left(\frac{m_{\tilde{e}_L}}{m_{\tilde{u}_L}} \right)^2 \right. \\
&\qquad \left. + \epsilon_{Ri}(u)\epsilon_{Li}(e) \left(\frac{m_{\tilde{d}_R}}{m_{\tilde{u}_L}} \right)^2 \right]
\end{aligned}
\tag{4.54}
$$

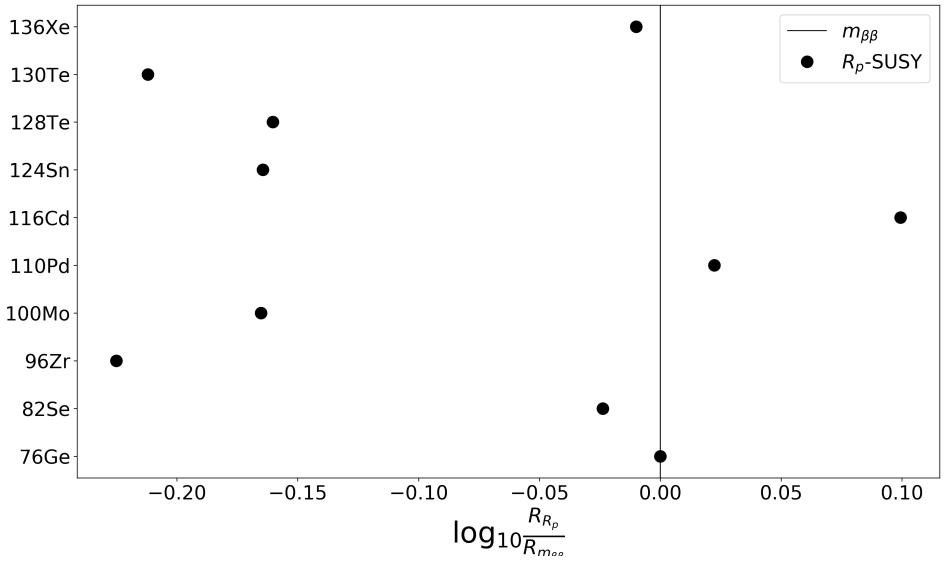

Figure 4.11.: Half-life ratios resulting from the $\not{R}_p$-SUSY contributions to $0\nu\beta\beta$ compared to the standard mass mechanism.

with

$$\Lambda = \frac{\sqrt{2\pi}}{3}\frac{\lambda'_{111}}{G_F m^2_{\tilde{d}_R}} \tag{4.55}$$

We can see that both gluino and neutralino exchange diagrams contribute to the same low-energy operators. We calculated the ratios in Figure 4.11. As we saw in the previous section, distinguishing effects coming from $C^{(9)\prime}_{2R}$ and $C^{(9)\prime}_{3R}$ is not achievable by any practical means within the current knowledge of LECs. Hence, there is no sense in studying different parameter settings here. Additionally, both operators contribute only to G_{01} such that there is not much information to gain when turning towards the phase-space observables as they are the same as for the mass mechanism.

4.2.3. Leptoquarks

Leptoquarks (LQs) are hypothetical bosons $(3, X, Y)$ with non-zero color charge which couple to both quarks and leptons. They arise in numerous Standard Model extensions such as technicolor and composite models [102, 103] or models of grand unification [104, 105]. Additionally, they can generate non-zero neutrino masses at 1 loop level [106]. For a comprehensive review on leptoquarks see [107].
Ignoring leptoquarks which do not directly couple to the Standard Model's particle content, one can add up to 10 different leptoquarks which obey the Standard Model sym-

LQ (Ω)	$SU(3)_C$	$SU(2)_L$	$U(1)_Y$	Q
S_0	3	1	-2/3	-1/3
$\tilde{S}_0$	3	1	-8/3	-4/3
$S_{1/2}$	$\overline{3}$	2	-7/3	$(-2/3, -5/3)$
$\tilde{S}_{1/2}$	$\overline{3}$	2	-1/3	$(1/3, -2/3)$
S_1	3	3	-2/3	$(2/3, -1/3, -4/3)$
V_0	$\overline{3}$	1	-4/3	-2/3
$\tilde{V}_0$	$\overline{3}$	1	-10/3	-5/3
$V_{1/2}$	3	2	-5/3	$(-1/3, -4/3)$
$\tilde{V}_{1/2}$	3	2	1/3	$(2/3, -1/3)$
V_1	$\overline{3}$	3	-4/3	$(1/3, -2/3, -5/3)$

Table 4.4.: List of possible scalar and vector leptoquarks and their transformation properties under the Standard Model symmetries.

metries [**?**][11] They are summarized in Table 4.4. By looking at the relevant Feynman diagrams in Figure 4.12 we can see that the contributions to $0\nu\beta\beta$ arise from leptoquarks with $Q^{(1)} = \pm 1/3$ (Figure 4.12 left) and $Q^{(2)} = \pm 2/3$ (Figure 4.12 right). The full set of renormalizable LQ-fermion interactions is given by [108]

$$\begin{aligned}\mathcal{L}_{S,f} = &\left(\lambda^R_{S_0}\right)_{ij} S_0^{R\dagger}\left[\overline{u^c}_i P_R e_j\right] + \left(\lambda^R_{\tilde{S}_0}\right)_{ij} \tilde{S}_0^{\dagger}\left[\overline{d^c}_i P_R e_j\right] \\ &+ \left(\lambda^R_{S_{1/2}}\right)_{ij} S_{1/2}^{R\dagger}\left[\overline{u}_i P_L L_j\right] + \left(\lambda^R_{\tilde{S}_{1/2}}\right)_{ij} \tilde{S}_{1/2}^{\dagger}\left[\overline{d}_i P_L L_j\right] \\ &+ \left(\lambda^L_{S_0}\right)_{ij} S_0^{L\dagger}\left[\overline{Q^c}_i P_L i\tau_2 L_j\right] + \left(\lambda^L_{S_{1/2}}\right)_{ij} S_{1/2}^{L\dagger}\left[\overline{Q^c}_i P_R i\tau_2 e_j\right] \\ &+ \left(\lambda^L_{S_1}\right)_{ij}\left[\overline{Q^c}_i P_L i\tau_2 S_1^{\dagger} L_j\right] + h.c.\end{aligned} \tag{4.56}$$

and

$$\begin{aligned}\mathcal{L}_{V,f} = &\left(\lambda^R_{V_0}\right)_{ij} V_{0\mu}^{R\dagger}\left[\overline{d}_i \gamma^\mu P_R e_j\right] + \left(\lambda^R_{\tilde{V}_0}\right)_{ij} \tilde{V}_{0\mu}^{R\dagger}\left[\overline{u}_i \gamma^\mu P_R e_j\right] \\ &+ \left(\lambda^R_{V_{1/2}}\right)_{ij} V_{1/2\mu}^{R\dagger}\left[\overline{d^c}_i \gamma^\mu P_L L_j\right] + \left(\lambda^R_{\tilde{V}_{1/2}}\right)_{ij} \tilde{V}_{1/2}^{\dagger}\left[\overline{u^c}_i \gamma^\mu P_L L_j\right] \\ &+ \left(\lambda^L_{V_0}\right)_{ij} V_{0\mu}^{L\dagger}\left[\overline{Q}_i \gamma^\mu P_L L_j\right] + \left(\lambda^L_{V_{1/2}}\right)_{ij} V_{1/2\mu}^{L\dagger}\left[\overline{Q^c}_i \gamma^\mu P_R e_j\right] \\ &+ \left(\lambda^L_{V_1}\right)_{ij}\left[\overline{Q}_i \gamma^\mu P_L V_{1\mu}^{\dagger} L_j\right] + h.c.\end{aligned} \tag{4.57}$$

for the scalar (S) and vector (V) leptoquarks respectively. Here we follow the notation of [108] which distinguishes leptoquarks coupling to left- and right-handed quarks. Additionally to the LQ-fermion interactions, one can write down gauge invariant and

[11] Note that one sometimes finds a different Y assignment. This is due to a different definition of Y which results in $Q = I_3 + Y$ instead of our definition $Q = I_3 + Y/2$.

renormalizable LQ-Higgs interactions

$$\begin{aligned}\mathcal{L}_{LQ,\Phi} =& h^i_{S_0}\tilde{\Phi}^\dagger \tilde{S}_{1/2} S^i_0 + h^i_{V_0}\tilde{\Phi}^\dagger \tilde{V}^\mu_{1/2} V^i_{0\mu} \\ &+ h_{S_1}\tilde{\Phi}^\dagger S_1 \tilde{S}_{1/2} + h_{V_1}\tilde{\Phi}_1^{\ \mu}\tilde{V}_{1/2\mu} \\ &+ Y^i_{S_{1/2}}\left(\tilde{\Phi}^\dagger S^i_{1/2}\right)\left(\tilde{S}^\dagger_{1/2}\Phi\right) + Y^i_{V_{1/2}}\left(\tilde{\Phi}^\dagger V^{\mu i}_{1/2}\right)\left(\tilde{V}^\dagger_{1/2\mu}\Phi\right) \\ &+ Y_{S_1}\left(\tilde{\Phi}^\dagger S^\dagger_1 \Phi\right)\tilde{S}_0 + Y_{V_1}\left(\tilde{\Phi}^\dagger V^\dagger_{1\mu}\Phi\right)\tilde{V}^\mu_0 \\ &+ \kappa^i_S\left(\Phi^\dagger S_1 \Phi\right) S^{i\,\dagger}_0 + \kappa^i_V\left(\Phi_1^{\ \mu}\Phi\right) V^{i\ \dagger}_{0\mu} + h.c. \\ &- \sum_\Omega \left(\eta_\Omega M^2_\Omega - g^{i_1 i_2}_\Omega \Phi^\dagger\Phi\right)\Omega^{i_1\dagger}\Omega^{i_2}\end{aligned} \tag{4.58}$$

where the leptoquark triplets are defined as

$$V_1 = \sum_i \tau_i V_{1i} \qquad S_1 = \sum_i \tau_i S_{1i}. \tag{4.59}$$

These LQ-Higgs interactions are essential when considering contributions to $0\nu\beta\beta$ because they result in non-zero correlation functions for, e.g.,

$$\left\langle S^i_0 \tilde{S}_{1/2}\right\rangle \propto \sum_{\tilde{I}} \mathcal{N}_{S^i_0\tilde{I}}\mathcal{N}_{\tilde{S}_{1/2}\tilde{I}} \tag{4.60}$$

where $\mathcal{N}$ is the mixing matrix which diagonalizes the mass matrix $\mathcal{N}^T\mathcal{M}^2\mathcal{N} = \mathcal{M}^2_{diag}$ and $\tilde{I} = \mathcal{N}^T I$ are the mass eigenstate fields. This particular example results in contributions to the right diagram in Figure 4.12. After electroweak symmetry breaking the relevant mass matrices are given by [108]

$$\mathcal{M}_{\mathcal{I}}{}^2\left(Q^{(1)}_I\right) = \eta_I \begin{pmatrix} \eta_I \overline{\mathbf{M}}_{\mathbf{I^L_0}}{}^2 & g^{LR}_{I_0} v^2 & \mathbf{h^L_{I_0}} v & \kappa^L_I v^2 \\ g^{LR}_{I_0} v^2 & \eta_I \overline{\mathbf{M}}_{\mathbf{I^R_0}}{}^2 & \mathbf{h^R_{I_0}} v & \kappa^R_I v^2 \\ \mathbf{h^L_{I_0}} v & \mathbf{h^R_{I_0}} v & \eta_I \overline{\mathbf{M}}_{\mathbf{I_{1/2}}}{}^2 & \mathbf{h_{I_1}} v \\ \kappa^L_I v^2 & \kappa^R_I v^2 & \mathbf{h_{I_1}} v & \overline{\mathbf{M}}_{\mathbf{I_1}}{}^2 \end{pmatrix} \tag{4.61}$$

and

$$\mathcal{M}^2_I\left(Q^{(2)}_I\right) = \eta_I \begin{pmatrix} \eta_I \overline{\mathbf{M}}_{\mathbf{I_{1/2}}}{}^2 & Y^L_{I_{1/2}} v^2 & Y^R_{I_{1/2}} v^2 & \sqrt{2}\mathbf{h_{I_1}} v \\ Y^L_{I_{1/2}} v^2 & \eta_I \overline{\mathbf{M}}_{\mathbf{I^L_{1/2}}}{}^2 & g^{LR}_{I_{1/2}} v^2 & 0 \\ Y^R_{I_{1/2}} v^2 & g^{LR}_{I_{1/2}} v^2 & \eta_I \overline{\mathbf{M}}_{\mathbf{I^R_{1/2}}}{}^2 & 0 \\ \sqrt(2)\mathbf{h_{I_1}} v & 0 & 0 & \eta_I \overline{\mathbf{M}}_{\mathbf{I_1}}{}^2 \end{pmatrix} \tag{4.62}$$

with $I = S, V$ $\eta_S = 1, \eta_V = -1$ and $\overline{M}^2 = M^2_I + \eta_I g_I v^2$. The **bold** constants are mass scales which are a priori completely free. Of course, they can arise dynamically from more complete models.

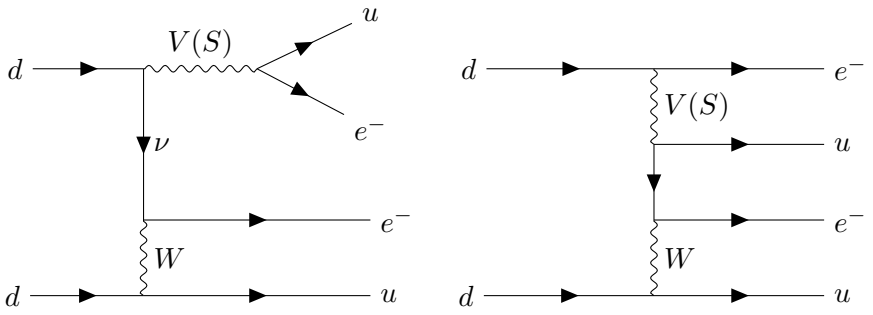

Figure 4.12.: Feynman diagrams of the vector (V) and scalar (S) leptoquark interactions contributing to $0\nu\beta\beta$.

After integrating out the heavy LQ degrees of freedom and rearranging the resulting EFT operators via Fierz transformations one arrives at the effective low-energy 4-Fermi interactions. The parts of the low-energy Lagrangian, that are relevant to $0\nu\beta\beta$, are then given by [109]

$$\begin{aligned}\mathcal{L}_{LQ} = &[\overline{e}P_L\nu^c]\left\{\frac{\epsilon_S}{M_S^2}[\overline{u}P_Rd] + \frac{\epsilon_V}{M_V^2}[\overline{u}P_Ld]\right\} \\ &- [\overline{e}\gamma^\mu P_L\nu^c]\left\{\left(\frac{\alpha_S^R}{M_S^2} + \frac{\alpha_V^R}{M_V^2}\right)[\overline{u}\gamma_\mu P_Rd] - \sqrt{2}\left(\frac{\alpha_S^L}{M_S^2} + \frac{\alpha_V^L}{M_V^2}\right)[\overline{u}\gamma_\mu P_Ld]\right\} + h.c.\end{aligned} \tag{4.63}$$

with the low-energy Wilson coefficients

$$\epsilon_I = 2^{-\eta_I}\left[\lambda_{I_1}^L\lambda_{\tilde{I}_{1/2}}^R\left(\tilde{\theta}_{43}^I\left(Q_I^1\right) + \eta_I\sqrt{2}\tilde{\theta}_{41}^I\left(Q_I^2\right)\right) - \lambda_{I_0}^L\lambda_{\tilde{I}_{1/2}}^R\tilde{\theta}_{23}^I\left(Q_I^1\right)\right] \tag{4.64}$$

$$\alpha_I^L = \frac{2}{3+\eta_I}\lambda_{I_{1/2}}^L\lambda_{I_1}^L\tilde{\theta}_{24}^I\left(Q_I^2\right), \qquad \alpha_I^R = \frac{2}{r+\eta_I}\lambda_{I_0}^R\lambda_{\tilde{I}_{1/2}}^R\tilde{\theta}_{23}^I\left(Q_I^1\right). \tag{4.65}$$

with

$$\tilde{\theta}_{ij}^I = \sum_k \mathcal{N}_{ik}\mathcal{N}_{jk}\frac{M_I^2}{M_{\tilde{I}_k}^2}. \tag{4.66}$$

Here, "common mass scales" M_S and M_V have been inserted for convenience. It should be noted that the exact choice of $M_{S,V}$ does not matter as they drop out. However, the exact LQ masses do enter into the calculation such that for leptoquark masses which are about the same order of magnitude one can choose $M_{S,V}$ such that it represents the supression factor. Looking at Eq. (4.64) and Eq. (4.65), there is a priori no reason from, e.g., naturalness arguments why any of the low energy coefficients α_I and ϵ_I should be suppressed or enhanced compared to the others. However, if the LQ interactions arise from a more complete model, hierarchical structures might appear. We will therefore study different settings in which some couplings dominate over the others.

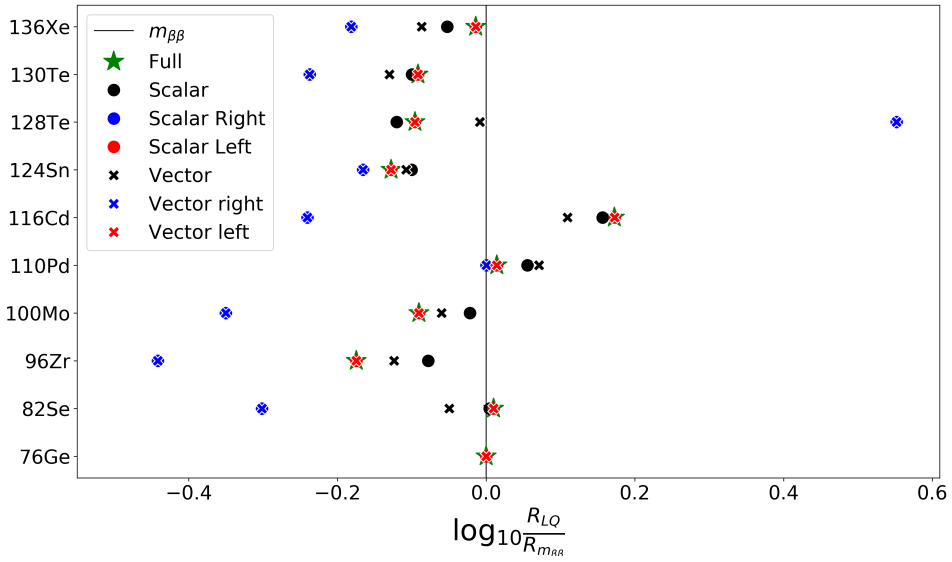

Figure 4.13.: Half-life ratios resulting from different leptoquark settings when taking ^{76}Ge as the reference isotope. The ratios are compared to the standard mass mechanism.

From Eq. (4.63) we can match the Wilson coefficients in Eq. (4.64) and Eq. (4.65) onto the *C-basis* and find

$$\begin{aligned} C_{SL}^{(6)} &= \frac{v^2}{M_V^2}\epsilon_V \\ C_{SR}^{(6)} &= \frac{v^2}{M_S^2}\epsilon_S \\ C_{VL}^{(6)} &= \sqrt{2}v^2\left(\frac{\alpha_S^L}{M_S^2}+\frac{\alpha_V^L}{M_V^2}\right) \\ C_{VR}^{(6)} &= -v^2\left(\frac{\alpha_S^R}{M_S^2}+\frac{\alpha_V^R}{M_V^2}\right). \end{aligned} \tag{4.67}$$

We study 7 different settings of LQ contributions to $0\nu\beta\beta$:

1. Full LQ Model: $\epsilon_S = \epsilon_V = \alpha_S^L = \alpha_S^R = \alpha_V^L = \alpha_V^R = 1$
2. Scalar LQs (S): $\epsilon_S = \alpha_S^L = \alpha_S^R = 1$
3. Scalar LQs coupling to LH fermions (SL): $\alpha_S^L = 1$
4. Scalar LQs coupling to RH fermions (SR): $\alpha_S^R = 1$

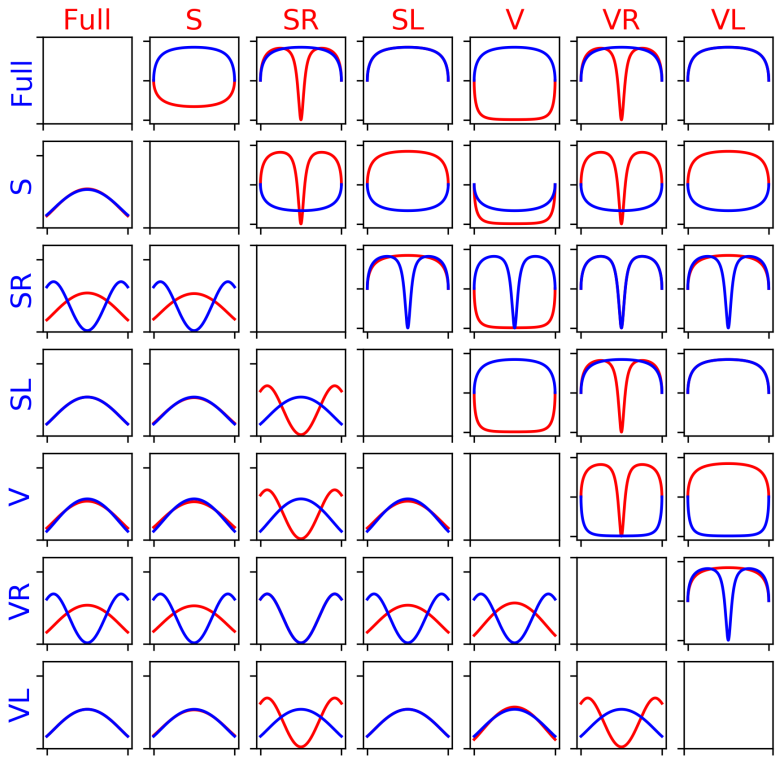

Figure 4.14.: Angular correlation coefficients (upper right) and single electron spectra (lower left) resulting from the different LQ contributions.

5. Vector LQs (V): $\epsilon_V = \alpha_V^L = \alpha_V^R = 1$
6. Vector LQs coupling to LH fermions (VL): $\alpha_V^L = 1$
7. Vector LQs coupling to RH fermions (VR): $\alpha_V^R = 1$

The resulting ratios normalized to the neutrino mass mechanism for each of the above cases are shown in Figure 4.13. The corresponding single electron spectra and angular correlation coefficients can be seen in Figure 4.14. We can see that distinguishability between scalar and vector LQs is only given if couplings to both left- and right-handed fermions are realized while distinguishability between leptoquarks coupling to left- or right-handed fermions is also possible.

5. Summary and Conclusions

In this thesis, we studied possibilities to distinguish and identify different mechanisms of $0\nu\beta\beta$-decay. We focused our efforts mainly towards low-energy $0\nu\beta\beta$-decay experiments but also shortly covered complementary high-energy collider experiments. To include all possible $0\nu\beta\beta$ mechanisms we utilized a low-energy effective field theory framework designed by [74] that contains a basis of 32 independent LEFT operators.
Studying the observables that can in principle be extracted from $0\nu\beta\beta$-decay experiments we found that one can organize these 32 different operators into 11 groups that are theoretically distinguishable from each other. To arrive at these 11 operator groups we assumed the NDA values for the unknown LECs. First we studied the impact of the different operators onto the phase space observables, i.e., the single electron spectrum as well as the angular correlation coefficient shown in Figure 4.2 and found that in principle one can distinguish 4 different groups of operators via these observables. Afterwards we turned towards studying how well different operator groups can be distinguished from each other utilizing half-life measurements in different isotopes. This approach resulted in the aforementioned 11 distinguishable groups. In Figure 4.6 we show the maximum half-life ratios and the corresponding combination of isotopes. We calculated these once setting the unknown LECs to 0 while keeping $g_{1,6,7}^{NN} = g_V^{\pi N} = \tilde{g}_V^{\pi N} = 1$ such that we do not omit contributions from the short-range vector operators and once setting the unknown LECs to their NDA values. The different choices mostly affect the contributions from short-range mechanisms. Next, from the results shown in Figure 4.6 we determined the experimental accuracy on the half-life measurement that is necessary to identify different operators at 1σ. The results are shown in Table 4.3. Again, we studied both LEC settings. Interestingly, we found that in both settings the mass mechanism can be identified or rejected at the 1σ level if the necessary accuracy of 5σ on the half-life of $0\nu\beta\beta$ is reached. Therefore, given the observation of $0\nu\beta\beta$ in the corresponding isotopes one can already see whether the mass mechanism is indeed the leading order mechanism or if some non-standard mechanism gives the leading order contribution.
While these findings encourage measurements in many different isotopes, we do not find measurements of different $0\nu\beta\beta$ modes to be very promising as they are typically expected to be highly suppressed.
We want to emphasize that while our findings should be qualitatively profound, especially for the short-range mechanism a precise knowledge of the currently unknown LECs is necessary if one wants to exactly predict quantitative half-life ratios. Additionally, better knowledge of the currently unknown LECs could enable us to distinguish between different short-range vector operators, increasing the number of operator groups that are distinguishable via $0\nu\beta\beta$ experiments to 12. Therefore, this work should be viewed as a motivation towards calculating these within lattice QCD.

Within our calculations we ignored uncertainties coming from the choice of the NME calculation method as it is currently not possible to set strict errorbars. However, while different calculation methods can lead to NMEs differing by factors of $2-3$ the difference of the ratios of NMEs are oftentimes smaller as one can expect that systematic errors cancel. Additionally, as ab initio methods will become more feasible also for heavier nuclei the uncertainty on the NMEs should become considerably smaller while it can become possible to safely quantify uncertainties in the NME calculation.
In the best case scenario we will observe lepton number violation in both $0\nu\beta\beta$ experiments as well as within collider experiments. Assuming the currently unknown LECs will allow us to distinguish the maximum of 12 operator groups within $0\nu\beta\beta$ experiments, one can additionally distinguish between operators of the same quark current but different lepton current structure using collider data. This would result in 17 different distinguishable operator groups.
In the last part of this work we applied the above methods onto full models rather than just single operators and compared them to the standard mass mechanism. While the assumption of a single operator dominance can be realized in full models such as, e.g., the mLRSM with vanishing $m_{\beta\beta} < 10\,\text{meV}$, this does not necessarily hold for every model or parameter setting. Here we studied three different types of models, mLRSM, $\not{R}_p$-SUSY and Leptoquarks. The obtained ratios are shown in Figures 4.8, 4.11 and 4.13. Of course one cannot hope to clearly identify a full BSM model utilizing only $0\nu\beta\beta$-decay experiments as many different high-energy models can result in the same low-energy effective theory. However, measuring and comparing the expected decay rate ratios can still help to reject certain models or parameter sets. Additionally, all three models that we studied can in principle be distinguished from the mass mechanism.[1]
In this work we only considered new-physics beyond the weak scale. However, especially the presence of light[2] right-handed sterile neutrinos is a notable exception that we do not cover by this approach. The impact of which has recently been studied by Dekens et al. [110] and should also be included in a future work. Especially masses around the scale of momentum transfer $\sim 100\,\text{MeV}$ could be interesting as resonances might appear.

[1] That is except parameter settings for the mLRSM in which the mass mechanism gave the dominant contribution.
[2] , i.e., that are dynamical also at the LEFT scale

Part I.

Appendix

A. Basis Translation

A.1. Fierz Tranformations

Fierz transformations [111, 112] give a relation between fermion quadrilinears of different Lorentz structures. Defining

$$e_S(1234) = [\overline{\omega}_1\omega_2]\,[\overline{\omega}_3\omega_4] \tag{A.1}$$
$$e_V(1234) = [\overline{\omega}_1\gamma^\mu\omega_2]\,[\overline{\omega}_3\gamma_\mu\omega_4] \tag{A.2}$$
$$e_T(1234) = [\overline{\omega}_1\sigma_{\mu\nu}\omega_2]\,[\overline{\omega}_3\sigma^{\mu\nu}\omega_4] \tag{A.3}$$
$$e_A(1234) = [\overline{\omega}_1\gamma^\mu\gamma_5\omega_2]\,[\overline{\omega}_3\gamma_\mu\gamma_5\omega_4] \tag{A.4}$$
$$e_P(1234) = [\overline{\omega}_1\gamma_5\omega_2]\,[\overline{\omega}_3\gamma_5\omega_4] \tag{A.5}$$

where Ψ_i are anti-commuting dirac spinors and with

$$\sigma_{\mu\nu} = \frac{i}{2}\,[\gamma_\mu, \gamma_\nu] \tag{A.6}$$

the standard Fierz transformation gives a relation of the form

$$e_I(1234) = \sum_{J=S}^{P} F_{IJ} e_J(1432) \tag{A.7}$$

with

$$F = \begin{pmatrix} -\frac{1}{4} & -\frac{1}{4} & -\frac{1}{8} & \frac{1}{4} & -\frac{1}{4} \\ -1 & \frac{1}{2} & 0 & \frac{1}{2} & 1 \\ -3 & 0 & \frac{1}{2} & 0 & -3 \\ 1 & \frac{1}{2} & 0 & \frac{1}{2} & -1 \\ -\frac{1}{4} & \frac{1}{4} & -\frac{1}{8} & -\frac{1}{4} & -\frac{1}{4} \end{pmatrix} \quad . \tag{A.8}$$

A.2. Basis translation $\epsilon \longleftrightarrow C$

Even though they are equal in some parts, in order to correctly translate the ϵ-*basis* into the C-*basis* one needs to consider a few steps:

1.: The prefactors of the two descriptions differ by a factor of

$$\begin{aligned}\mathcal{L}_9^{\epsilon} &= \frac{G_F^2}{2m_N}... \\ &= \frac{1}{4v^4 m_N}... \\ &= \frac{1}{v^5}\frac{v}{4m_N}... \ .\end{aligned}$$

Additionally, the chiral fermion currents in the *ϵ-basis* are defined by

$$\overline{\Psi}(1\pm\gamma_5)\Psi = \overline{\Psi}2P_{R,L}\Psi \tag{A.9}$$

$$= 2\overline{\Psi_L}\Psi_R \ . \tag{A.10}$$

Thus, for every chiral fermion current there is a factor of 2 which has to be taken into account.

2.: The *ϵ-basis* contains quark tensor currents. Instead, the *C-basis* contains color-octet operators. These are related via Fierz transformations. One can express the color-octet operators as a mixture of two terms

$$\Big[\overline{u}\lambda^A d\Big]\Big[\overline{u}\lambda^A d\Big] = 2\overline{u}^\alpha d^\beta \overline{u}^\beta d^\alpha - \frac{2}{3}\overline{u}^\alpha d^\alpha \overline{u}^\beta d^\beta \tag{A.11}$$

where α, β are color indices. To get rid of the tensor currents within the *ϵ-basis* one needs the following Fierz transformation

$$\begin{aligned}&\Big[\overline{\Psi}_1\sigma^{\mu\nu}\Psi_2\Big]\Big[\overline{\Psi}_3\sigma_{\mu\nu}\Psi_4\Big] \\ =& -3\Big[\overline{\Psi}_1\Psi_4\Big]\Big[\overline{\Psi}_3\Psi_2\Big] + \frac{1}{2}\Big[\overline{\Psi}_1\sigma^{\mu\nu}\Psi_4\Big]\Big[\overline{\Psi}_3\sigma_{\mu\nu}\Psi_2\Big] - 3\Big[\overline{\Psi}_1\gamma_5\Psi_4\Big]\Big[\overline{\Psi}_3\gamma_5\Psi_2\Big] \\ =& -3\Big(\Big[\overline{\Psi}_1\Psi_4\Big]\Big[\overline{\Psi}_3\Psi_2\Big] + \Big[\overline{\Psi}_1\gamma_5\Psi_4\Big]\Big[\overline{\Psi}_3\gamma_5\Psi_2\Big]\Big) \\ &+ \frac{1}{2}\Big(-3\Big[\overline{\Psi}_1\Psi_2\Big]\Big[\overline{\Psi}_3\Psi_4\Big] + \frac{1}{2}\Big[\overline{\Psi}_1\sigma^{\mu\nu}\Psi_2\Big]\Big[\overline{\Psi}_3\sigma_{\mu\nu}\Psi_4\Big] - 3\Big[\overline{\Psi}_1\gamma_5\Psi_2\Big]\Big[\overline{\Psi}_3\gamma_5\Psi_4\Big]\Big)\end{aligned} \tag{A.12}$$

which results in

$$\begin{aligned}&\Big[\overline{\Psi}_1\sigma^{\mu\nu}\Psi_2\Big]\Big[\overline{\Psi}_3\sigma_{\mu\nu}\Psi_4\Big] \\ =& -4\Big[\overline{\Psi}_1\Psi_4\Big]\Big[\overline{\Psi}_3\Psi_2\Big] - 4\Big[\overline{\Psi}_1\gamma_5\Psi_4\Big]\Big[\overline{\Psi}_3\gamma_5\Psi_2\Big] \\ &-2\Big[\overline{\Psi}_1\Psi_2\Big]\Big[\overline{\Psi}_3\Psi_4\Big] - 2\Big[\overline{\Psi}_1\gamma_5\Psi_2\Big]\Big[\overline{\Psi}_3\gamma_5\Psi_4\Big] \ .\end{aligned} \tag{A.13}$$

Plugging in chiral fermion currents one finds

$$\begin{aligned}&\Big[\overline{\Psi_{1R,L}}\sigma^{\mu\nu}\Psi_{2L,R}\Big]\Big[\overline{\Psi_{3R,L}}\sigma_{\mu\nu}\Psi_{4L,R}\Big]\\ =-8&\Big[\overline{\Psi_{1R,L}}\Psi_{4L,R}\Big]\Big[\overline{\Psi_{3R,L}}\Psi_{2L,R}\Big]-4\Big[\overline{\Psi_{1R,L}}\Psi_{2L,R}\Big]\Big[\overline{\Psi_{3R,L}}\Psi_{4L,R}\Big]\end{aligned} \tag{A.14}$$

and

$$\Big[\overline{\Psi_{1R,L}}\sigma^{\mu\nu}\Psi_{2L,R}\Big]\Big[\overline{\Psi_{3L,R}}\sigma_{\mu\nu}\Psi_{4R,L}\Big]=0 \tag{A.15}$$

With the help of the above relation we can match operators of the type $\epsilon_2 J^{\mu\nu}J_{\mu\nu}j$ e.g.

$$\begin{aligned}&\epsilon_2^{LLL}\Big[\overline{u}_R^\alpha\sigma^{\mu\nu}d_L^\alpha\Big]\Big[\overline{u}_R^\beta\sigma_{\mu\nu}d_L^\beta\Big]\overline{e}_L e_L^c\\ =&\epsilon_2^{LLL}\Big(-8\Big[\overline{u}_R^\alpha d_L^\beta\Big]\Big[\overline{u}_R^\beta d_L^\alpha\Big]-4\Big[\overline{u}_R^\alpha d_L^\alpha\Big]\Big[\overline{u}_R^\beta d_L^\beta\Big]\Big)\overline{e}_L e_L^c\\ =&\epsilon_2^{LLL}\Big(-8\mathcal{O}_3-4\mathcal{O}_2\Big)\overline{e}_L e_L^c\ .\end{aligned} \tag{A.16}$$

Operators with different chiralities can be transformed accordingly. The remaining operators in the ϵ-*basis* which contain tensor currents are of the form $\epsilon_4 J^\mu J_{\mu\nu}j^\nu$. Obviously, we cannot use the same trick here again to get rid of the tensor current. Instead, we have to treat the tensor current as a combination of two vector currents

$$\begin{aligned}J^\mu J_{\mu\nu}&=\overline{\Psi}_1\gamma^\mu\Psi_2\overline{\Psi}_3\sigma_{\mu\nu}\Psi_4\\ &=\frac{i}{2}\Big[\overline{\Psi}_1\gamma^\mu\Psi_2\overline{\Psi}_3\gamma_\mu\gamma_\nu\Psi_4-\overline{\Psi}_1\gamma^\mu\Psi_2\overline{\Psi}_3\gamma_\nu\gamma_\mu\Psi_4\Big]\\ &=\frac{i}{2}\Big[2\overline{\Psi}_1\gamma^\mu\Psi_2\overline{\Psi}_3\gamma_\mu\gamma_\nu\Psi_4-2\overline{\Psi}_1\gamma^\mu\Psi_2\overline{\Psi}_3 g_{\mu\nu}\Psi_4\Big]\\ &=i\Big[\overline{\Psi}_1\gamma^\mu\Psi_2\overline{\Psi}_3\gamma_\mu\Big(\gamma_\nu\Psi_4\Big)-\overline{\Psi}_1\gamma_\nu\Psi_2\overline{\Psi}_3\Psi_4\Big]\\ &=i\Big[-\overline{\Psi}_1\Big(\gamma_\nu\Psi_4\Big)\overline{\Psi}_3\Psi_2\\ &\quad+\frac{1}{2}\overline{\Psi}_1\gamma_\mu\Big(\gamma_\nu\Psi_4\Big)\overline{\Psi}_3\gamma^\mu\Psi_2\\ &\quad+\frac{1}{2}\overline{\Psi}_1\gamma_\mu\gamma_5\Big(\gamma_\nu\Psi_4\Big)\overline{\Psi}_3\gamma^\mu\gamma_5\Psi_2\\ &\quad+\overline{\Psi}_1\gamma_5\Big(\gamma_\nu\Psi_4\Big)\overline{\Psi}_3\gamma_5\Psi_2\\ &\quad-\overline{\Psi}_1\gamma_\nu\Psi_2\overline{\Psi}_3\Psi_4\Big]\\ &=i\begin{cases}-2\overline{\Psi}_1\gamma_\nu\Psi_4\overline{\Psi}_3\Psi_2-\overline{\Psi}_1\gamma_\nu\Psi_2\overline{\Psi}_3\Psi_4 & \text{for LLX and RRX}\\ \overline{\Psi}_1\gamma^\mu\Psi_2\overline{\Psi}_3\gamma_\mu\gamma_\nu\Psi_4-\overline{\Psi}_1\gamma_\nu\Psi_2\overline{\Psi}_3\Psi_4 & \text{for LRX and RLX}\end{cases}\end{aligned} \tag{A.17}$$

with

$$\gamma_\mu\gamma_\nu = -\gamma_\nu\gamma_\mu + 2g_{\mu\nu} \tag{A.18}$$

If we switch the step from line 2 to line 3 to

$$\begin{aligned}
&\frac{i}{2}\Big[\overline{\Psi}_1\gamma^\mu\Psi_2\overline{\Psi}_3\gamma_\mu\gamma_\nu\Psi_4 - \overline{\Psi}_1\gamma^\mu\Psi_2\overline{\Psi}_3\gamma_\nu\gamma_\mu\Psi_4\Big] \\
=&\frac{i}{2}\Big[- 2\overline{\Psi}_1\gamma^\mu\Psi_2\left(\overline{\Psi}_3\gamma_\nu\right)\gamma_\mu\Psi_4 + 2\overline{\Psi}_1\gamma^\mu\Psi_2\overline{\Psi}_3 g_{\mu\nu}\Psi_4\Big] \\
&\cdot \\
&\cdot \\
&\cdot \\
=&i\begin{cases}\overline{\Psi}_1\gamma_\nu\Psi_2\overline{\Psi}_3\Psi_4 - \overline{\Psi}_1\gamma^\mu\Psi_4\overline{\Psi}_3\gamma_\nu\gamma_\mu\Psi_2 & \text{for LLX and RRX} \\ \overline{\Psi}_1\gamma_\nu\Psi_2\overline{\Psi}_3\Psi_4 + 2\overline{\Psi}_1\Psi_4\overline{\Psi}_3\gamma_\nu\Psi_2 & \text{for LRX and RLX}\end{cases}
\end{aligned} \tag{A.19}$$

we finally get

$$\begin{aligned}
J^\mu J_{\mu\nu} &= \overline{\Psi}_1\gamma^\mu\Psi_2\overline{\Psi}_3\sigma_{\mu\nu}\Psi_4 \\
&= i\begin{cases}-2\overline{\Psi}_1\gamma_\nu\Psi_4\overline{\Psi}_3\Psi_2 - \overline{\Psi}_1\gamma_\nu\Psi_2\overline{\Psi}_3\Psi_4 & \text{for LLX and RRX} \\ \overline{\Psi}_1\gamma_\nu\Psi_2\overline{\Psi}_3\Psi_4 + 2\overline{\Psi}_1\Psi_4\overline{\Psi}_3\gamma_\nu\Psi_2 & \text{for LRX and RLX}\end{cases}
\end{aligned} \tag{A.20}$$

We can then use the above relation to get rid of the remaining tensor currents e.g.

$$\begin{aligned}
\epsilon_4^{LL} J_L^\mu J_{\mu\nu L} j_L^\nu &= \epsilon_4^{LL}\Big[\overline{u}_L^\alpha\gamma^\mu d_L^\alpha\Big]\Big[\overline{u}_R^\beta\sigma_{\mu\nu}d_L^\beta\Big]\overline{e}\gamma_\mu\gamma_5 e^c \\
&= \epsilon_4^{LL}\Big(- 2i\Big[\overline{u}_L^\alpha\gamma_\nu d_L^\beta\Big]\Big[\overline{u}_R^\beta d_L^\alpha\Big] - i\Big[\overline{u}_L^\alpha\gamma_\nu d_L^\alpha\Big]\Big[\overline{u}_R^\beta d_L^\beta\Big]\Big)\overline{e}\gamma_\mu\gamma_5 e^c \\
&= i\epsilon_4^{LL}\Big(- \Big[\overline{u}_L\lambda^A\gamma_\nu d_L\Big]\Big[\overline{u}_R\lambda^A d_L\Big] - \frac{5}{3}\Big[\overline{u}_L^\alpha\gamma_\nu d_L^\alpha\Big]\Big[\overline{u}_R^\beta d_L^\beta)\Big]\Big)\overline{e}\gamma_\mu\gamma_5 e^c \\
&= i\epsilon_4^{LL}\Big(- \mathcal{O}_9^\mu - \frac{5}{3}\mathcal{O}_8^\mu\Big)\overline{e}\gamma_\mu\gamma_5 e^c
\end{aligned} \tag{A.21}$$

Again, similar operators with different chiralities can be transformed accordingly.
The translation of the remaining operators which do not contain tensor currents is straight-forward.

B. Phase Space Factors - Trace calculations

When taking the absolute square of (3.136), the 5 different lepton currents result in 11 different trace calculations. To calculate these one needs the relations given in (3.81)

plus some additional relations concering traces of γ_5. For convenience we summarize all the necessary relations and trace identities including the ones from (3.81)

$$\begin{aligned}
&\mathrm{Tr}\{ABC\} = \mathrm{Tr}\{CAB\} = \mathrm{Tr}\{BCA\} \qquad \text{(Cyclic Permutation)}\\
&\mathrm{Tr}\{A+B\} = \mathrm{Tr}\{A\} + \mathrm{Tr}\{B\}\\
&\left.\begin{array}{l}\sum_{\text{spins}} u(p)\overline{u}(p) = \not{p} + m_e\\ \sum_{\text{spins}} u^c(p)\overline{u^c}(p) = \not{p} - m_e\end{array}\right\} \qquad \text{(Completeness relation)}\\
&\left.\begin{array}{l}\mathrm{Tr}\{\gamma^\mu\} = 0\\ \mathrm{Tr}\{\gamma^\mu\gamma_5\} = 0\end{array}\right\} \qquad \text{(Trace of odd number of } \gamma^\mu \text{ vanishes)}\\
&\mathrm{Tr}\{\gamma_5\} = \mathrm{Tr}\{\gamma^\mu\gamma^\nu\gamma_5\} = 0\\
&\mathrm{Tr}\{\gamma^\mu\gamma^\nu\gamma^\rho\gamma^\sigma\gamma_5\} = -4i\epsilon^{\mu\nu\rho\sigma}\\
&\mathrm{Tr}\{\gamma^\mu\gamma^\nu\} = 4g^{\mu\nu}\\
&\mathrm{Tr}\{\gamma^\mu\gamma^\nu\gamma^\rho\gamma^\sigma\} = 4\left(g^{\mu\nu}g^{\rho\sigma} - g^{\mu\rho}g^{\nu\sigma} + g^{\mu\sigma}g^{\nu\rho}\right)\\
&(\gamma_5)^2 = 1\\
&\{\gamma_5, \gamma^\mu\} = 0
\end{aligned} \tag{B.1}$$

where $\epsilon^{\mu\nu\rho\sigma}$ is the anti-symmetric Levi-Civita tensor. Using these relations the lepton current traces can be calculated which leads to

$$\begin{aligned}
\mathrm{Tr}\Big\{|\overline{u}_1 u_2^c|^2\Big\} &= 4\left(E_1E_2 - \vec{p}_1\cdot\vec{p}_2 - m_e^2\right)\\
\mathrm{Tr}\Big\{|\overline{u}_1 P_{R,L} u_2^c|^2\Big\} &= 2\left(E_1E_2 - \vec{p}_1\cdot\vec{p}_2\right)\\
\left(\frac{E_1-E_2}{m_e}\right)^2 \mathrm{Tr}\Big\{|\overline{u}_1\gamma_0 u_2^c|^2\Big\} &= 4\left(E_1E_2 + \vec{p}_1\cdot\vec{p}_2 - m_e^2\right)\\
\mathrm{Tr}\Big\{|\overline{u}_1\gamma_0\gamma_5 u_2^c|^2\Big\} &= 4\left(E_1E_2 + \vec{p}_1\cdot\vec{p}_2 + m_e^2\right)
\end{aligned} \tag{B.2}$$

for the simple squared currents and

$$\begin{aligned}
&\mathrm{Tr}\Big\{\big[\overline{u}_1 P_{R,L} u_2^c\big]\ \big[\overline{u_2^c} u_1\big]\Big\} = \frac{1}{2}\,\mathrm{Tr}\Big\{|\overline{u}_1 u_2^c|^2\Big\} = 2\left(E_1E_2 - \vec{p}_1\cdot\vec{p}_2 - m_e^2\right)\\
&\mathrm{Tr}\Big\{\big[\overline{u}_1 P_{R,L} u_2^c\big]\ \big[\overline{u_2^c} P_{R,L} u_1\big]\Big\} = \frac{1}{2}\,\mathrm{Tr}\Big\{|\overline{u}_1 u_2^c|^2\Big\} - \mathrm{Tr}\Big\{|\overline{u}_1 P_{R,L} u_2^c|^2\Big\} = -2m_e^2\\
&\frac{E_1-E_2}{m_e}\,\mathrm{Tr}\Big\{\big[\overline{u}_1 P_{R,L} u_2^c\big]\ \big[\overline{u_2^c}\gamma_0 u_1\big]\Big\} = -2\left(E_1-E_2\right)^2\\
&\mathrm{Tr}\Big\{\overline{u}_1 P_{R,L} u_2^c\overline{u_2^c}\gamma_0\gamma_5 u_1\Big\} = \pm 2\left(E_1+E_2\right)m_e\\
&\frac{E_1-E_2}{m_e}\,\mathrm{Tr}\Big\{\big[\overline{u}_1\gamma_0 u_2^c\big]\ \big[\overline{u_2^c} u_1\big]\Big\} = 2\frac{E_1-E_2}{m_e}\,\mathrm{Tr}\Big\{\big[\overline{u}_1 P_{R,L} u_2^c\big]\ \big[\overline{u_2^c}\gamma_0 u_1\big]\Big\} = -4\left(E_1-E_2\right)^2\\
&\frac{E_1-E_2}{m_e}\,\mathrm{Tr}\Big\{\big[\overline{u}_1\gamma_0 u_2^c\big]\ \big[\overline{u_2^c}\gamma_0\gamma_5 u_1\big]\Big\} = 0\\
&\mathrm{Tr}\Big\{\big[\overline{u}_1 u_2^c\big]\ \big[\overline{u_2^c}\gamma_0\gamma_5 u_1\big]\Big\} = 0
\end{aligned} \tag{B.3}$$

for the mixed currents. In the above formulas we used the abbreviation

$$u_{1,2} = u\left(p_{1,2}\right) \quad . \tag{B.4}$$

We see that, while many different traces appear, there are actually only 6 independent results.

C. Lists

List of Figures

List of Tables

Bibliography

[1] M. J. Herrero. The standard model, 1998.

[2] J. Erler and M. Schott. Electroweak precision tests of the standard model after the discovery of the higgs boson. *Progress in Particle and Nuclear Physics*, 106:68–119, May 2019.

[3] A. Aguilar-Arevalo et al. Evidence for neutrino oscillations from the observation of $\bar{\nu}_e$ appearance in a $\bar{\nu}_\mu$ beam. *Phys. Rev. D*, 64:112007, 2001.

[4] Y. Fukuda, T. Hayakawa, E. Ichihara, K. Inoue, K. Ishihara, H. Ishino, Y. Itow, T. Kajita, J. Kameda, S. Kasuga, and et al. Evidence for oscillation of atmospheric neutrinos. *Physical Review Letters*, 81(8):1562–1567, Aug 1998.

[5] S. Davidson, E. Nardi, and Y. Nir. Leptogenesis. *Physics Reports*, 466(4-5):105–177, Sep 2008.

[6] J. Schechter and J. W. F. Valle. Neutrinoless double-β decay in su(2)u(1) theories. *Phys. Rev. D*, 25:2951–2954, Jun 1982.

[7] H. Pas, M. Hirsch, H.V. Klapdor-Kleingrothaus, and S.G. Kovalenko. Towards a superformula for neutrinoless double beta decay. *Phys. Lett. B*, 453:194–198, 1999.

[8] H. Pas, M. Hirsch, H.V. Klapdor-Kleingrothaus, and S.G. Kovalenko. A Superformula for neutrinoless double beta decay. 2. The Short range part. *Phys. Lett. B*, 498:35–39, 2001.

[9] C. Giunti and C. W. Kim. *Fundamentals of Neutrino Physics and Astrophysics*. 4 2007.

[10] P.A. Zyla et al. (Particle Data Group). *to be published in Prog. Theor. Exp. Phys. 2020, 083C01 (2020).*

[11] S. Floerchinger and C. Wetterich. Lectures on quantum field theory. 2018.

[12] E. Kh. Akhmedov. Neutrino physics, 2000.

[13] S. Weinberg. Baryon- and lepton-nonconserving processes. *Phys. Rev. Lett.*, 43:1566–1570, Nov 1979.

[14] C. Giunti. Neutrino wave packets in quantum field theory. *Journal of High Energy Physics*, 2002(11):017–017, Nov 2002.

[15] N. Cabibbo. Unitary symmetry and leptonic decays. *Phys. Rev. Lett.*, 10:531–533, Jun 1963.

[16] M. Kobayashi and T. Maskawa. CP-Violation in the Renormalizable Theory of Weak Interaction. *Progress of Theoretical Physics*, 49(2):652–657, 02 1973.

[17] L. Chau and W. Keung. Comments on the parametrization of the kobayashi-maskawa matrix. *Phys. Rev. Lett.*, 53:1802–1805, Nov 1984.

[18] W. Grimus. Neutrino physics - models for neutrino masses and lepton mixing, 2006.

[19] F. R. Klinkhamer and N. S. Manton. A saddle-point solution in the weinberg-salam theory. *Phys. Rev. D*, 30:2212–2220, Nov 1984.

[20] E. Ma and R. Srivastava. Dirac or inverse seesaw neutrino masses with bl gauge symmetry and s3 flavor symmetry. *Physics Letters B*, 741:217–222, Feb 2015.

[21] J.W.F. Valle and C.A. Vaquera-Araujo. Dynamical seesaw mechanism for dirac neutrinos. *Physics Letters B*, 755:363–366, Apr 2016.

[22] S. Jana, V. P.K., and S. Saad. Minimal realizations of dirac neutrino mass from generic one-loop and two-loop topologies at d=5. *Journal of Cosmology and Astroparticle Physics*, 2020(04):018–018, Apr 2020.

[23] L. Canetti, M. Drewes, and M. Shaposhnikov. Matter and antimatter in the universe. *New Journal of Physics*, 14(9):095012, Sep 2012.

[24] M. Drewes and S. Eijima. Neutrinoless double β decay and low scale leptogenesis. *Phys. Lett. B*, 763:72–79, 2016.

[25] R. Kallosh, A. Linde, D. Linde, and L. Susskind. Gravity and global symmetries. *Physical Review D*, 52(2):912–935, Jul 1995.

[26] J. Wing and P. Fong. Semiempirical nuclidic mass equation. *Phys. Rev.*, 136:B923–B932, Nov 1964.

[27] M.I. Krivoruchenko, F. Šimkovic, D. Frekers, and A. Faessler. Resonance enhancement of neutrinoless double electron capture. *Nuclear Physics A*, 859(1):140–171, Jun 2011.

[28] Schwab D.J. Tsai J.J. Coursey, J.S. and R.A. Dragoset. Atomic weights and isotopic compositions (version 4.1)., 2015. [Online] Available: `http://physics.nist.gov/Comp` [2019, 12, 12] National Institute of Standards and Technology, Gaithersburg, MD.

[29] J. Kotila and F. Iachello. Phase-space factors for double-decay. *Physical Review C*, 85(3), Mar 2012.

[30] Yong-Hamb Kim. Neutrinoless double beta decay experiment, 2020.

[31] M. J. Dolinski, A.W.P. Poon, and W. Rodejohann. Neutrinoless double-beta decay: Status and prospects. *Annual Review of Nuclear and Particle Science*, 69(1):219–251, Oct 2019.

[32] K-H Ackermann, M Agostini, M Allardt, M Altmann, E Andreotti, AM Bakalyarov, M Balata, I Barabanov, M Barnabé Heider, N Barros, et al. The gerda experiment for the search of 0 $\nu\beta\beta$ decay in 76 ge. *The European Physical Journal C*, 73(3):1–29, 2013.

[33] W. Xu, N. Abgrall, F. T. Avignone, A. S. Barabash, F. E. Bertrand, V. Brudanin, M. Busch, M. Buuck, D. Byram, A. S. Caldwell, and et al. The majorana demonstrator: A search for neutrinoless double-beta decay of76ge. *Journal of Physics: Conference Series*, 606:012004, May 2015.

[34] C. E. Aalseth, N. Abgrall, E. Aguayo, S. I. Alvis, M. Amman, I. J. Arnquist, F. T. Avignone, H. O. Back, A. S. Barabash, P. S. Barbeau, C. J. Barton, P. J. Barton, F. E. Bertrand, T. Bode, B. Bos, M. Boswell, A. W. Bradley, R. L. Brodzinski, V. Brudanin, M. Busch, M. Buuck, A. S. Caldwell, T. S. Caldwell, Y-D. Chan, C. D. Christofferson, P.-H. Chu, J. I. Collar, D. C. Combs, R. J. Cooper, C. Cuesta, J. A. Detwiler, P. J. Doe, J. A. Dunmore, Yu. Efremenko, H. Ejiri, S. R. Elliott, J. E. Fast, P. Finnerty, F. M. Fraenkle, Z. Fu, B. K. Fujikawa, E. Fuller, A. Galindo-Uribarri, V. M. Gehman, T. Gilliss, G. K. Giovanetti, J. Goett, M. P. Green, J. Gruszko, I. S. Guinn, V. E. Guiseppe, A. L. Hallin, C. R. Haufe, L. Hehn, R. Henning, E. W. Hoppe, T. W. Hossbach, M. A. Howe, B. R. Jasinski, R. A. Johnson, K. J. Keeter, J. D. Kephart, M. F. Kidd, A. Knecht, S. I. Konovalov, R. T. Kouzes, B. D. LaFerriere, J. Leon, K. T. Lesko, L. E. Leviner, J. C. Loach, A. M. Lopez, P. N. Luke, J. MacMullin, S. MacMullin, M. G. Marino, R. D. Martin, R. Massarczyk, A. B. McDonald, D.-M. Mei, S. J. Meijer, J. H. Merriman, S. Mertens, H. S. Miley, M. L. Miller, J. Myslik, J. L. Orrell, C. O'Shaughnessy, G. Othman, N. R. Overman, G. Perumpilly, W. Pettus, D. G. Phillips, A. W. P. Poon, K. Pushkin, D. C. Radford, J. Rager, J. H. Reeves, A. L. Reine, K. Rielage, R. G. H. Robertson, M. C. Ronquest, N. W. Ruof, A. G. Schubert, B. Shanks, M. Shirchenko, K. J. Snavely, N. Snyder, D. Steele, A. M. Suriano, D. Tedeschi, W. Tornow, J. E. Trimble, R. L. Varner, S. Vasilyev, K. Vetter, K. Vorren, B. R. White, J. F. Wilkerson, C. Wiseman, W. Xu, E. Yakushev, H. Yaver, A. R. Young, C. H. Yu, V. Yumatov, I. Zhitnikov, B. X. Zhu, and S. Zimmermann. Search for neutrinoless double-β decay in ^{76}Ge with the majorana demonstrator. *Phys. Rev. Lett.*, 120:132502, Mar 2018.

[35] N. Abgrall, A. Abramov, N. Abrosimov, I. Abt, M. Agostini, M. Agartioglu, A. Ajjaq, S. I. Alvis, F. T. Avignone, X. Bai, and et al. The large enriched germanium experiment for neutrinoless double beta decay (legend). 2017.

[36] K. Ni, Y. Lai, A. Abdukerim, W. Chen, X. Chen, Y. Chen, X. Cui, Y. Fan, D. Fang, C. Fu, and et al. Searching for neutrino-less double beta decay of 136xe with pandax-ii liquid xenon detector. *Chinese Physics C*, 43(11):113001, Oct 2019.

[37] NEXT Collaboration, V. Álvarez, M. Ball, M. Batallé, J. Bayarri, F. I. G. Borges, S. Cárcel, J. M. Carmona, J. Castel, J. M. Catalá, S. Cebrián, A. Cervera-Villanueva, D. Chan, C. A. N. Conde, T. Dafni, T. H. V. T. Dias, J. Díaz, R. Esteve, P. Evtoukhovitch, L. M. P. Fernandes, P. Ferrario, E. Ferrer-Ribas, A. L. Ferreira, E. D. C. Freitas, A. Gil, I. Giomataris, A. Goldschmidt, E. Gómez, H. Gómez, J. J. Gómez-Cadenas, K. Gónzález, R. M. Gutiérrez, J. A. Hernando-Morata, D. C. Herrera, V. Herrero, F. Iguaz, I. G. Irastorza, V. Kalinnikov, A. Kustov, I. Liubarsky, J. A. M. Lopes, D. Lorca, M. Losada, G. Luzón, J. Martín-Albo, A. Méndez, T. Miller, A. Moisenko, J. P. Mols, F. Monrabal, C. M. B. Monteiro, J. M. Monzó, F. J. Mora, J. Muñoz-Vidal, H. Natal da Luz, G. Navarro, M. Nebot, D. Nygren, C. A. B. Oliveira, R. Palma, J. L. Pérez-Aparicio, J. Renner, L. Ripoll, A. Rodríguez, J. Rodríguez, F. P. Santos, J. M. F. dos Santos, L. Seguí, L. Serra, C. Sofka, M. Sorel, H. Spieler, J. F. Toledo, A. Tomás, Z. Tsamalaidze, D. Vázquez, E. Velicheva, J. F. C. A. Veloso, J. A. Villar, R. Webb, T. Weber, J. White, and N. Yahlali. The next-100 experiment for neutrinoless double beta decay searches (conceptual design report), 2011.

[38] V. Álvarez, F. I. G. M. Borges, S. Cárcel, J. M. Carmona, J. Castel, J. M. Catalá, S. Cebrián, A. Cervera, D. Chan, C. A. N. Conde, and et al. Next-100 technical design report (tdr). executive summary. *Journal of Instrumentation*, 7(06):T06001–T06001, Jun 2012.

[39] G. Anton, I. Badhrees, P.S. Barbeau, D. Beck, V. Belov, T. Bhatta, M. Breidenbach, T. Brunner, G.F. Cao, W.R. Cen, and et al. Search for neutrinoless double-decay with the complete exo-200 dataset. *Physical Review Letters*, 123(16), Oct 2019.

[40] nEXO Collaboration, S. Al Kharusi, A. Alamre, J. B. Albert, M. Alfaris, G. Anton, I. J. Arnquist, I. Badhrees, P. S. Barbeau, D. Beck, V. Belov, T. Bhatta, F. Bourque, J. P. Brodsky, E. Brown, T. Brunner, A. Burenkov, G. F. Cao, L. Cao, W. R. Cen, C. Chambers, S. A. Charlebois, M. Chiu, B. Cleveland, R. Conley, M. Coon, M. Côté, A. Craycraft, W. Cree, J. Dalmasson, T. Daniels, D. Danovitch, L. Darroch, S. J. Daugherty, J. Daughhetee, R. DeVoe, S. Delaquis, A. Der Mesrobian-Kabakian, M. L. Di Vacri, J. Dilling, Y. Y. Ding, M. J. Dolinski, A. Dragone, J. Echevers, L. Fabris, D. Fairbank, W. Fairbank, J. Farine, S. Ferrara, S. Feyzbakhsh, P. Fierlinger, R. Fontaine, D. Fudenberg, G. Gallina, G. Giacomini, R. Gornea, G. Gratta, G. Haller, E. V. Hansen, D. Harris, J. Hasi, M. Heffner, E. W. Hoppe, J. Hößl, A. House, P. Hufschmidt, M. Hughes, Y. Ito, A. Iverson, A. Jamil, C. Jessiman, M. J. Jewell, X. S. Jiang, A. Karelin, L. J. Kaufman, C. Kenney, R. Killick, D. Kodroff, T. Koffas, S. Kravitz, R. Krücken, A. Kuchenkov, K. S. Kumar, Y. Lan, A. Larson, B. G. Lenardo, D. S. Leonard, C. M. Lewis, G. Li,

S. Li, Z. Li, C. Licciardi, Y. H. Lin, P. Lv, R. MacLellan, K. McFarlane, T. Michel, B. Mong, D. C. Moore, K. Murray, R. J. Newby, T. Nguyen, Z. Ning, O. Njoya, F. Nolet, O. Nusair, K. Odgers, A. Odian, M. Oriunno, J. L. Orrell, G. S. Ortega, I. Ostrovskiy, C. T. Overman, S. Parent, M. Patel, A. Peña-Perez, A. Piepke, A. Pocar, J. F. Pratte, D. Qiu, V. Radeka, E. Raguzin, T. Rao, S. Rescia, F. Retière, A. Robinson, T. Rossignol, P. C. Rowson, N. Roy, J. Runge, R. Saldanha, S. Sangiorgio, S. Schmidt, J. Schneider, A. Schubert, J. Segal, K. Skarpaas VIII, A. K. Soma, K. Spitaels, G. St-Hilaire, V. Stekhanov, T. Stiegler, X. L. Sun, M. Tarka, J. Todd, T. Tolba, T. I. Totev, R. Tsang, T. Tsang, F. Vachon, B. Veenstra, V. Veeraraghavan, G. Visser, P. Vogel, J. L. Vuilleumier, M. Wagenpfeil, Q. Wang, M. Ward, J. Watkins, M. Weber, W. Wei, L. J. Wen, U. Wichoski, G. Wrede, S. X. Wu, W. H. Wu, Q. Xia, L. Yang, Y. R. Yen, O. Zeldovich, X. Zhang, J. Zhao, Y. Zhou, and T. Ziegler. nexo pre-conceptual design report, 2018.

[41] XENON Collaboration. Observation of two-neutrino double electron capture in 124xe with xenon1t. *Nature*, 568(7753):532–535, Apr 2019.

[42] J. Aalbers, F. Agostini, M. Alfonsi, F.D. Amaro, C. Amsler, E. Aprile, L. Arazi, F. Arneodo, P. Barrow, L. Baudis, and et al. Darwin: towards the ultimate dark matter detector. *Journal of Cosmology and Astroparticle Physics*, 2016(11):017–017, Nov 2016.

[43] S. Andringa, E. Arushanova, S. Asahi, M. Askins, D. J. Auty, A. R. Back, Z. Barnard, N. Barros, E. W. Beier, A. Bialek, and et al. Current status and future prospects of the sno+ experiment. *Advances in High Energy Physics*, 2016:1–21, 2016.

[44] The KamLAND-Zen Collaboration. Results from kamland-zen, 2014.

[45] S. Umehara, T. Kishimoto, M. Nomachi, S. Ajimura, T. Iida, K. Nakajima, K. Ichimura, K. Matsuoka, M. Saka, T. Ishikawa, D. Tanaka, M. Tanaka, T. Maeda, S. Yoshida, K. Suzuki, G. Ito, H. Kakubata, W. Wang, V.T.T. Trang, W.M. Chan, J. Takemoto, M. Doihara, T. Ohata, K. Tetsuno, Y. Tamagawa, I. Ogawa, T. Ueno, S. Maeda, A. Yamamoto, S. Tomita, G. Fujita, A. Kawamura, T. Harada, Y. Inukai, K. Sakamoto, M. Yoshizawa, K. Fushimi, R. Hazama, N. Nakatani, H. Ohsumi, and K. Okada. Search for neutrino-less double beta decay with candles. *Physics Procedia*, 61:283 – 288, 2015. 13th International Conference on Topics in Astroparticle and Underground Physics, TAUP 2013.

[46] D. Poda and A. Giuliani. Low background techniques in bolometers for double-beta decay search. *International Journal of Modern Physics A*, 32(30):1743012, Oct 2017.

[47] C. Alduino, K. Alfonso, D.R. Artusa, F.T. Avignone III, O. Azzolini, M. Balata, T.I. Banks, G. Bari, J.W. Beeman, F. Bellini, and et al. Cuore-0 detector: design, construction and operation. *Journal of Instrumentation*, 11(07):P07009–P07009, Jul 2016.

[48] The CUPID Interest Group. Cupid pre-cdr, 2019.

[49] S. Soldner-Rembold. Search for neutrinoless double beta decay with nemo 3 and supernemo. *Journal of Physics: Conference Series*, 110(8):082019, May 2008.

[50] A.S. Barabash, A. Basharina-Freshville, S. Blot, M. Bongrand, Ch. Bourgeois, D. Breton, V. Brudanin, H. Burešovà, J. Busto, A.J. Caffrey, and et al. Calorimeter development for the supernemo double beta decay experiment. *Nuclear Instruments and Methods in Physics Research Section A: Accelerators, Spectrometers, Detectors and Associated Equipment*, 868:98–108, Oct 2017.

[51] M. D. Schwartz. *Quantum field theory and the standard model*. Cambridge University Press, 2014.

[52] M. Peskin. *An introduction to quantum field theory*. CRC press, 2018.

[53] S. Bilenky. *Introduction to the physics of massive and mixed neutrinos*, volume 947. Springer, 2018.

[54] S. M. Bilenky. Neutrinoless double beta-decay. *Physics of Particles and Nuclei*, 41(5):690–715, Sep 2010.

[55] M. Salmhofer. Methoden der mathematischen physik 1 (mmp1) skript zur vorlesung im frühling 2016. 2016.

[56] M. Aker, K. Altenmüller, M. Arenz, M. Babutzka, J. Barrett, S. Bauer, M. Beck, A. Beglarian, J. Behrens, T. Bergmann, and et al. Improved upper limit on the neutrino mass from a direct kinematic method by katrin. *Physical Review Letters*, 123(22), Nov 2019.

[57] P. A. R. Ade, N. Aghanim, M. Arnaud, M. Ashdown, J. Aumont, C. Baccigalupi, A. J. Banday, R. B. Barreiro, J. G. Bartlett, and et al. Planck2015 results. *Astronomy Astrophysics*, 594:A13, Sep 2016.

[58] J. Kotila and F. Iachello. Phase space factors for++decay and competing modes of double-decay. *Physical Review C*, 87(2), Feb 2013.

[59] S. M. Bilenky and C. Giunti. Neutrinoless double-beta decay: A probe of physics beyond the standard model. *International Journal of Modern Physics A*, 30(04n05):1530001, Feb 2015.

[60] P. A. R. Ade et al. Planck 2015 results. XIII. Cosmological parameters. *Astron. Astrophys.*, 594:A13, 2016.

[61] F. Deppisch, M. Hirsch, and H. Päs. Neutrinoless double-beta decay and physics beyond the standard model. *Journal of Physics G: Nuclear and Particle Physics*, 39(12):124007, Nov 2012.

[62] E. Takasugi. Can the neutrinoless double beta decay take place in the case of dirac neutrinos? *Physics Letters B*, 149(4-5):372–376, 1984.

[63] J. F. Nieves. Dirac and pseudo-dirac neutrinos and neutrinoless double beta decay. *Physics Letters B*, 147(4-5):375–379, 1984.

[64] M. Duerr, M. Lindner, and A. Merle. On the quantitative impact of the schechter-valle theorem. *Journal of High Energy Physics*, 2011(6), Jun 2011.

[65] Y. Chikashige, R. N. Mohapatra, and R. D. Peccei. Spontaneously broken lepton number and cosmological constraints on the neutrino mass spectrum. *Phys. Rev. Lett.*, 45:1926–1929, Dec 1980.

[66] J.B. Albert, D.J. Auty, P.S. Barbeau, E. Beauchamp, D. Beck, V. Belov, C. Benitez-Medina, M. Breidenbach, T. Brunner, A. Burenkov, and et al. Search for majoron-emitting modes of double-beta decay ofxe136with exo-200. *Physical Review D*, 90(9), Nov 2014.

[67] A. V. Manohar. Introduction to effective field theories, 2018.

[68] B. Gripaios. Lectures on effective field theory, 2015.

[69] A. V. Manohar. Effective field theories. *Lecture Notes in Physics*, page 311–362.

[70] I. Z. Rothstein. Tasi lectures on effective field theories, 2003.

[71] W. D. Goldberger. Les houches lectures on effective field theories and gravitational radiation, 2007.

[72] M. L. Graesser. An electroweak basis for neutrinoless double decay. *Journal of High Energy Physics*, 2017(8), Aug 2017.

[73] V. Cirigliano, W. Dekens, J. de Vries, M. L. Graesser, and E. Mereghetti. Neutrinoless double beta decay in chiral effective field theory: lepton number violation at dimension seven. *Journal of High Energy Physics*, 2017(12), Dec 2017.

[74] V. Cirigliano, W. Dekens, J. de Vries, M. L. Graesser, and E. Mereghetti. A neutrinoless double beta decay master formula from effective field theory. *Journal of High Energy Physics*, 2018(12), Dec 2018.

[75] Hao-Lin Li, Zhe Ren, Ming-Lei Xiao, Jiang-Hao Yu, and Yu-Hui Zheng. Complete set of dimension-9 operators in the standard model effective field theory, 2020.

[76] Yi Liao and Xiao-Dong Ma. An explicit construction of the dimension-9 operator basis in the standard model effective field theory, 2020.

[77] S. Scherer. Introduction to chiral perturbation theory. *Adv. Nucl. Phys.*, 27:277, 2003.

[78] D. Štefánik, R. Dvornický, F. Šimkovic, and P. Vogel. Reexamining the light neutrino exchange mechanism of the0decay with left- and right-handed leptonic and hadronic currents. *Physical Review C*, 92(5), Nov 2015.

[79] J. Hyvärinen and J. Suhonen. Nuclear matrix elements for $0\nu\beta\beta$ decays with light or heavy majorana-neutrino exchange. *Phys. Rev. C*, 91:024613, Feb 2015.

[80] T. Bhattacharya, V. Cirigliano, S. D. Cohen, R. Gupta, H.-W. Lin, and B. Yoon. Axial, scalar, and tensor charges of the nucleon from2+1+1-flavor lattice qcd. *Physical Review D*, 94(5), Sep 2016.

[81] A. Nicholson, E. Berkowitz, H. Monge-Camacho, D. Brantley, N. Garron, C.C. Chang, E. Rinaldi, M.A. Clark, B. Joó, T. Kurth, and et al. Heavy physics contributions to neutrinoless double beta decay from qcd. *Physical Review Letters*, 121(17), Oct 2018.

[82] J. Engel and J. Menéndez. Status and future of nuclear matrix elements for neutrinoless double-beta decay: a review. *Reports on Progress in Physics*, 80(4):046301, Mar 2017.

[83] J. Menéndez. Neutrinoless $\beta\beta$ decay mediated by the exchange of light and heavy neutrinos: The role of nuclear structure correlations. *Journal of Physics G: Nuclear and Particle Physics*, 45(1):014003, 2017.

[84] J. Barea, J. Kotila, and F. Iachello. Nuclear matrix elements for double-decay. *Physical Review C*, 87(1), Jan 2013.

[85] J. Barea, J. Kotila, and F. Iachello. 0and2nuclear matrix elements in the interacting boson model with isospin restoration. *Physical Review C*, 91(3), Mar 2015.

[86] J.M. Yao, B. Bally, J. Engel, R. Wirth, T.R. Rodríguez, and H. Hergert. Ab initio treatment of collective correlations and the neutrinoless double beta decay of ca48. *Physical Review Letters*, 124(23), Jun 2020.

[87] F. Deppisch and H. Päs. Pinning down the mechanism of neutrinoless doubledecay with measurements in different nuclei. *Physical Review Letters*, 98(23), Jun 2007.

[88] J. Kotila, J. Barea, and F. Iachello. Neutrinoless double-electron capture. *Physical Review C*, 89(6), Jun 2014.

[89] A. Babič, D. Štefánik, M. I. Krivoruchenko, and F. Šimkovic. Bound-state double-decay. *Physical Review C*, 98(6), Dec 2018.

[90] J. C. Pati and A. Salam. Lepton number as the fourth "color". *Phys. Rev. D*, 10:275–289, Jul 1974.

[91] R. N. Mohapatra and J. C. Pati. "natural" left-right symmetry. *Phys. Rev. D*, 11:2558–2561, May 1975.

[92] G. Senjanovic and R. N. Mohapatra. Exact left-right symmetry and spontaneous violation of parity. *Phys. Rev. D*, 12:1502–1505, Sep 1975.

[93] P. Duka, J. Gluza, and M. Zrałek. Quantization and renormalization of the manifest left–right symmetric model of electroweak interactions. *Annals of Physics*, 280(2):336–408, Mar 2000.

[94] W. Dekens and D. Boer. Viability of minimal left–right models with discrete symmetries. *Nuclear Physics B*, 889:727–756, Dec 2014.

[95] Y. Zhang, H. An, X. Ji, and R. N. Mohapatra. General cp violation in minimal left–right symmetric model and constraints on the right-handed scale. *Nuclear Physics B*, 802(1-2):247–279, Oct 2008.

[96] J.L. Díaz-Cruz and D.A. López-Falcón. Probing the mechanism of ewsb with a rho-parameter defined in terms of higgs couplings. *Physics Letters B*, 568(3-4):245–253, Aug 2003.

[97] STEPHEN P. MARTIN. A supersymmetry primer. *Advanced Series on Directions in High Energy Physics*, page 1–98, Jul 1998.

[98] M. Hirsch, H. V. Klapdor-Kleingrothaus, and S. G. Kovalenko. Supersymmetry and neutrinoless double decay. *Physical Review D*, 53(3):1329–1348, Feb 1996.

[99] M. Hirsch, H. V. Klapdor-Kleingrothaus, and S. G. Kovalenko. New constraints on R-parity-broken supersymmetry from neutrinoless double beta decay. *Phys. Rev. Lett.*, 75:17–20, Jul 1995.

[100] H. E. Haber and G. L. Kane. The Search for Supersymmetry: Probing Physics Beyond the Standard Model. *Phys. Rept.*, 117:75–263, 1985.

[101] H. P. Nilles. Supersymmetry, Supergravity and Particle Physics. *Phys. Rept.*, 110:1–162, 1984.

[102] S. Dimopoulos and L. Susskind. Mass without scalars. *Nuclear Physics B*, 155(1):237 – 252, 1979.

[103] B. Gripaios. Composite leptoquarks at the lhc. *Journal of High Energy Physics*, 2010(2), Feb 2010.

[104] H. Fritsch. and P. Minkowski. Unified interactions of leptons and hadrons. *Annals of Physics*, 93(1):193 – 266, 1975.

[105] I. Dorsner and P. Fileviez Pérez. Unification without supersymmetry: Neutrino mass, proton decay and light leptoquarks. *Nuclear Physics B*, 723(1-2):53–76, Sep 2005.

[106] I. Doršner, S. Fajfer, and N. Košnik. Leptoquark mechanism of neutrino masses within the grand unification framework. *The European Physical Journal C*, 77(6), Jun 2017.

[107] I. Doršner, S. Fajfer, A. Greljo, J.F. Kamenik, and N. Košnik. Physics of leptoquarks in precision experiments and at particle colliders. *Physics Reports*, 641:1–68, Jun 2016.

[108] M. Hirsch, H.V. Klapdor-Kleingrothaus, and S.G. Kovalenko. New low-energy leptoquark interactions. *Physics Letters B*, 378(1-4):17–22, Jun 1996.

[109] M. Hirsch, H. V. Klapdor-Kleingrothaus, and S. G. Kovalenko. New leptoquark mechanism of neutrinoless doubledecay. *Physical Review D*, 54(7):R4207–R4210, Oct 1996.

[110] W. Dekens, J. de Vries, K. Fuyuto, E. Mereghetti, and G. Zhou. Sterile neutrinos and neutrinoless double beta decay in effective field theory. *Journal of High Energy Physics*, 2020(6), Jun 2020.

[111] M. Fierz. Zur fermischen theorie des β-zerfalls. *Zeitschrift für Physik*, 104(7-8):553–565, 1937.

[112] J. F. Nieves and P. B. Pal. Generalized fierz identities. *American Journal of Physics*, 72(8):1100–1108, Aug 2004.

Danksagung

Zum Abschluss möchte ich die letzten Zeilen dazu nutzen mich bei einigen Menschen zu bedanken, die mich nicht nur während dieser Arbeit sondern auch während meines Studiums unterstützt und begleitet haben.
Zunächst möchte ich mich daher bei Prof. Dr. Dr. h.c. Manfred Lindner für die außerordentlich gute Betreuung sowohl meiner Bachelor- als auch meiner Masterarbeit sowie die Möglichkeit, diese am Max-Planck-Institut für Kernphysik anzufertigen, bedanken. Ebenfalls möchte ich mich bei Dr. Lukas Graf bedanken, der mir während dieser Arbeit zu jeder Zeit hilfreich mit Rat und Tat zur Seite stand. Auch bei Herrn Prof. Dr. Joerg Jaeckel möchte ich mich bedanken, der sich freundlicherweise bereiterklärt hat, diese Arbeit als Zweitkorrektor zu bewerten.
Des Weiteren gilt mein Dank Jakob Stegmann, Julian Bollig, Ingolf Bischer, Thomas Rink, Dr. Thomas Hugle, Ken Laudor und Tiffany Kilian, die sich die Arbeit gemacht haben diese Thesis vorab zu lesen. Auch bei Christian Döring möchte ich mich für eine angenehme Arbeitsathmosphäre sowie viele hilfreiche und interessante Diskussionen bedanken.
Bei meinen Kommilitonen Alex Matskevych, Kian Tadjalli Mehr, Paul Oppelt, Jakob Stegmann, Fritz Schelten und Martin Weinreich möchte ich mich ebenfalls für viele Abende und Nächte voller Übungszetteln und Protokolle sowie eine tolle Studienzeit im Allgemeinen bedanken. Ohne euch wäre es erheblich weniger spaßig gewesen.
Bei Ina Michelsen möchte ich mich besonders für ihre Geduld und Unterstützung nicht nur während der Anfertigung dieser Arbeit sondern die gesamten letzten Jahre bedanken.
Abschließend gilt der größte Dank meiner Familie und natürlich insbesondere meinen beiden Eltern.

Erklärung:

Ich versichere, dass ich diese Arbeit selbstständig verfasst habe und keine anderen als die angegebenen Quellen und Hilfsmittel benutzt habe.

Heidelberg, den 31.07.2020

Oliver Scholer